Study of Resonant Reflection in Helicoidal Photonic Band Gap Structures

Thèse

Karen Allahverdyan

Doctorat en physique

Philosophiae doctor (Ph.D.)

Québec, Canada

Résumé

Étude de la réflexion résonante dans des structures hélicoïdales à bande photonique interdite

La présente thèse de doctorat rapporte une étude expérimentale sur la réflexion résonante de la lumière dans des structures hélicoïdales à bande photonique interdite. Plusieurs aspects optiques et électro-optiques des cristaux liquides cholestériques sont abordés en concentrant l'attention sur deux effets principaux: l'influence des conditions aux limites (mécaniques et optiques) sur les propriétés optiques des couches de cristaux liquides cholestériques et le contrôle de la bande interdite de ces dernières.

On présente un élément à double-rétroaction optique basé sur une cavité de Fabry-Pérot remplie de cristal liquide cholestérique. Les propriétés spectrales et de polarisation de cet élément sont caractérisées expérimentalement et par des simulations théoriques.

Un changement mineur dans la structure en haut (cavité de Fabry-Pérot) nous a permis d'obtenir une transmission non-réciproque de la lumière sans application d'un champ externe à l'élément en question. Nous avons observé une transmission non-réciproque de la lumière par un système qui ressemble beaucoup aux structures naturelles observées sur certaines carapaces d'insectes (par exemple, sur les élytres de certains coléoptères): une simple couche de matière transparente linéaire dans son état fondamental. L'effet est défini par deux facteurs principaux: la chiralité et la périodicité de la matière ainsi que les conditions asymétriques aux surfaces limites.

Concernant la partie sur le contrôle de la bande interdite, nous présentons la création et l'utilisation du mélange de cristal liquide cholestérique à deux fréquences pour le 'déroulement' et la reconstruction dynamique de la structure hélicoïdale. Le processus de reconstruction est accéléré d'un ordre de grandeur par l'application de champs électriques modérés.

L'étape suivante du contrôle de la bande interdite est l'accord en longueur d'onde de la bande interdite. Un effet électromécanique est utilisé pour générer et étudier l'auto-adaptation du pas d'hélice de la couche de cristal liquide cholestérique. L'anisotropie négative diélectrique a permis d'assurer la stabilisation de la structure hélicoïdale de la couche pendant l'application du champ électrique qui a aussi changé l'épaisseur de la couche de cristal liquide en pliant un des substrats minces de la cellule. Cette déformation de la couche a généré un d'accord (et des sauts) des longueurs d'onde de la bande interdite. Les études spectrales et morphologiques pendant les changements de la bande interdite sont présentées et discutées.

Summary

Study of Resonant Reflection in Helicoidal Photonic Band Gap Structures

The present PhD thesis reports experimental study of resonant reflection in helicodal photonic band gap structures. Several optical and electro-optical properties of cholesteric liquid crystals are investigated where attention was concentrated on two principal phenomena: the influence of mechanical and optical boundary conditions on optical properties of cholesteric liquid crystal layers and control of photonic band gap of cholesteric liquid crystals.
The creation of a double-feedback optical element based on a Fabry-Perot cavity filled with a planar aligned cholesteric liquid crystal mixture is presented. The polarization and spectral properties of this element are characterized experimentally and simulated theoretically. Experimental results are obtained for the transmittance dependence upon the orientation of the linear polarization plane and the polarization state of incident probe beam.
A slight change in above mentioned structure (Fabry-Perot cavity) let us obtain a non-reciprocal transmittance of light without applying any external field. We observed an optical non reciprocity in a material system that is very close to natural structures, such as insect skin: a single layer of linear transparent material in its ground state. The process is shown to be defined by two key parameters: the chiral and periodic nature of the material and its asymmetric boundary conditions.

In the part of band gap control, we present the creation and the use of dual frequency cholesteric liquid crystal mixtures for the dynamic electrical unwinding and forced (accelerated) restoring of their molecular helix. The restoring process is accelerated almost by an order of magnitude for quite moderate voltages used.

The next step of band gap control is the tuning of band gap (wavelength). Strong electromechanical effect was used to generate and study self-adaptation and pitch jumps in a layer of cholesteric liquid crystal. The negative dielectric anisotropy of the material allowed its stabilization by the electric field and important thickness changes, achieved thanks to the use of a very thin substrate, allowed the observation of multiple dynamic jumps at fixed deformation conditions. Spectral and morphological studies of the material during those jumps were performed and are presented.

Contents

Table of Figures

Acknowledgments

Several people have supported me during my studies and assisted in my integration into the social life of Quebec City, since my first arrival These individuals have always been there to help me with advice and assistance. Without them, my PhD project simply could not have progressed to its final stage.

The first person who met me in Quebec, and who helped me overcome the challenges facing a newcomer was my research director, Professor Tigran Galstian. Professor Galstian guided my first steps, personally introducing me to Laval University and its personnel. Professor Galstian provided key professional support, scientific discussions, advice and direction in respect of project proposals. I am deeply grateful to Professor Galstian.

I would also like to thank Professor Michel Piché for doing a revision of a version of the present thesis. His valuable remarks and advice helped to increase the value of work.

I would also like to thank all the staff of the COPL (Center for Optics Photonics and Lasers) who were always kind and ready to help with any service I asked. Remarkably, I would like to thank all the personnel of technicians, principally Patrick Larochelle and Souleymane Toubou Bah who provided a high quality support in laboratories.

I thank the Natural Sciences and Engineering Research Council of Canada (NSERC) for their financial support.

I also acknowledge TLCL Research Optics and its staff for material support, discussions and advice during my entire project.

I am grateful to the Armenian community of Quebec City (notably to Gurgen Melkonyan), for advice and support in daily life that were especially valuable during the starting phase of my stay in Quebec.

Finally, and most of all, I am deeply grateful to my family (in Armenia) and my friends who encouraged me and provided all the necessary help to make the decision to move to Canada and to start the PhD project.

My very last and a special acknowledgment is dedicated to my grandfather. Being a physics teacher at a village school, he is the person who inspired me to choose physics as my profession.

Karen Allahverdyan

Foreword

The present thesis is based on four manuscripts of articles published in peer-reviewed journals (during my PhD project). I am the principal author in all of them. Two of them are realized in collaboration with Professors Rafik Hakobyan and Ashot Gevorgyan, from Yerevan State University:

- K. Allahverdyan, A. Gevorgyan, T. Galstian, R. Hakopyan. "*Polarization and spectral properties of a cholesteric liquid crystal Fabry-Perot slab"*. Molecular Crystals and Liquid Crystals 560, 23 (**2012**).
- K. R. Allahverdyan, A. H. Gevorgyan, R. R. Hakobyan, T. V. Galstian, "*Observation of optical non reciprocity in a single layer of transparent linear chiral media with asymmetric boundaries"*. Pis'ma v ZhETF, vol. 96, iss. 11, pp. 778 - 782 (**2012)**.

The roles of authors are the following. All the authors participated in the subject discussions. The experimental part was discussed with Professor T. Galstian and entirely realized by me. The theoretical part (simulations) was realized by Professors Rafik Hakobyan and Ashot Gevorgyan. The writing of manuscripts was principally realized by Professor Tigran Galstian and me. After discussing the content and structure with Professor Galstian, I provided my version of manuscript to him who edited, added some missing parts and completed it.

The next two articles are authored by Professor T. Galstian and me:

- K. Allahverdyan, T. Galstian, "Electrooptic jumps in natural helicoidal photonic bandgap structures", ***Optics Express***, Vol. 19, 5, pp. 4611-4617 (**2011)**.
- K. Allahverdyan, T. Galstian . "*Accelerating the cholesteric helix restoring by a dual frequency cmpound*". Crystals Molecular Crystals and Liquid Crystals 560, 35 (**2012**)

The subjects and experiment strategies were discussed with Professor T. Galstian. The experiments were entirely realized by me. After discussing the manuscript content and structure with Professor T. Galstian, I provided my version of manuscript to him who then edited and completed it.

Co-authors:

Tigran Galstian: Center for Optics, Photonics and Laser, Department of Physics, Engineering Physics and Optics, Laval University, Pav. d'Optique-Photonique, 2375 Rue de la Terrasse, Québec, G1V 0A6, Canada.

e-mail: galstian@phy.ulaval.ca

Rafik Hakobyan: Department of Physics, Yerevan State University, 1 Alex Manoogian, 0025 Yerevan.

e-mail: rhakob@ysu.am

Ashot Gevorgyan: Department of Physics, Yerevan State University, 1 Alex Manoogian, 0025 Yerevan.

e-mail: agevorgyan@ysu.am

Karen Allahverdyan

Publications (during the PhD project)

Reviewed periodicals

1. **K. Allahverdyan**, T. Galstian, "Electrooptic jumps in natural helicoidal photonic bandgap structures", ***Optics Express***, Vol. 19, 5, pp. 4611-4617, **2011**.

2. **K. Allahverdyan** , T. Galstian. "*Accelerating the cholesteric helix restoring by a dual frequency compound"*. Crystals Molecular Crystals and Liquid Crystals 560, 35 (**2012**)

3. **K. Allahverdyan**, A. Gevorgyan, T. Galstian, R. Hakopyan. "*Polarization and spectral properties of a cholesteric liquid crystal Fabry-Perot slab"*. Molecular Crystals and Liquid Crystals 560, 23 (**2012**)

4. **K. R. Allahverdyan**. *Experimental study of influence of external electric field on the photonic band gap of chiral liquid crystals*. Journal of Contemporary Physics (Armenian Academy of Sciences), Volume 47, Issue 4, pp 168-172, **2012.**

5. **K. R. Allahverdyan**, A. H. Gevorgyan, R. R. Hakobyan, T. V. Galstian. *Observation of optical non reciprocity in a single layer of transparent linear chiral media with asymmetric boundaries*. Pis'ma v ZhETF, vol. 96, iss. 11, pp. 778 - 782, **2012**.

6. **Karen Allahverdyan**, Ashot Gevorgyan, Tigran Galstian, Refik Hakobyan. *Could the cuticle of beetles serve also for their radiative thermoregulation?,* Optics and Photonics Journal (OPJ) Vol.3 No.7A, **2013**

7. **K. Allahverdyan** , T. Galstian. *Focusing unpolarized light with a single nematic liquid crystal layer,* **submitted** to OE (SPIE)

Conference Presentations

1. Ismaël Duchesne, Guillaume Paradis, **Karen Allahverdyan**, Tigran Galstian and Simon Rainville. *The motility of bacteria in an anisotropic liquid environment,* CAP 2013 (annual congress). Montreal, 27-31 May, **2013.**

2. **Karen Allahverdyan** and Tigran Galstian, *Study of chiral molecular diffusion in anisotropic liquid,* CAP 2014 (annual congress). Sudbury, 16- 20 June, **2014.**

3. **K. Allahverdyan**, G. Agez, M. Mitov, T. Galstian, *Spectral and polarization study of self-organized cholesteric oligomers,Montreal,* 28-30 May, **2014.**

Chapter 1
Introduction

Matter is usually considered to have three main phases: gas, liquid and solid. Each of those states has different properties and is separated into different classes. Gases for example, are almost always isotropic and they adopt the shape and the volume of the container they are filled in: they homogenously fill the entire container. We will not concentrate our attention on gases, as these are not the subject of the present work. Liquids take the shape of the container where they are located and very often are considered as isotropic media without any organized structure in the molecular level. Finally, in the solid phase matter conserves both its shape and volume. The solid state could be referred as the most complex of the three above mentioned phases: matter in this state can be isotropic or anisotropic, amorphous or crystalline, sometimes possessing complex molecular organization such as the cubic, tetragonal or hexagonal molecular (or atomic) arrangements [1] or without any organized structure in the case of amorphous solids. What if between two condensed phases of matter (solid and liquid) there were to exist an "intermediate" phase?

In 1888, the Austrian chemist Friedrich Reinitzer, working in the Institute of Plant Physiology at the University of Prague, discovered a strange phenomenon. Reinitzer was conducting experiments with a cholesterol based substance, trying to figure out the exact formula and molecular weight of the cholesterol. When he tried to precisely determine the melting point, which is an important purity indicator of a substance, he was struck by the fact that this substance seemed to have two melting points. At 145.5°C the solid crystal melted into a cloudy liquid, which existed until 178.5°C, when the cloudiness suddenly disappeared, giving way to a clear transparent liquid. At first Reinitzer thought that this might have been a sign of impurities in the material, but further purification did not lead to any changes of such behavior and Reinitzer, being a chemist, asked for help of a physicist, Otto Lehmann. Lehmann examined the intermediate cloudy fluid and reported seeing crystallites.

This new state of matter was an "intermediate'' state between the liquid and solid states of matter, and was called liquid crystal (LC). Not all materials pass through the LC phase; those that do can have many different physical properties (optical, dielectric, magnetic, mechanical, etc.). What unites all LCs is that they can form a collectively organized molecular structure; they are usually elongated, rod-like molecules, having anisotropic characteristics and they assume a liquid phase (they are able to flow).

The name "liquid crystal" was coined historically because it exhibits the properties of crystals such as molecular order and, yet these "crystals" are liquids: they flow. The scientific name that better represents this state of matter might be "anisotropic liquids".

LCs have been intensively investigated and applied in diverse fields of science and technology, since the 1960s. From the point of view of scientific interest LCs are useful, among other reasons, because being anisotropic and liquid (less anchoring energies between molecules) they appear to show nonlinear effects at extremely low intensities of probe light. For example, the electro - optical Kerr coefficient is in the order of 10^{-14} - 10^{-13} m/V^2 for conventional liquids (electro-optical Kerr effect), while it is usually in the order of 10^{-10} for LCs [2]. Hence, liquid crystalline media show non-linear optical response at much lower intensities than conventional liquids or the solids [2]. The non-linear response of LCs has found different applications, such as the all-optical light switches, self-focusing (defocusing), phase modulation, nonlinear wave-guiding [2] etc. However, in technology LCs have found massive applications thanks mainly to their electro-optical properties; applying low electric fields to LC layers, one can easily control their optical properties and control the propagation of light through thin films of LC [3]. The most obvious example of LC based electro-optical device is the LC display.

1.1 Liquid Crystals

The difference between crystals and liquids (or amorphous solids) is that the molecules in crystals are ordered over long range, whereas, they are not in common liquids. The order in crystals is usually both positional and orientational, that is, the molecules are confined both to occupy specific sites in a lattice and to point molecular axes (if they exist) in specific directions. The molecules in liquids are usually distributed randomly throughout the sample

with their molecular axes fluctuating. Interestingly, many phases with molecular order greater than that of liquids, but less than typical crystals, also exist in nature. These phases are grouped together and called LC, since they share some properties that are normally associated with liquids and others associated with crystals.

The molecules in many LC phases are distributed much like molecules of a liquid, but they also do maintain some degree of order, notably orientational. The amount of order in LCs is quite small – with respect to crystals. There is only a slight tendency for the majority of molecules to be pointed in one direction than in any other, or to spend more time in certain positions than in others. The fact that most of the order ("the order energy'') of a crystal is lost when it transforms from the solid to LC phase is revealed by the value of the latent heat. The values are around 250 J/g, which is typical for a crystal transforming into a liquid. When an LC transforms to a liquid the latent heat is much smaller; typically about 5J/g. Yet, a small amount of order in LCs reveals itself by mechanical and electromagnetic properties, which resemble those of crystals [4]

The molecules in most common types of LC are rod-like, elongated molecules. The LC molecules possess a unique tendency to collectively organize, which is key to numerous fascinating phenomena occurring in LC materials. Once the rod-like LC molecules are in bulk, each molecule tends to orient in the same direction as its neighbours and, as a result, they form domains. In each domain the molecules are oriented in one direction, described by unit vector, $\vec{n}$, called the director. This unique property separates LCs from other (isotropic) liquids. Because of thermal motion, there are some fluctuations (deviations) from this preferred direction. The amount of these fluctuations from the perfectly ordered system is described by the so called order parameter, S:

$$S = \langle \frac{3}{2} \cos^2 \theta - \frac{1}{2} \rangle \qquad (1.\ 1)$$

where the brackets denote an average over many molecules at any given instant of time, or the average over time for a single molecule (Figure 1.(a)). The decrease of the order parameter with increase of temperature (Figure 1. (b)) appears because of the rise of thermal motion which becomes more intense and chaotic near the LC - isotropic phase

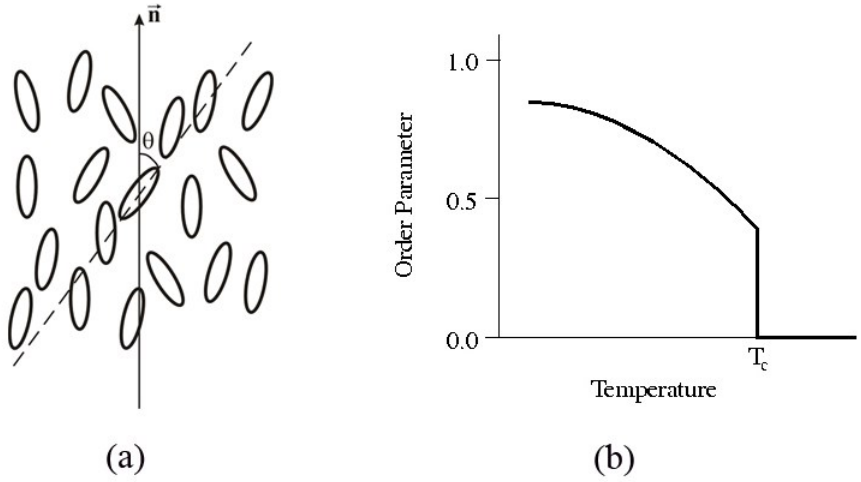

Figure 1.1 (after Ref. [4]): a) The molecular order in a nematic liquid crystal. b) The typical temperature dependence of the order parameter, S. Tc is the temperature of the liquid crystal transition to liquid.

transition temperature. At the phase transition temperature T_c, the LC transforms into an isotropic phase and the molecular order sharply vanishes, yielding a value of 0 for the order parameter. The order parameter, **S**, approaches unity in perfectly ordered systems such as the crystals and it tends to zero in non - organized systems, such as conventional liquids or amorphous solids. When we consider the LC in a bulk where there is no external force, and the above-mentioned domains are oriented chaotically, that is, the director ($\vec{n}$) changes its direction from one domain to the other without any long range order. In this case, the order parameter, ***S***, adopts some relatively high value if we take into account only one ordering domain, while it approaches zero if we take into account the entire bulk. Usually, it is desired to have highly organized structures, where instead of being chaotically oriented, the molecules point their axes towards some (initially predicted) direction for all domains. To achieve this, LCs are almost always used as thin films, sandwiched between two glass substrates. This configuration is used to impose generalized orientational anisotropy, avoiding major orientational defects that might, for example, result in optical scattering when light passes through the LC layer. The use of a thin LC layer in a sandwich structure also allows one to control molecular orientation by external forces such as those derivd from electric or magnetic fields, and those based on mechanical interventions.

From a structural point of view, there are three main types of liquid crystals: nematic liquid crystals (NLC), cholesteric liquid crystals (CLC) and smectic liquid crystals (SLC) [5]. In this project we use the first two types, NLC and CLC, so we concentrate our attention on these types.

1.2 Nematic Liquid Crystals

The NLC has the simplest structure among all LC phases. Perhaps, it is also the most applied in technology: LC displays [6] (e.g. computer monitors, cellphone, electronic watch and calculator displays), tunable LC lenses [7-9], tunable LC phase retarders [10], etc. Even if the NLCs are not the main subject of investigation in the present work, we will present in detail the NLCs and their properties because it's a compound that is very often used in CLCs.

As already mentioned, the molecules of most LCs have rod-like shape. There exist some other LC molecules such as disc like [5] molecules, but the present thesis is concerned exclusively with LCs based on rod-like molecules, thus we will always consider the LC molecules as rod-like. Being rod-like, the LC molecule possesses a long axis and a short axis (actually the short axis is not definitely defined; it is laid on a surface perpendicular to the long axis of the molecule). Hence, if it is not specified, we will always talk about the long axis and we will sometimes simply call it the "molecular axis".

Molecules of NLC tend to point their axes parallel to the axis of their neighboring molecules and, once in bulk, they "create" a general axis along which they orient. As mentioned earlier, the molecules are oriented in the same direction in domains, but (in general) the director varies from domain to domain. That "complicates" the application possibilities (both in science and in technology). In terms of orientation in a bulk, the situation changes dramatically, once we somehow give a preferred direction to the molecules in the bulk. The preferred direction could be given by external action such as electric or magnetic fields or different mechanical actions. The mechanical action can, for example, be some flow of the LC. The rod-like molecules usually adopt the flow direction, pointing their axes along the movement direction. These and other hydrodynamic

properties of LCs are well investigated and are known as hydrodynamic effects in LCs [11], [12-14]. The method to give a preferred direction to LC molecules that is efficient and widely used in both science and technology is the method called “rubbing”. The rubbing is done by a soft (usually silk) cloth that “grooves” nano - scratches on the surface of limiting glass substrates. This is the most common technique that is used to align the molecules of LC layer. As mentioned before, thin layers of LC sandwiched between two glass substrates are used in investigations and they are called LC cells (Figure 1.2). The LC layer thickness can be different, depending on the purposes; usually it varies from a few micrometers up to a few hundreds of micrometers. The dimension ratio is not respected in the figure below: in our experiments, the LC layer thickness is usually tens of micrometers, while the substrates usually are 0.1-1 mm thick.

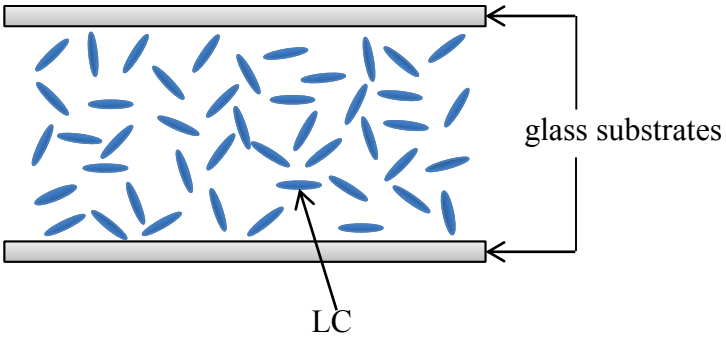

Figure 1.2: The schematic of a standard liquid crystal cell.

As one can see in Figure 1.2, the LC molecules point their long axes in random directions if there is no preferred direction given to the LC molecules. In this case, the LC molecules align randomly and, over time, they randomly change their alignment due to thermal motion. In reality (not illustrated in the figure) some coherence exists between molecules which forces the molecules to form the microscopic domains where they are aligned in the same direction, but that direction chaotically changes from one domain to another. In order to have a uniform LC cell with a single direction of director in the whole cell, one needs to give a preferred direction to molecules.

The two main types of uniform molecular organizations in a LC cell are the planar and homeotropic alignment (Figure 1.3) [10]. In the case of planar alignment (Figure 1.3(a)) the molecular axes are pointed parallel to the glass substrates while in the case of homeotropic

alignment (Figure 1.3(b)) all the molecules in the layer point their axes perpendicular to limiting glass substrates.

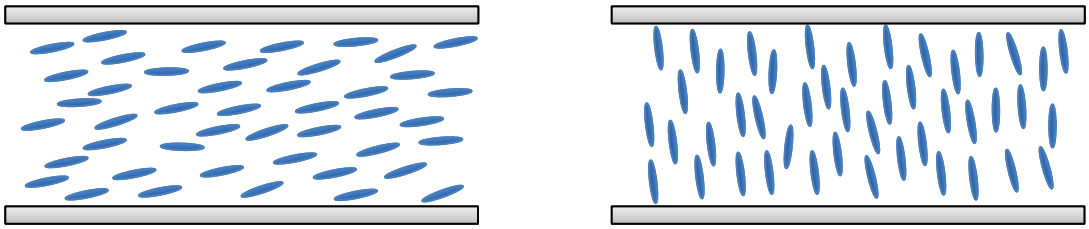

a: planar b: homeotropic

Figure 1.3: The schematic illustration of molecular arrangement in a planar (a) and homeotropic (b) aligned liquid crystal cells

In other words, the homeotropic and planar orientations are the orientations where the LC director has, on average, the same direction over the entire cell: it is perpendicular to limiting substrates in the homeotropic case and parallel in the planar case. Because of thermal motion, there are always deivations from the above mentioned directions, but these are around the same direction. They are not large in amplitude and do not influence the alignment of the average director. Apart from planar and homeotropic alignments, there are other alignments, such as the twist and hybrid orientations which in some way, are combinations or modifications of planar and homeotropic alignments [10]. These orientations, for example, are used to make NLC displays [6].

1.3 Smectic Liquid Crystals

The smectic phase of LC is of lesser concern to the present thesis. In separated layers, the molecular orientation of smectics is much similar to nematics; all the molecules pointing their axes in the same direction. The particularity of SLCs is their layered structure with well-defined interlayer spacing that can be measured by X-ray diffraction [5]. A comparison of molecular arrangements in NLCs and SLCs is shown in the Figure 1.4. We can see that unlike the nematics, the molecular layers are not interfused in the case of smectics and they can even slide with respect to their neighbour layers [5]. The smectic phase of LCs is more ordered than the nematic one. For a given material, the smectic phases usually occur at temperatures below the temperatures of nematic phase.

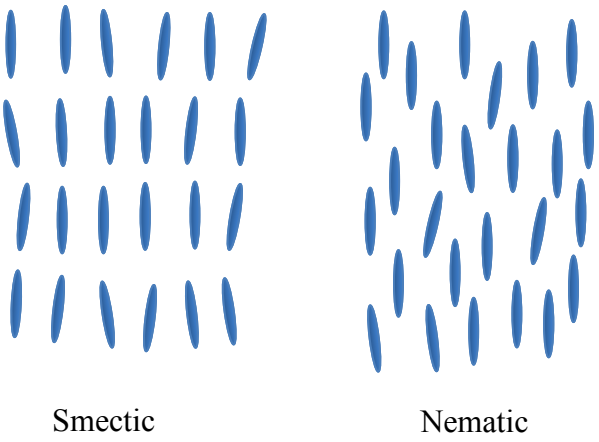

Figure 1.4: The arrangement of molecules in smectic (left) anf nematic (rigth) liquid crystals

The name smectic comes from Greek word smēktikos (clean) and the Latin, smecticus, meaning, having the properties of soap. That is because of similarities in mechanical properties of smectics and soap. At certain concentrations the soap solution in water passes to SLC phase.

The SLCs have not found notable technological applications yet, but they can still be useful for academic investigations. For example, having a closer molecular organization to crystals and being easily manipulated (as liquids) they can be used to better understand diverse phenomena in crystals.

1.4 Chirality

The word "*chiral*" comes from Greek word for hand, "$\chi\varepsilon\iota\rho$". Macroscopic objects, molecules or structures that appear to be non-superposable on their mirror images are said to be chiral [15]. The most common, and also evident, example of a chiral object is the human hand. If we carefully observe our two hands (we already know they are similar), we can notice that they are not identical: we cannot superpose them. Our left hand is the mirror image of our right hand and they are not superposable. This is the basic definition of chirality: a molecule, an object or a structure is chiral if it is not superposable with its own mirror image. Alongside with the human hand, there exist different types of chiral molecules, structures or objects in nature or in our daily life. Some examples (a human

hand, a screw and a propeller) are presented in Figure 1.5. The helicoidal structure of a CLC phase is an example of chiral molecular order: the molecular structures of right and left handed CLCs are non-superposable mirror images of each other. In addition, our galaxy itself has chiral properties [16]: it has right handed structure.

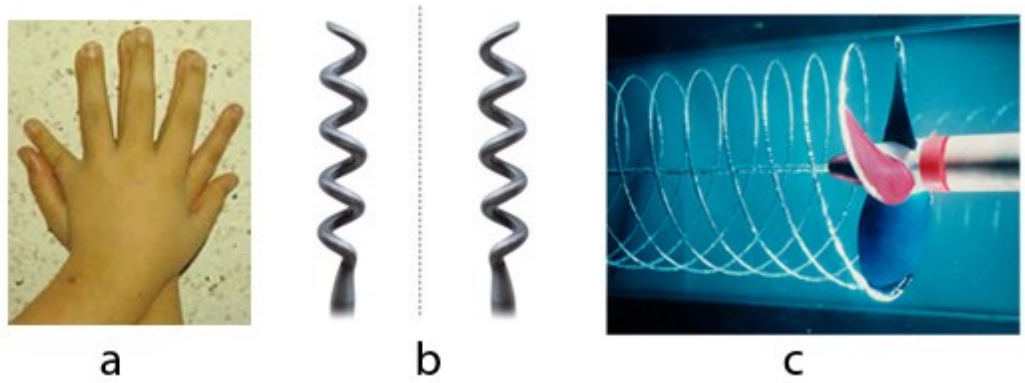

Figure 1.5: Examples of chiral objects. a) Human hand, b) screw and c) propeller.

By saying right handed we mean a helicoidal structure, the rotation sign of which corresponds to "right-hand rule": to move forward through the structure and follow the helix, one needs to make clockwise rotations. Obviously, the left handed structure is the structure corresponding to "left-hand rule". The definition is exactly the same as that of right handed structure with a single difference: one has to make counter-clockwise rotations. In Figure 1.5, the helix designated by the propeller is a right-handed helix(c), the screw on the right is right handed and that on the left is left-handed (b). There are several definitions of handedness of chiral structures [5, 17, 18], sometimes confusing, and even controversial. To be systematic, we will always follow the above presented definition and will also adapt it to the sign of circular polarized light. Helicoidal chiral structures or objects are naturally associated with the above definition. However, other chiral objects and structures can also be associated with rotations, so that the definition can be adapted to them as well.

Molecular chirality is well investigated in chemistry, biology and in medicine. Two chiral molecules that are mirror-images one of the other seem to have the same properties as they contain the same atoms and those atoms are arranged in the similar way. But interestingly, this pair of molecules can have radically different properties that can be manifested in an

organism digestive system. For example, the human body utilizes sugars which are right – handed molecule, whereas the mirror image of some sugars is utilized in artificial sweeteners such as Tagatose or Natrulose. The human metabolism cannot fully metabolize left - handed molecules, and they therefore have zero or low calories [15]. Similarly, the two mirror-image forms of a chiral molecule may have very different odours or even may be harmful (poison) or helpful (drug) for human organism. So the choice of the "correct" handedness is sometimes extremely important, especially in medicine.

In the present work, we concentrate on media that contain a small amount of chiral molecules, resulting in formation of chiral molecular structure. Particularly, the propagation of light through such media in different states is considered as one of the objectives of present work. As we will discuss later, the presence of chiral molecules in a medium can significantly change the propagation of light [19]: transmission, reflection and scattering (backward and forward) are in question. There are two major mechanisms for chiral molecules to act on light propagation: chiral molecules act themselves "directly on light" or they change the structure of the host media and afterwards, the structure acts on the light. One of the commonly used examples of the first mechanism is the optical activity [19] of sugar solution in water. This phenomenon is used to precisely measure the concentration of chiral molecules in different solutions [20], e.g., the method of measuring the concentration of sugar in blood (the glucose level). An example of the second mechanism is a solution of chiral molecules in a NLC to induce a periodic – helicoidal structure (CLC) and if certain conditions are satisfied, light may be reflected from such a periodic structure [2, 5, 18].

1.5 Cholesteric Liquid Crystals

Historically, CLCs were the first type of LCs to be observed. The Austrian chemist Friedrich Reinitzer was investigating a cholesterol based substance when he discovered the LC phase. This is why this type of LC is called cholesteric. CLCs are sometimes called twisted NLCs (or just twisted nematics) or chiral NLCs (or chiral nematics), because very often CLCs are obtained by adding some little amount of chiral dopant in a NLC host which results in formation of a twisted (helicoidal) structure (Figure 1.6). The CLCs possess a structure that is identical to nematics in separated molecular layers. So, farther in

the present work, all the above mentioned names will refer to the same type of material: CLC.

The director $\vec{n}$ of CLC is not constant in space. The preferred conformation of CLC molecules in bulk is helicoidal (Figure 1.6). As we can see, the director is constant in separated layers while it slightly inclines if one moves from one layer to its neighbouring layer. The distance $\boldsymbol{p}$ at which the director rotates at 360^o is called helix pitch. The helix pitch $\boldsymbol{p}$ can be presented as the "geometrical period" of the structure. As the form of LC molecules is geometrically symmetric, from an optical point of view the period $\boldsymbol{L}$ of the structure is the distance at which the director rotates at 180^o, i.e., the half-pitch ($L = p/2$) [5]. If we call the helical axis the z-axis, we have the following distribution for $\vec{n}$ components:

$$\begin{aligned} n_x &= \cos(q_0 z + \varphi) \\ n_y &= \sin(q_0 z + \varphi) \\ n_z &= 0 \end{aligned} \tag{1.2}$$

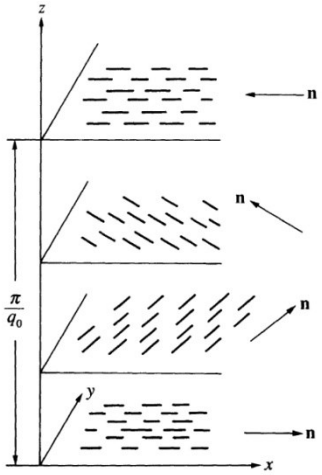

Figure 1.6 (after Ref. [5]): The arrangement of molecules in the cholesteric mesophase. The successive planes have been drawn for convenience; they do not have any specific physical meaning.

Both the helical axis (z) and the value of φ are arbitrary. As we see from the equations above and from Figure 1.6, the structure is periodic along **z** and (since the states $\vec{n}$ and, $-\vec{n}$**,** are equivalent) the spatial period *L* is equal to one-half to the pitch:

$$L = \frac{\pi}{|q_0|} \tag{1.3}$$

The twisting power q_0 (thus the pitch length) can be extremely different. It depends of course on the chiral molecules, on their concentration in NLC, on temperature etc. It can even change its sign (positive for the right-handed helix and negative for the left-handed one) not only from a chiral molecule to a chiral molecule, but also, in particular cases, $q_0(T)$ $\mathrm{q_0(T)}$ can even change its sign at particular temperature [21, 22].

So, the period *L* responsible for optical properties of CLCs can be presented in two ways:

$$L = \frac{p}{2} \text{ or } L = \frac{\pi}{|q_0|} \tag{1.4}$$

Once again, *p* is the pitch of cholesteric structure and q_0 is the helical twisting power (HTP): the rotation angle of director $\vec{n}$ per unit length along the axis of helix.

Periodic and helicoidal structures occur in the nature in different forms, such as the cuticle of different scarab beetles, the wings of some butterfly species [23, 24], and in *Pollia condensata*, a type of blueberry found in Western Africa. Some examples of iridescent structures existing in the nature are shown in Figure 1.7. These periodic formations usually exhibit similar optical properties as the CLCs. However, some inevitable light scattering usually occurs in natural forms that can be edited in CLCs by different methods such as the use of LC cells.

As mentioned above, the CLCs are usually obtained by adding some dopant to NLC. The dopant consists of chiral molecules and the presence of these chiral molecules dramatically changes the molecular organization in a bulk of CLC (NLC & chiral dopant mixture). What is more important, the presence of chiral molecules in the matrix of NLC drastically changes the optical characteristics of NLC as well. If a preferred alignment direction (parallel to layer surfaces) is given to external molecular layers of CLC, the molecules in

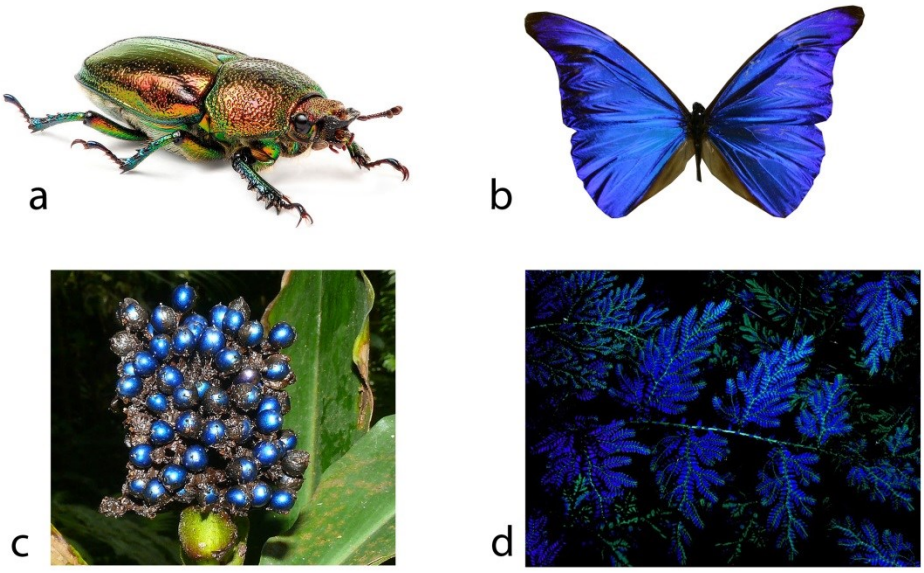

Figure 1.7: a) Golden stag beetle, b) Morpho Butterfly, c) *Pollia condensata*, d) *Selaginella willdenowii*.

the entire LC layer form a helicoidal structure with a helix axis perpendicular to the layer surfaces. In separated monomolecular layers, parallel to the layer surfaces, the molecules have a single preferred direction to point their axes, just like nematics. The difference from nematics is that in the case of cholesterics there is a slight tilt of that preferred direction (director) between neighbouring monomolecular layers. Thus, the director is always parallel to the surface of LC film, with its end drawing a helix, while we move from one surface to the other. The organization of molecules in CLC is shown in Figure 1.6 and Figure 1.8. If the CLC is free of external forces it forms helicoidal structures in little domains with chaotically oriented helix axes in different domains.

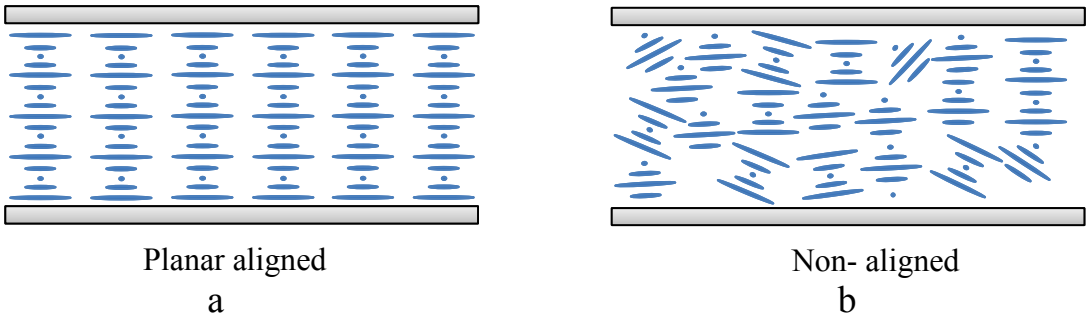

Figure 1.8: The helicoidal organization of cholesteric liquid crystal molecules in aligned (planar) and non - aligned cholesteric liquid crystal cells.

In Figure 1.8 one observes a schematic illustration of molecular organization in planar (a) and un-oriented (b) cells filled with CLC. The lines with different lengths represent molecule (or the director) projections at the plane of paper. One can see that if the cell substrates are treated for planar orientation (a), all the molecules stay parallel to glasses and form the above mentioned helicoidal structure. A schematic of chaotically oriented helicoidal domains in a cell, the substrates of which are not treated, is illustrated in Figure 1.8 b. The CLC can form different molecular structures depending on cell gap (the distance between the glass substrates) if the substrates are treated for homeotropic orientation. They can, for example, form a helix whose axis is parallel to glasses (fingerprint texture) [25] in thin cells (comparable to helix pitch, see Figure 1.9b) or a helix with perpendicular (to

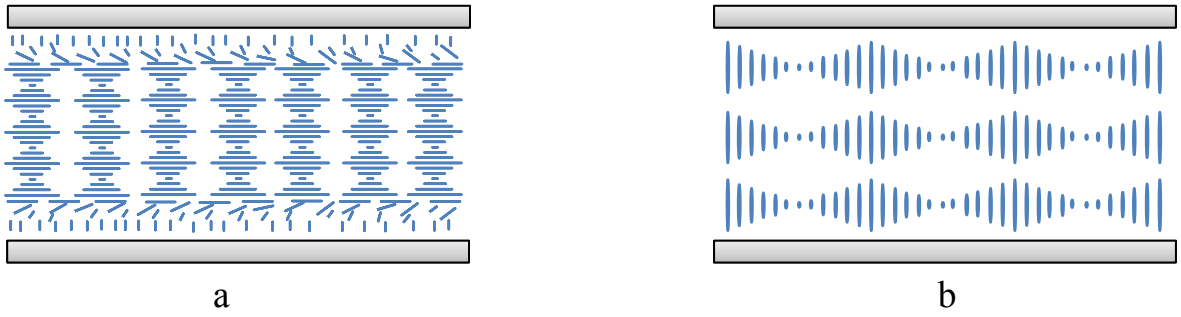

Figure 1.9: The helicoidal organization of cholesteric liquid crystal molecules in homeotropic aligned cells. a: the helix pitch is much smaller than the cell thickness, and b: the helix pitch is comparable with the cell thickness.

glass substrates) axis in relatively thick cells (see Figure 1.9a). In the last case, molecules that are close to substrates (treated for homeotropic orientation) are arranged perpendicular and they gradually incline while one moves farther from the substrate. Some electro-optical properties and applications of CLCs will be discussed further.

1.6 Anisotropy of Liquid Crystals

Almost all the peculiarities of the three kinds of LCs come from the anisotropic nature of their molecules. As already mentioned, LC molecules have a rod-like shape that gives them anisotropic characteristics such as the optical and electrical anisotropies: the most investigated and the most utilized in diverse applications. Along with electrical and optical anisotropies which are both the results of the anisotropy of dielectric permittivity (ε), LCs

exhibit also anisotropic characteristics with respect to movements (flow), deformations (elastic constants), thermal conductivity [2] etc.

As it is well known, the propagation of waves in diverse media can be described by Maxwell's equations combined with constitutive equations [19, 26]:

$$\vec{D} = \bar{\varepsilon}\vec{E} \text{ and } \vec{B} = \mu_0\vec{H} \tag{1.5}$$

where the $\bar{\varepsilon}$ is the permittivity of the material through which the electromagnetic wave is propagating and the μ_0 is the free space (magnetic) permeability. As the magnetic response of typical materials is slow in the optical range of frequencies, the relative magnetic permeability of the material in question is assumed to be one: $\mu_r = 1$, and in the general case the permittivity $\bar{\varepsilon}$ is assumed to be a second-rank tensor, which takes the form of 3x3 matrix [19, 26]. The solution of Maxwell`s equation is sought in the form of plane waves:

$$\vec{E} = E_0\vec{s}e^{i(\omega t - \vec{k}\cdot\vec{r})}, \tag{1.6}$$

where E_0 is the field amplitude, $\vec{s}$ is a unit vector of field polarization, ω is the circular frequency and $\vec{k}$ is the wave vector. The diagonal elements of $\bar{\varepsilon}$ matrix are identical ($\varepsilon_{11} = \varepsilon_{22} = \varepsilon_{33} = \varepsilon$) in isotropic media. That equivalence results in the following relation between $\vec{k}$ and ω:

$$k^2 = \omega^2\mu\varepsilon, \tag{1.7}$$

which defines a sphere with a radius $\sqrt{\omega^2\mu\varepsilon}$ in three dimensional k - space for any given ω. This shows the equivalence of directions of wave propagation in the material: $|\vec{k}|$ is invariant with direction, and consequently, so is the refractive index n of the material ($n = \frac{c}{v}$, $|\vec{k}|^2 = \frac{\omega^2}{v^2}$, where v is the speed of light in the medium in question). In anisotropic media the diagonal elements of the $\bar{\varepsilon}$ matrix are different. An important case based on so-called uniaxial materials: materials having two (out of three) equivalent diagonal elements of $\bar{\varepsilon}$ matrix: $\varepsilon_{11} = \varepsilon_{22} = \varepsilon \neq \varepsilon_{33}$. In that case, the relation between k - components (k_x, k_y, k_z) and ω is the following [26]:

$$\left(\frac{k^2}{\omega^2\mu\varepsilon}-1\right)\left(\frac{{k_x}^2+{k_y}^2}{\omega^2\mu\varepsilon_{33}}+\frac{{k_z}^2}{\omega^2\mu\varepsilon}+1\right)=0. \tag{1.8}$$

The last equation defines two surfaces in the three dimensional k - space: a sphere and an ellipsoid (Figure 1. 10).

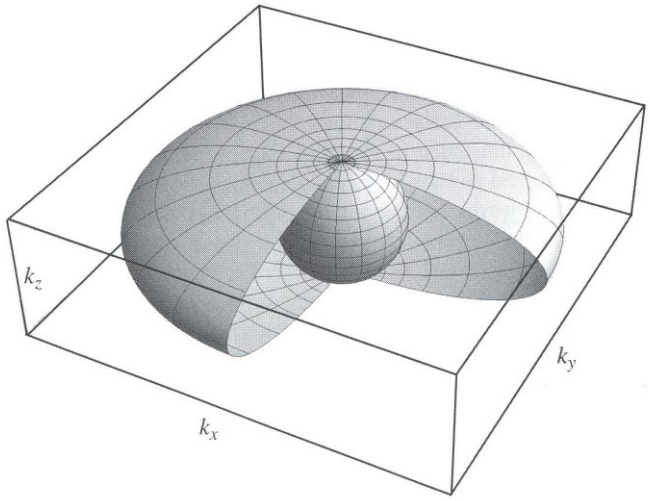

Figure 1. 10 (after ref [26]): The equi-frequency surfaces of uniaxial materials. For every frequency and every direction of wave propagation (with the exception of propagation along the z-direction), there are two different phase velocities that correspond to two polarizations of the wave. Along the z-direction, the plane waves propagate with phase velocity independent of polarization. For illustration, the ratios of the eigenvalue are chosen as $\varepsilon_{11}=\varepsilon_{22}\neq\varepsilon_{33}$. Part of the outer surface is cut out to show the inner surface.

For a given frequency and direction of propagation, two waves with different phase velocities, hence with different refractive indexes, are allowed. As one can see, the above mentioned sphere and the ellipsoid intersect with each other at two points lying on a line that is parallel to the z-axis. Thus in the case of a wave, propagating along the z-axe, the phase velocity is independent of polarization and there is no birefringence. For every other direction of propagation, there are two orthogonally polarized beams that possess different phase velocities and different refractive indexes. Those two beams, corresponding to the sphere and the ellipsoid, are called ordinary and extraordinary beams, respectively. The wave-vector (and the refractive index) of ordinary polarized beam is invariant on the

direction of propagation, while that of extraordinary polarized beam changes upon the direction of propagation (more specifically upon the direction of wave-vector, $\vec{k}$).

Generally the beam propagates at some other direction than parallel or perpendicular to the anisotropy axis and the vectors $\vec{k}$ and $\vec{S}$ (Pointing vector) have different directions for the extraordinary wave. This results in different directions of propagation of ordinary and extraordinary waves.

Hereafter, we will usually use the following simplified notation of ordinary and extraordinary waves:

The optical anisotropy (Δn) is the difference of extraordinary (n_e) and ordinary (n_o) refractive indexes: $\Delta n = n_e - n_o$. The extraordinary refractive index is the refractive index of an electromagnetic wave, electrical field of which oscillates parallel to the LC director (parallel to long axes of molecules) and the ordinary refractive index is that of one oscillating perpendicular to the director. The dielectric anisotropy is described by the difference between parallel and perpendicular dielectric permittivities: $\Delta\varepsilon = \varepsilon_{\parallel} - \varepsilon_{\perp}$. As one would expect, $\varepsilon_{\parallel}$is the dielectric permittivity of electric field that is parallel to LC director and the $\varepsilon_{\perp}$ is that of an electric field that is perpendicular to LC director. Usually, the optical anisotropy (Δn) of LCs varies around the value of 0.2 (n_e of the order of 1.7 and the n_o of the order of 1.5).

The optical anisotropy is often used to make retarding films in order to control beam polarization which is then used (among other applications) in LC modulators or in LC displays [6, 10]. The dielectric anisotropy is then used to control the orientation of molecules so that LC based devices can be tunable. Thanks to relatively high dielectric anisotropy and small interaction between molecules (as liquids), LCs require very low electric fields to introduce changes in their molecular structure (less than 1V).

The above presented definition of anisotropy is not the strict definition of it, but it is reasonable since in the present work, light propagation is almost always considered perpendicular or parallel to the anisotropy axis.

1.7 Periodic Media

The propagation of waves through a medium with a periodic modulation of material properties on the scale of the wavelength is often profoundly different from that of the homogeneous case. The fact is well known in solid-state physics, in which periodicity in the electrostatic potential associated with atoms in crystalline solids is responsible for the formation of energy bands and energy gaps of electronic states in metals, semiconductors and dielectrics [1, 26, 27].

Electromagnetic waves that propagate through a periodic medium may exhibit many interesting and potentially useful phenomena. Examples include diffraction of light from periodic strain and the diffraction of X-rays. These phenomena have been used in many optical devices, such as diffraction gratings, holograms, distributed-feedback lasers [28, 29], high-reflectance Bragg mirrors or filters [30, 31] and acousto-optic modulators [32].

Periodic structures are well described and classified in solid-state physics, where different types of symmetries and periodicities are considered [1]. Here we will not focus on the types of symmetry, but we will discuss the types of periodicities following the classification of materials called photonic crystals (PC).

In the course of the last decades, significant attention has been paid to develop photonic devices that can confine, control and route light on a scale corresponding to modern electronic devices, namely the nanometer scale. The beginning of investigations into PCs is marked by the almost simultaneous publications of E. Yalblonovich [33] and S. John [34] in 1987. The key motivation of this activity is the promise of photonic devices: light path controllers, modulators, “ultra-compact” and low threshold lasers [35], etc. However, for this promise to be realized such devices must possess the ability to confine light on a sub-wavelength scale and they must be fabricated in a material system that is compatible with microelectronics manufacturing infrastructure. Although the latter requirement is readily satisfied through a proper choice of materials, i.e. silicon, the former was historically more elusive. The reason for this is the nature of confinement in conventional materials. There are two major types of material used in optics to confine, control and route light: conductors and dielectrics. Conductive materials usually have high refractive indexes in the

optical range and are usually used as reflectors. These materials are usually lossy and are not the ideal materials to be used for light path control. Dielectrics (refractive materials) can provide low losses but they do not confine the optical modes in a sufficiently small scale. In searches to solve the above mentioned problems, scientists have turned to photonic devices, particularly to PCs or photonic band-gap (PBG) materials, which can provide low losses and high confinement for optical wavelengths. Also, they may be fabricated from dielectric materials [26, 27].

The important property of PCs (or PBG materials) is the periodic modulation of optical properties (e.g., refractive index). This periodic modulation leads to selective reflectance of incident light [26, 27]. There is a wavelength band (corresponding to the Bragg condition [19, 36]) that does not transmit through PC: the light having a wavelength inside this band reflects from the PC. This band is called photonic band – gap (PBG) or it is usually called the band - gap (BG) and that is why the PCs are sometimes called PBG materials.

According to the periodicity, PCs are classified into three groups: one- (1D), two- (2D) and three (3D) – dimensional PCs [27]. Naturally, the one dimensional PCs possess the less complicated structure. They are easier to fabricate and to be investigated or interpreted as well. Being the main subject of the present thesis, the CLCs have 1D periodic structure.

PC optical characteristics, e.g., the refractive index, are periodically modulated. In the case of 1D PCs, there is only one axis along which the refractive index is modulated: the optical characteristics are constant along directions perpendicular to this axis. In Figure 1.11 one can see an example of a 1D PC. They consist usually (not always) of an alternation of two different transparent materials (having different refractive indexes). By choosing the "right" material with the "right" refractive index and depositing them with the required thickness, one can have a PBG with the desired central wavelength and desired width as well. The schematic illustration of a beam's reflection from a 1D PC is presented in Figure 1.11. So, the 1D PC is a distributed Bragg reflector. If, for example, the chosen material refractive indexes (n_1 and n_2) and thicknesses (d_1 and d_2) provide the same optical path ($n_1 \times d_1 = n_2 \times d_2$), all the beams reflected from layer surfaces, due to Fresnel reflection, will constructively interfere for selected wavelengths, corresponding to following condition:

$$m\lambda = n_1 \times 2d_1 \cos\theta = n_2 \times 2d_2 \cos\theta \qquad (1.9)$$

where λ is the constructively interfering wavelength and the m is a integer number ($m = 1, 2, 3$ ....…). Henceforth, we will use common terms for λ and m: BG wavelength and diffraction order, respectively.

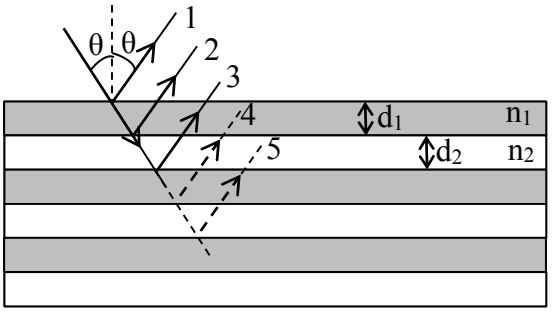

Figure 1.11: The schematic illustration of ligth reflection from one dimensional photonic crystal.

The principle of the Bragg condition is the following: from each interface, because of the refractive index mismatch, the beam is partly reflected [19]. If all the reflected waves oscillate at the same phase (the phase shift is multiple to 2π), they interfere constructively and the resulting reflected beam intensity equals to the sum of intensities of all the reflected beams from inner interfaces of Bragg reflector [19, 36]. The difference of refractive indexes of the two materials defines the width of the band-gap [26, 31] and the intensity of the reflected beam from each interface. Thus, in order to have the same value of reflectance, the number of alternating layers is supposed to be higher if the used materials have close refractive indexes.

One can see the drastic boundaries of PBG and oscillations near the PBG in Figure 1.12, which are not always there in Bragg reflectors with disruption of periodicity. Very often, there are also high order reflections: $m = 2, 3$ ... in Eq. (1.9) (not illustrated in Figure 1.12).

Bragg reflectors are well applied in diverse optical devices such as dielectric mirrors or fiber Bragg gratings [37] (with their wide field of applications in telecommunication, in medicine, etc.).

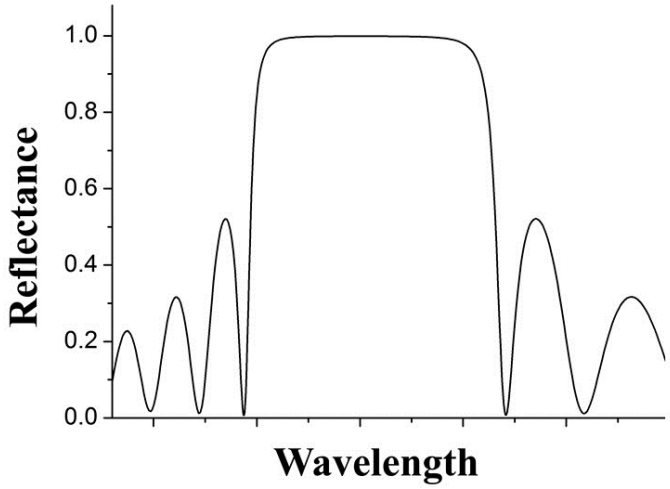

Figure 1.12 (after Ref [26]): The typical transmittance spectrum form of one dimensional photonic crystal.

An ideal (without any impurity or structural defect) Bragg mirror was considered above, which provides reflectance spectra shown in Figure 1.12. But, in reality, because of non-identical thicknesses of layers or different non-uniformities, there are always some deviations from the ideal periodic structure. The next section discusses some peculiarities of non-ideal Bragg reflectors are considered.

1.8 Non Ideal Bragg Reflectors

For various reasons we usually have to use non-ideal periodic structures where some disruption of periodicity is present. In fact, in reality we can never achieve ideal (absolute) periodic structure; there are always some variations from absolute periodicity. However, in many cases those variations are minor and one can neglect them, considering the system as discussed in the previous section. The cases where one cannot neglect the disruptions of periodicity can be separated in two groups: desirable and undesirable. Almost parallel with the intensive investigation of PCs, a sub-section of PC applications started to develop (in 1990s). That is the PCs with planar defect. It was both theoretically and experimentally shown that the existence of a thin layer in the middle of a PC somehow disrupting the periodicity can significantly change the propagation of light with specific wavelengths [38],

[39, 40]; more specifically, it can introduce a narrow band in reflection spectrum (or transmittance spectrum) inside the BG that is transmitted (or reflected). That band is called defect mode and its spectral position and the width can be controlled by tuning the properties (e.g. the optical thickness) of the defect layer [41, 42].The number of defect modes depends on defect layer optical properties as well. The presence of a defect mode in the BG can be used for preparation of low-threshold tunable laser [35, 43, 44], narrow-band tunable mirrors [45], optical non-reciprocal elements [46, 47] etc. So this kind of disruption of periodicity is desirable and it is introduced for certain targeted purposes.

Another kind of perturbation is the variation of periodic characteristics such as the period or the amplitude of modulation. If the period is changing throughout a PC layer, the PBG can widen [48, 49], as different sub-layers possess different PBGs. The gradient of the pitch can also result in quenching of oscillations near the PBG edges [50].

Finally, the most undesirable and sometimes inevitable case of disruptions are the orientational defects or impurities in PCs. Speaking about CLCs, for example, we can say that in real conditions there are always thermal fluctuations, non-ideal parallel surfaces of limiting substrates or impurities that cause disclination lines [51, 52] introducing some scattering of light. In fact, the impurities themselves scatter light. Because of imperfection in the orientational order, tilted domains (tilted helix axis) can exist which can also scatter the light. The last case of light scattering is selective and it is mostly back scattering: correctly speaking, it is mostly reflection at various angles. If we combine all the above mentioned possible contributions in light scattering we will have complicated situation where due to anisotropy, depolarization and multiple reflections from different domains should also be considered [50]. It is a significantly complicated task to solve the general case of above mentioned problem, and very often, an individual approach to a specific case is more suitable.

1.9 Cholesteric Liquid Crystals as Tunable Distributed Bragg Gratings

As it has already been mentioned, CLCs are obtained by mixing some amount of chiral dopant (CD) in a NLC. Proportions of given CD and the host NLC define the helix pitch of final CLC: the more CD is mixed with the NLC, the smaller the pitch will be. Naturally, the helix pitch depends also on molecular structures of both CD and NLC compounds [2]. Compound proportions that provide helix pitches comparable to the visible wavelengths are usually chosen in photonic applications. This provides a PBG inside or near the visible spectrum of wavelengths thus it allows manipulating visible light. By tuning the compound proportions one can finely tune the PBG position in the spectrum and choose the one which corresponds to requirements of any specific application. It is possible to determine the required proportions (of compounds) theoretically, before preparing the mixture. To do that, one needs to analyse the chemical structures of both compound molecules, where specific connections are responsible for different properties of the final mixture such as the helix pitch, the pitch dependence on temperature or the viscosity [2]. But these provisions usually are complicated and in practice they are rarely used. In practice the helix pitch dependence (the other properties also) are usually determined experimentally. Very often the final proportions are important not only for the PBG spectral position but also for its dependence upon temperature [5, 53]. In order to visualize that, we present the Figure 1.13, where the helix pitch dependence on temperature is presented for three different CLC mixtures. As one can see, the dependence is extremely strong for certain temperatures while it is rather weak for others. Depending on the application one can be in need of strong or weak dependence. For example: CLC thermometers [54] require specific and precise temperature dependence of the helix pitch and for precise measurements strong dependence is required. In applications such as the smart windows or LC displays, weak temperature dependence is required - the weaker the better. So for the first case one needs to locate on the left wing and for the second case, on the right wing of the curve (Figure 1.13). In order to tune not only the pitch, but also its dependence on temperature, usually three component mixtures are used: left and right twisting chiral molecules and an NLC [53]. The opposed twisting chiral molecules are used to tune the strength of temperature

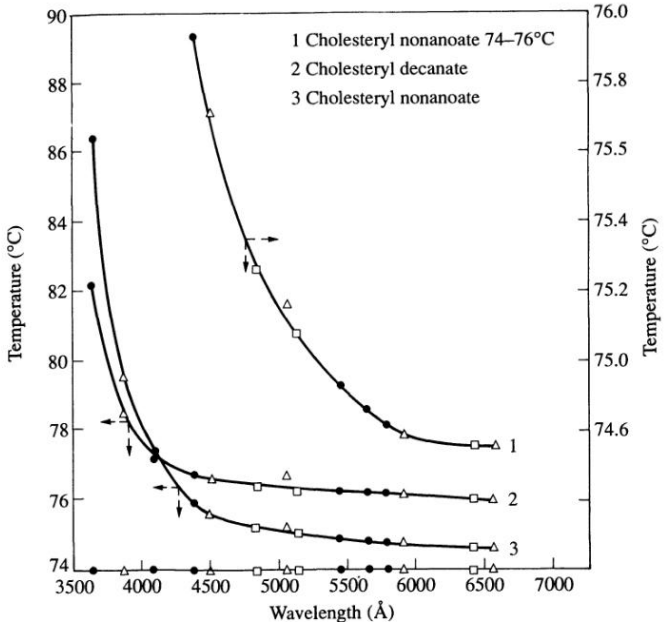

Figure 1.13: (after Ref. [5]): The relation between pitch and temperature in typical cholesterics. What is plotted horizontally is the optical wavelength for Bragg reflection from the helicoidal structure.

dependence and the addition of NLC is to tune the helix pitch (and thus theP BG spectral position) for any specific temperature range.

Consider a light wave propagating along the helix axis (z direction). In a locally uniaxial medium, the electric displacement $\vec{D}$ and the electric field $\vec{E}$ are related by

$$\vec{D} = \hat{\varepsilon}\,\vec{E} = \varepsilon_{\perp}\vec{E} + \Delta\varepsilon\,(\vec{n}\cdot\vec{E})\vec{n} \qquad (1.10)$$

where $\hat{\varepsilon}$ is the dielectric anisotropy tensor

$$\hat{\varepsilon} = \begin{pmatrix} \varepsilon_{\perp} & 0 & 0 \\ 0 & \varepsilon_{\perp} & 0 \\ 0 & 0 & \varepsilon_{\parallel} \end{pmatrix}. \qquad (1.11)$$

The two electric field components, E_x and E_y, in plane wave form, are given by

$$E_x = \mathrm{Re}\left[E_x(z)\, e^{-i\omega t}\right] \qquad (1.12)$$

$$E_y = \mathrm{Re}\left[E_y(z)\, e^{-i\omega t}\right] \qquad (1.13)$$

And they satisfy the Maxwell equation:

$$-\frac{d^2}{dz^2}\begin{pmatrix}E_x\\E_y\end{pmatrix} = \left(\frac{\omega}{c}\right)^2 \hat{\varepsilon}(z)\begin{pmatrix}E_x\\E_y\end{pmatrix}. \tag{1. 14}$$

Using $\hat{n} = (\cos\theta\,, \sin\theta, 0)$ and $\theta = q_0 Z$ in $\hat{\varepsilon}(z)$, we get

$$\hat{\varepsilon}(z) = \frac{\varepsilon_{\parallel}+\varepsilon_{\perp}}{2}\begin{pmatrix}1 & 0\\0 & 1\end{pmatrix} + \frac{\Delta\varepsilon}{2}\begin{pmatrix}\cos 2q_0 & \sin 2q_0 z\\ \sin 2q_0 z & -\cos 2q_0 z\end{pmatrix}. \tag{1. 15}$$

In terms of circular right (+) and left (-) polarized waves: $\hat{\varepsilon}_{\pm} = \frac{\hat{x}\pm i\hat{y}}{\sqrt{2}}$, Eq. 1.14 becomes

$$-\frac{d^2E^+}{dz^2} = k_0^2\,E^+ + k_1^2 \exp(2iq_0 z)\,E^- \tag{1. 16}$$

$$-\frac{d^2E^-}{dz^2} = k_0^2\,E^+ + k_1^2 \exp(-2iq_0 z)\,E^+ \tag{1. 17}$$

where $k_0^2 = (\omega/c)^2\langle\varepsilon\rangle$ and $k_1^2 = (\omega/c)^2\Delta\varepsilon$, and $\langle\varepsilon\rangle = \frac{\varepsilon_{\parallel}+\varepsilon_{\perp}}{2}$.

The solutions for E^+ and E^- are of the form of

$$E^+ = a\,exp(i(l+q_0)z) \tag{1. 18}$$

$$E^- = b\,exp(i(l-q_0)z). \tag{1. 19}$$

The substitution of Eq. 1.18 and Eq. 1.19 into Eq. 1.16 and Eq. 1.17 gives the following dispersion relationship between ω and l:

$$\left(-\left(\frac{\omega}{c}\right)^2\langle\varepsilon\rangle + l^2 + q_0^2\right)^2 - 4q_0^2 l^2 - \left(\frac{\omega}{c}\right)^4\Delta\varepsilon^2 = 0. \tag{1. 20}$$

For $cq_0/n_{\perp} < \omega < cq_0/n_{\perp}$, only one wave with circular polarization may propagate. [2] This is the Bragg reflection regime: the PBG position is in agreement with Bragg's law. The central wavelength of the BG (λ_0) corresponds to the following equation:

$$\boldsymbol{\lambda_0 = \bar{n} \cdot p}, \tag{1.21}$$

where $\bar{n} = (n_o + n_e)/2$ is the average refractive index of the CLC mixture and the p is the pitch of the helix. The BG short-wave (λ_1) and long-wave (λ_2) sides (Figure 1.14) correspond to

$$\boldsymbol{\lambda_1 = n_0 \cdot p},\ \boldsymbol{\lambda_2 = n_e \cdot p}, \tag{1.22}$$

where the n_0 and n_e are the ordinary and extraordinary refractive indexes of the CLC. Consequently, the PBG width $\Delta\lambda = \Delta n \times p$, where $\Delta n = n_e - n_0$ is the optical birefringence of the material. It is worth mentioning that in the equations above (and in most part of present work) a normal incidence of the incoming beam on the CLC layer (propagating parallel to helix axis) is considered. Otherwise, all the above equations should include $\cos\theta$ (as in Eq. (1.9)).

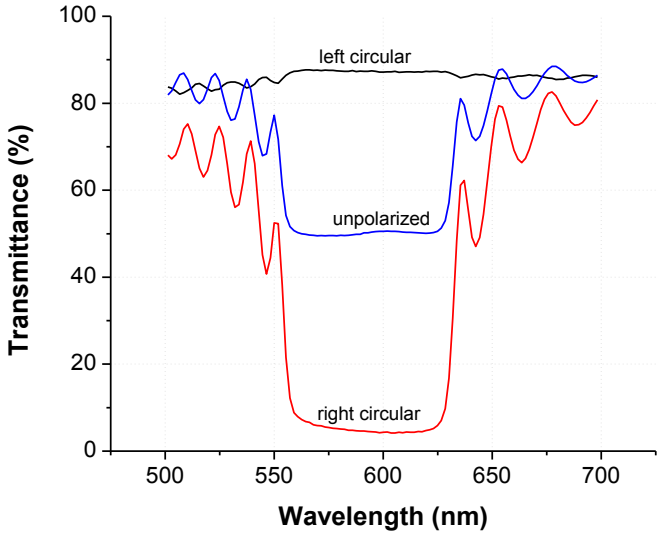

Figure 1.14: Transmittance spectra of the planar aligned CLC cell for un-polarized, resonant circularly polarized (right) and non – resonant (left) circularly polarized probe beams.

In spite the apparent good agreement with Bragg's law the law cannot accurately explain the effect of reflection from a CLC layer. The reason is the helicoidal structure of CLCs, which not considered within conventional Bragg theory. According to Bragg's theory, if the CLC possesses a sufficient number of layers then reflection from the PBG can theoretically reach 100%. The reflectance is independent polarization and thus, ordinary

Bragg mirrors exhibit selective reflection only with respect to the wavelength. Moreover, the reflected wavelength corresponds to the general Bragg condition:

$$m\lambda_0 = \frac{\bar{n}\times p}{\cos\theta}, \tag{1.23}$$

where $m = 1, 2 \ldots$. In the case of conventional Bragg mirrors, high order reflections ($\lambda = \frac{\lambda_0}{2}, \frac{\lambda_0}{3}, \ldots$) corresponding to $m = 2, 3 \ldots$, respectively, are always present, while only the first order ($m = 1$) reflection is present in the case of helicoidal Bragg mirrors. We can see that Eq. (1.21) is a special case of Eq. (1.23) ($m = 1$ and $\theta = 0$). That is the zero order diffraction of a normal incident probe beam. This is the case usually considered (generally and in this thesis as well). So, when speaking of a PBG mirror one usually refers to the first order reflection of a normal incident beam.

The reason for the above described differences can be found in the helicoidal nature of CLCs, the periodic structure of which is formed, not by abrupt change of the material (refractive index), but thanks to a gradual change of molecule orientation from one side of the cell to the other. All these properties can be explained in terms of scattering amplitude $\alpha = \boldsymbol{f} \cdot \varepsilon(\boldsymbol{q}) \cdot \boldsymbol{i}$, where $\boldsymbol{f}$ and $\boldsymbol{i}$ represent the polarizations of the reflected wave (of wave vector $\boldsymbol{k_1}$) and the incident wave (wave vector $\boldsymbol{k_0}$). $\mathbf{q} = \boldsymbol{k_0} - \boldsymbol{k_1}$ is the scattering wave vector, and the $\varepsilon(q)$ the Fourier transform of the dielectric tensor [5]. Using the dielectric tensor distribution for CLC one can achieve to the above mentioned differences, more specifically, the absence of higher order reflections in the case of normal incidence and their presence in the case of oblique incidence (See in Ref. [5]).

1.10 Optical Activity

It is well known [19] that the rotation of the plane of polarization of light in a material (optical activity) is the result of a difference in phase velocities of two orthogonal circular polarized waves. The two waves interact with CLCs in different ways: one of them strongly interacts with the CLC (diffraction) while the opposite one interacts slightly without sensing the periodic structure. In consequence, the two opposed circular polarized beams can have different phase velocities and rotate the polarization plane of linearly polarized

probe beam. The rotation (optical activity) is notably higher inside the PBG or at its wings. The optical rotatory power differs qualitatively from that of molecules, the former usually being much higher. For example, the optical activity of CLCs is usually on the order of 10^4 degrees/mm [50] whereas it is about 10 degree/mm, in conventional optically active materials such as a water-sugar solutions or a quartz crystals. So we will separate two cases of optical activity: the optical activity caused by interaction of light with the molecules of a material and the optical activity caused by interaction of light with the molecular structure of the material (the case of CLCs). There are several differences between those two optical activities.

In the case of "classic" optically active materials, such as sugar, only the polarization plane of the wave is rotated, whereas the polarization state can also be changed after passage through a CLC layer. This takes place for wavelengths inside the BG or near to its wings and the reason is the reflection of one of two circular polarizations. The ellipticity (ratio of short and long axes) of the transmitted beam polarization is given by following the equation if the incident beam has linear polarization

$$b = \frac{1-\sqrt{T^+}}{1+\sqrt{T^+}}, \tag{1.24}$$

where the T^+ is the transmittance of a resonantly polarized beam through the CLC layer in question and is given by [50]. One can easily notice that the ellipticty value b changes significantly inside the PBG where T^+differs from zero and depends upon the CLC layer thickness. For thick CLC layers one observes little optical activity inside the PBG as one of the circular polarized components is totally reflected ($T^+ = 0$) and the transmitted beam appears to have circular polarization. By saying thick CLC layer one usually refers to CLC layers possessing several complete helix pitches [50].

Other features that distinguish CLCs from conventional gyrotropic materials are that the optical activity of CLCs depends strongly upon wavelength, even far from the absorption band, and it changes the sign at different sides of the PBG [50]. By "gyrotropic" we mean a material that has chiral properties: either a medium with chiral molecular organization (such as CLC structures) or simply a medium with chiral molecules in the material (such as

the sugar solution in water). In other words, gyrotropic materials are the materials that exhibit optical activity of light. Gyrotropic materials usually exhibit different refractive indices (n+ and n-) for circular right and left polarizations of the incident light.

The last difference we would like to mention is that in contrast to conventional optically active materials, the rotation of the polarization axis (long axis of the ellipse) depends non-linearly upon the thickness of the CLC layer. The peculiarities of optical activity in CLCs, such as the influences of the thickness or the temperature of the CLC layer, are discussed in ref. [50]

1.11 Electric Field Induced Reorientation

As mentioned, the most reliable and reproducible way to control the alignment of LC molecules is by means of an electric field. This form of control is well investigated and has various technological and academic applications for both nematics and cholesterics [3]. Despite the fact that those two types of LC usually consist of similar molecules (remember that the CLC is obtained by adding a little amount of chiral molecules in NLC), their electro-optical properties are completely different. We have already discussed some optical and structural differences of those two types of LCs. Here we will discuss how the CLCs respond to an external electric field and we will make some parallel comparisons with NLCs.

Since LCs are dielectrically anisotropic materials, for a general direction of an electric field strength $\vec{E}$, the relation between the electric displacement $\vec{D}$ and the field strength $\vec{E}$ has the form:

$$\vec{D} = \varepsilon_{\perp}\vec{E} + (\varepsilon_{\parallel} - \varepsilon_{\perp})(\vec{n} \cdot \vec{E})\vec{n}. \quad (1.25)$$

In the second term, a molecular torque, $\vec{\Gamma}_e$, is associated with the electric field through:

$$\vec{\Gamma}_e = \vec{D} \times \vec{E} = \Delta\varepsilon(\vec{n} \cdot \vec{E})(\vec{n} \times \vec{E}) \quad (1.26)$$

The dielectric anisotropy, $\Delta\varepsilon = \varepsilon_{\parallel} - \varepsilon_{\perp}$, can be positive or negative, depending on the specific chemical structure of the constituent molecules. Depending on its sign, the molecular torque changes its direction forcing the molecules to reorient parallel or perpendicular to the external electric field. If each molecule caries a permanent dipole that

is parallel (or nearly parallel) to its long axis, the dipole can be oriented (by the field $\vec{E}$) along the nematic axis ($\varepsilon_{\parallel} > \varepsilon_{\perp}$, positive dielectric anisotropy). And if there is a permanent dipole, which is more or less perpendicular to the long axis ($\varepsilon_{\parallel} < \varepsilon_{\perp}$ negative dielectric anisotropy) [2], the situation is reversed; the dipole is oriented parallel to the external electric field and thus, the long axis of molecule is pointed perpendicular to the electric field (see Figure 1.15).

Once the dipole is induced (it is "oriented" parallel, or perpendicular to the long axis of molecule), the electric field will act on the molecule in a way similar to how it acts on a simple dipole (see Figure 1.15) in any medium (in our case the medium is an LC having viscosity, molecular interactions, etc.) Thus, we can control LC molecule orientation by the electric field.

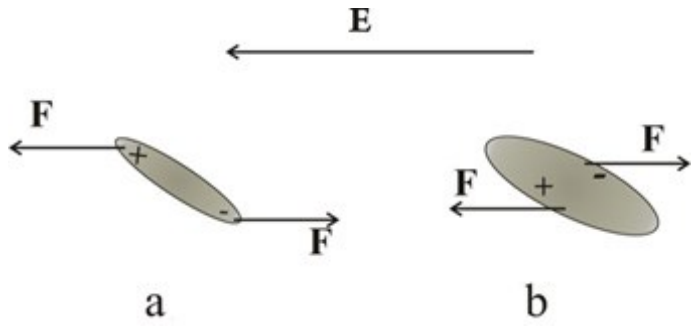

Figure 1.15: a) The dielectrically positive (having a positive dielectric anisotropy) LC molecule in an electric field. b) The dielectrically negative (having a positive dielectric anisotropy) LC molecule in an electric field.

We see from Eq. (1.25) that the higher is the dielectric anisotropy of the material, the higher would be the dipole momentum for a given electric field. Consequently, the higher is the dielectric anisotropy of the material the lower electric fields are required to control molecular orientations. The required voltages depend also upon the viscosity and the elastic constants of the material [2, 3].

So the required electric field strength to control the director is different from LC to LC. However, the characteristic fields for nematics are less than $\sim 1V/\mu m$ [2, 3]. Cholesterics require higher electric fields for reorientation. For example, for one of the CLCs we used (MDA 02-3211, from **Merck LC**) with $\varepsilon_{\parallel} = 26.1$ and $\varepsilon_{\perp} = 5.9$ ($\Delta\varepsilon = 20.2$), the electric field-induced reorientation in a 5μm thick planar cell only started at ~1.4V/μm and

complete reorientation (all the molecules are aligned parallel to the electric field) was obtained at $\sim 6.4V/\mu m$.

Given the fact that the applied electric field is usually perpendicular to the glass substrates of the LC cell, the above mentioned complete reorientation assumes a homeotropic alignment of molecules (Figure 1.15b). The voltage that is required for transition of a CLC cell from planar (helicoidal) state to homeotropic state is given by the following equation [3, 55]

$$V_{th} = d \times E_{th} = d \times \frac{\pi^2}{P_0}\sqrt{\frac{K_{22}}{\varepsilon_0 \Delta\varepsilon}}, \tag{1.27}$$

where the $E_{th}$is the threshold values of electric field, d is the cell gap, P_0 is the helical pitch in the absence of an electric field, K_{22} is the elastic constant responsible for twist deformation, ε_0 is the dielectric constant of vacuum and the $\Delta\varepsilon$ is the dielectric anisotropy of the CLC. This voltage will hereafter be referred as the helix unwinding voltage. If the applied electric field is less than the unwinding voltage but sufficient to start the reorientation, the CLC cell adopts a complex orientation which highly scatters light. The state is called "focal conic" state [18, 25]. A detailed investigation of transitions of a CLC cell between planar and homeotropic states will be presented in chapter 4.

If the LC in question has a negative dielectric anisotropy the external electric field does not reorient the molecules of a planar cell (both nematic and cholesteric) since the molecules are already aligned perpendicularly to the field. The response of negative (dielectric anisotropy) CLC to an external electric field is discussed in chapter 4 as well.

The situation is more complicated when we have a mixture of two LCs with opposite dielectric anisotropies. The electric field tends to orient a part of molecules parallel to the field and orient the other part perpendicularly. On the other hand, the molecules interact with each other and they tend to point their axes parallel to each other (collective behaviour). So, these two mechanisms compete, and it is interesting, from both scientific and technological points of view, to observe the tendencies. It is evident that the tendencies

will depend on the proportions of the molecular species, on the electric field frequencies, on the constants of elasticity, and so on.

Compared with NLCs, CLCs require higher voltages to reorient because in addition to all sorts of molecular interactions that NLCs possess, CLCs possess an additional free energy "forcing" the molecules to turn and form the helicoidal structure. To give an idea of the mentioned difference, NLC molecules usually start to reorient if the strength of applied electrical field is less than $0.1V/\mu m$. This is called the Fréedericksz transition threshold [56] and is given by the following equation:

$$V_{th} = \sqrt{\frac{K_{11}+(K_{33}-2K_{22})/4}{\varepsilon_0 \Delta\varepsilon}}, \tag{1.28}$$

where K_{11}, K_{22} and K_{33} are so called elastic constants of the LC in question and are associated with splay, twist and bend deformations of the LC director, respectively [2, 3].

1.12 Applications of Cholesteric Liquid Crystals

Thermometers: As demonstrated earlier, CLCs reflect a band of wavelength that depends upon the helix pitch. As the pitch itself depends on temperature, the reflected color is also dependent upon temperature. CLCs make it possible to accurately measure temperature just by looking at the color of the thermometer. By mixing different compounds, a device for practically any temperature range and of a big range of accuracy can be built [54, 57].

The "mood ring", a popular novelty a few years ago, took advantage of the unique color travel ability of the chiral NLC. More important and practical applications have been developed in such diverse areas as medicine and electronics. Special CLC films can be attached to human skin or to any surface to show a "map" of temperature. This is useful because often physical problems, such as tumors, have a different temperature than the surrounding tissue. Liquid crystal temperature sensors can also be used to find bad connections on a circuit board by detecting the characteristic higher temperature [58]. The above mentioned examples use the dependence of CLCs' pitch upon temperature. These thermometers are more useful and important for mapping temperature as they can be applied as a thin layer overthe entire surface in question. They are also "interesting" and

advantageous over other “mapping thermometers” such as the infrared thermometers, because they show the temperature map directly without any additional device and without conversion or treatment of any data. The human eye can directly observe the result.

Electro-optical elements: CLCs can be used for fabrication of different electro-optical elements such as wavelength tuneable mirrors or filters, tuneable circular polarizers, optical diodes, etc. Low threshold, mirrorless lasers can be built by the use of CLCs that have a planar defect where, as shown in [59], even sun light can be sufficient to achieve population inversion.

Bistable Reflective Cholesteric Liquid Crystal Displays: The inclusion of polymer networks in the cholesteric texture can provide important advantages to the helicoidal structure of cholesterics leading to unusual electro-optical properties.

When the pitch of the cholesteric material lies in the range of visible wavelengths, selective reflection from the *planar* cholesteric texture, in contrast to the partial or full transmission through the focal conic and homeotropic textures, provides opportunities for a variety of display applications. For example, in the planar state, a polymer stabilized cholesteric cell reflects incident light, and appears bright. In the focal-conic state [25], the incident light is transmitted through the cell and reveals the color of the coating on the rear of the window. Fortunately, both of these states are stable at E=0. This means that the textures are "locked in" and will remain intact until acted upon again (i.e. the device is bistable). Switching from planar to focal conic requires a low voltage pulse while the return from focal conic to planar requires a higher voltage pulse to drive the device into a homeotropic state which then relaxes through a transient planar texture to the final planar state [60].

Bistable reflective cholesteric cells are prepared in connection with the formation of networks in polymer stabilised cholesterics to have an appropriately short pitch. The combination is then photopolymerized in the initial planar state. The polymer network breaks up the planar texture into small domains, which are only slightly mis-oriented with respect to each other [61]. These polydomains respond more rapidly to a switching waveform than does a bulk material, an important factor for many display purposes. In addition, a good gray scale operation can be achieved through choice of polydomain size

distribution. Even more exciting is the fact that color displays are now possible through the use of either layered cholesteric cells, or the formation of CLC pixels. For the layered cholesterics, each layer is set to a different optical pitch to reflect different colors. The pixel cells work much like in other systems [6] by having each pixel contain one specific color and available to be turned on or off.

Among other advantages of devices employing bistable reflective cholesteric materials, is their relatively low power consumption due to the ability to hold pixels in either reflective or transmitting states at zero field. Another advantage is their use of reflected light which also decreases the power consumption (in comparison with the traditional LCDs which require backlighting and polarizers [6]). They also offer the possibilities of highly multiplexed passive displays and of the use of plastic substrates which have non-uniform birefringence but, in this case, do not change the transmission / reflection characteristics of the LC layer. The use of polymer network bonding to plastic substrates offers mechanical stability, as well. Finally, while video rates are not yet available, and reflective brightness still needs improvement, research in materials and in drive methods continues to show promising developments. In the meantime, some improvements in current technology should yield several possible applications including electronic books and newspapers, where fast responses are not needed.

Light Shutters: Polymer dispersed or polymer stabilized LC films are widely investigated. They have found applications in both nematics and cholesterics [10].

By lengthening the CLC pitch to the order of infra-red wavelengths, the bistable effect at zero applied electric field is avoided [62]. Instead, the choice of either planar or focal conic stable state is determined by initial conditions at the time of polymer network formation, as discussed below. The starting materials are the same as those used in the bistable reflecting cholesterics except for a reduction in concentration of the chiral agent to lengthen the cholesteric pitch. Depending on the LC texture in the stable state, shutters operating in reverse or in normal mode are possible to build [63].

1.13 Cell fabrication

There are two commonly used methods of cell assemblage. According to the situation (the phenomenon that is investigated) one or the other method is appropriate to use. If one needs to avoid the orientation of molecules caused by any flow during the fabrication process, the so - called "drop-fill" method is appropriate. Briefly, a droplet of LC is dropped on the "first" glass substrate and then the other substrate is put on it and the glasses are glued to each other. As a result, a thin layer of LC is obtained that is sandwiched between two glass substrates. Once again, what is important for the "drop-fill" method is that during the cell fabrication the LC does not flow in a certain direction which would give a preferred direction for molecules to point their long axis [11, 12].

If the initial orientation of LC molecules (due to flow) is not important, the other so-called "capillarity" method can be adopted. Usually, the "capillarity" method of cell preparation is used if strong boundary conditions are required to impose on the LC layer, because the LC molecules will anyway adopt the orientation given (forced) by the boundaries and they will "forget" the flow direction. The "capillarity" method can also be adopted if the cell is heated up to the isotropic phase after fabrication. Below, the "capillarity" method of cell fabrication is presented in detail as that is the principal way of cell assemblage used in the present thesis. In the following paragraphs we present the cell assembly process.

LC cell fabrication starts with the cleaning of the glass substrate. Cleaning consists of washing the glass substrates in an ultrasonic bath in three steps: in soap and water solution, in acetone and in isopropanol. Each step lasts 8-10 minutes. To finalize the cleaning process, the glasses are slowly moved up from the isopropanol (~ 1cm/min) and are let do dry in an oven at ~ 100℃ temperature for approximately 15 minutes. Note that in the case of electro-optical investigation, ITO (indium tin oxide) coated glasses are used, in order to be able to apply an electric field between the glasses (to the LC layer). The ITO layer thickness is usually of the order of 20 nm; it is transparent and conductive at the same time.

The next step is the coating of glass substrates with a surfactant layer to orient the LC molecules. As planar aligning agent, polyimide PI 150 solution (1 wt. %) in S21 (solvent) is used and 1 wt. % solution of PI 1211 in S26 is used as a homeotropic aligning agent.

Both the polyimides and the solvents are purchased from Nissan Chemicals. In order to obtain a uniform and thin layer of polyimide, a spin coater was used with the following rotation rates: 5 seconds at 500 rpm followed by 25 seconds at 3000 rpm. For the case of planar alignment, the PI 150 coated substrates are unidirectionally rubbed using a silk coat. The rubbing gives the LC molecules a preferred direction to point their long axes while staying parallel to substrates.

The following step is the attaching of two substrates. To do that, NOA 65 ultraviolet (UV) curable adhesive was used. Spherical glass spacers were dispersed in the adhesive in order to control the thickness of the space between glasses: that space is where the LC will be filled later. The diameter of glass spacers usually changes from ~1 μm to dozens or hundreds of micrometers. One can see the adhesive application form in Figure 1.16. The assembly procedure is schematically illustrated in the figure as well as in Figure 1.16. The UV curable adhesive is cured under UV light for approximately 10-15 minutes, after which the cell is ready to be filled with the LC. The LC is filled in the cell by two canals (Figure 1.16) using the capillarity effect and finally, when the cell is filled the canals are closed by the same adhesive (NOA 65) and the adhesive is cured for another 10-15 minutes. While curing, the LC is covered by aluminum foil in order to be sure that the UV exposure does not cause any degradation in LC layer [64, 65]. The cell is ready to be tested.

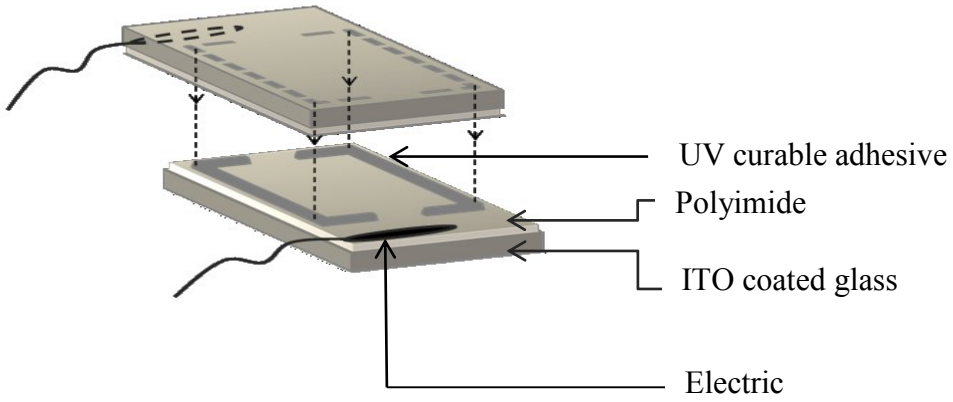

Figure 1.16: The schematic illustration of a standard liquid crystal cell

1.14 Problematics

As mentioned, LCs have found a wide range of applications thanks to their optical and electrical anisotropies. Among the conventional LC based devices the NLC based ones have the leading position. Almost all applications of NLCs use one principal electro-optical property of LCs and that is the tunable birefringence. Needless to say, that is already a huge advantage but such a material changes only the polarization of transmitted light. So usually, in display applications or in modulators, two polarizers are used to control the color or the intensity of transmitted light [6].

As previously mentioned, a CLC layer has the ability to reflect a certain range of wavelengths and/or a certain polarization (circular). This is an advantage over other LCs for two reasons. They can help us fabricate various optical elements such as circular polarizers or reflectors, narrow band filters or mirrors etc. Those elements can be tuned by electric or magnetic fields [3], by temperature [5] or by mechanical action such as pressure [66]. CLC films can also be used to control the flow of energy which can help to reduce energy consumption in buildings where people use electricity (or other sources) to heat in cold weather and to cool down in hot weather. Such films can be "inserted" into the windows to make the windows smart: let the energy (the sunlight) pass through and heat the room when it is cold and block the energy flow (reflect) into the room when it is hot.

Because of their helicoidal (more complex) structure, CLCs need more time to reorient their molecules. Especially, these times are long when processes are not forced, e.g., the relaxation after a forced reorientation, or structure changes caused by thermal or mechanical actions. So one of the challenges for CLCs to find wide application in technology, is the relatively long time of reorientation. The resolution of this problem can open many applications for CLCs.

The other factor making the CLCs interesting for investigation is the presence of similar structures in nature in the form of cuticles such as those of certain beetles (for example). There are many unanswered questions about insect cuticle optics. The questions raised are whether there is an evolutionary benefit for those organisms to form such a refined and complex structure. Is the benefit in the area of camouflage, sexual attraction, defence from

predators, thermoregulation, etc. There is much research on helicoidal structured cuticles in verity of scarab species but they are largely limited to structural (as opposed to optical) investigations, confirming only that the helicoidal-periodic structure is responsible for iridescence. There are only a few works [67] raising more fundamental questions.

1.15 Main Objectives

The boundary conditions applied on a CLC slab play an important role from both optical and orientational points of view. Usually ITO coated glass substrates are used to fabricate CLC cells which have relatively high refractive index; $\sim 1.8-2$ in the visible range of wavelengths, and ~ 2.5 in the near infrared NIR region (1321nm). For comparison, the average refractive index of E7 (a widely used NLC) is ~ 1.6 and ~ 1.58 in visible and NIR regions, respectively [68]. That mismatch of refractive indexes can cause multiple reflections inside the cell. In the case of CLCs, in addition to the Fresnel reflection [19] from boundaries, the Bragg reflection from inside the CLC layer is also present. Those two reflections different by their nature and their peculiarities are coupled together inside the CLC cell, creating a Fabry-Perot resonator filled with a CLC [69]. Those effects can significantly change the light propagation through a CLC cell. A part of the present thesis is dedicated to investigation of light propagation trough CLC cells with mismatch of optical boundary conditions. Cases of symmetric and asymmetric boundaries are considered. Particularly interesting is the asymmetric case, present in the nature: scarabs, for example, possess a cuticle which has the same helicoidal structure as the CLCs and that is surrounded by the body of the scarab from one side and by air from the other side. A question and a hypothesis about the role of this asymmetric Bragg reflector in the nature has been raised [70].

Mechanical boundary conditions (rubbing of substrates) can slightly influence over the structure of CLC. The effect discovered by Cano [25, 71], shows that the pitch of CLC helix adapts to strong boundary conditions and in consequence can be slightly different from its natural value defined by the helical twisting power (HTP) of the CLC. It can be used as a method to tune the pitch of CLC (hence the PBG position) by external fields. The possibilities and limits of electromechanical tuning of the PBG are investigated in chapter

5. This can be an alternative to thermal, purely electrical or magnetic field tunings of the PBG [5].

Finally, as CLCs tend to be used in CLC displays, the dynamics of transitions between different states is important to understand. This is a domain that is relatively "less" investigated, perhaps because of the fact that the transition (especially the restoration of helicoidal structure) times are long, sometimes they can last days. At present this is one of the key reasons why the CLCs are not used in dynamic displays; instead, they are used in static reflective displays [72]. So in order to widen the technological applications of CLCs, an understanding of transition dynamics and the process of helix formation is crucial. Only after that, can one try to interact with those processes and make them faster. One of the principal objectives of the present thesis is to investigate the dynamics of transitions between planar- helicoidal and homeotropic phases of CLCs.

Chapter 2
Light Propagation through a Chiral Medium with Symmetric Boundaries

As CLCs are almost always used in thin layers, they have boundaries that can sometimes play an important role in light propagation. Both optical and mechanical boundary conditions can be significant factors for optical and mechanical behaviour of a CLC layer. By optical behaviour, we mean effects appearing during the propagation of light through the layer. Those effects include the transmission, reflection, absorption and scattering. By mechanical behaviour, we mean variations of molecular texture of CLCs under different boundary conditions. Mechanical boundary conditions are usually given to a LC layer by treating glass substrates between which the LC layer is filled. In the present chapter and in the next chapter as well, we will discuss some particularities of light propagation through a CLC layer, concentrating our attention on the optical boundary conditions of the layer. Boundary conditions are always present regardless of the application (academic, scientific and in the Nature as well, [23, 24]). The reason why boundary conditions and their impact are not often considered is because their impact is usually small: but there are conditions that arise when the boundary conditions effectively change the optical properties of the system (CLC layer combined with the boundaries).

The present chapter is based on an article manuscript that discusses light propagation through a layer with symmetric optical boundaries. Here, by optical boundary conditions, we mean the optical properties of matter that surround the CLC layer. As mentioned above, LCs are almost always used in thin film form, where the film is sandwiched between two transparent substrates. The optical properties of the substrates should be viewed as optical boundary conditions. In this chapter we used identical glass substrates to provide symmetric optical boundary conditions on the CLC layer. The main influence of these boundaries on light propagation is due to the refractive index (mainly the difference between the CLC layer and the limiting substrate), and the fact that the CLC is an anisotropic and gyrotropic medium, while the glass substrates are isotropic.

Résumé de l'article inséré

Les propriétés de polarisation et spectrales d'une cavité de Fabry-Pérot au cristal liquide cholestérique

Nous présentons un élément à double-rétroaction optique basé sur une cavité de Fabry-Pérot remplie de cristal liquide cholestérique aligné planairement. La bande interdite du cristal liquide utilisé est dans la région du proche infrarouge. Les propriétés spectrales et de polarisation de cet élément sont caractérisées expérimentalement ainsi que par des simulations théoriques. Des résultats expérimentaux sont obtenus pour la dépendance de la transmission par rapport à l'orientation du plan de la polarisation linéaire et de l'état de polarisation du faisceau incident. La longueur d'onde du faisceau en question est hors de la bande interdite. Les résultats de la simulation théorique correspondante sont en accord avec les résultats expérimentaux.

Mol. Cryst. Liq. Cryst., Vol. 560: pp. 23–34, 2012

Polarization and Spectral Properties of a Cholesteric liquid Crystal Fabry-Perot Slab

Karen Allahverdyan[1, 2], Ashot Gevorgyan[2], Tigran Galstian[1] and Rafik Hakopyan[2]*

[1] Center for Optics, Photonics and Laser,

Department of Physics, Engineering Physics and Optics, Laval University,

Pav. d'Optique-Photonique, 2375 Rue de la Terrasse, Québec, G1V 0A6, Canada

[2] Department of Physics, Yerevan State University,1 Alex Manoogian, 0025 Yerevan,

Armenia

* author for communication, E-mail: galstian@phy.ulaval.ca; Phone: 1-418-6562025

Abstract

We report the creation of a double-feedback optical element based on a Fabry-Perot cavity filled with a planar aligned cholesteric liquid crystal mixture. The reflection band of the liquid crystal is in the near infra-red region. The polarization and spectral properties of this element are characterized experimentally and simulated theoretically. Preliminary experimental results are obtained for the transmission's dependence upon the orientation of the linear polarisation plane and the polarization state of the incident probe beam, with a wavelength out of resonance. The corresponding theoretical simulation results are in qualitative agreement with the experimental results.

KEYWORDS

Liquid crystals, cholesteric liquid crystals, dual frequency liquid crystal, distributed feedback, Fabry-Perot resonator, polarimetry, resonant reflection, electro-optic switch.

2.1 Introduction

Cholesteric liquid crystals (CLC) are fascinating examples of molecular self-organization into helicoidal (chiral) quasi-macroscopic structures generating wavelength and polarization selective reflection [5, 73, 74, 75]. They have generated important promise of applications in light reflectors and polarization-free modulators. Indeed, significant effort was devoted to manipulate their reflective properties, such as reflection strength, bandwidth, etc. (see, e.g., [53, 66, 76-83], and references therein).

The electrical modulation tool being very interesting (from practical point of view), we have focused our efforts on achieving a fast electrical modulation of the reflection of the CLC by destroying and then restoring its helix as quickly as possible [84]. To achieve that goal, we have used a mixture of a CLC and a dual frequency nematic liquid crystal (DF-NLC). The addition of the DF-NLC has shifted the resonant reflection band into near infra-red spectral band. The commercially purchased Indium Tin Oxide (ITO) layers being optimized only for the visible spectral band, the spectral analysis of the obtained cells has shown very strong Fabry-Perot oscillations overlapping with the resonant reflection band of the CLC. We have obtained thus a double-feedback system, the first one thanks to the classical Fabry-Perot effect and the second one due to the distributed feedback of the helicoidal structure of the CLC. The present work describes the preliminary results of the linear characterization of the obtained cells from spectral and polarization points of view.

2.2 Materials and Cells

The material compositions used as well as the cell fabrication are described in details in the Ref. [84] (see chapter 4 of this thesis). In short the material was obtained by mixing two materials: the CLC, called CB15, and the DF-NLC, called MLC 2048, (both purchased from Merck). The final compound (studied in the present work) contains 33 wt % of CB15 and 67 wt% of MLC 2048. The choice of those compounds was based on the desired dielectric parameters as well as the material availability. The MLC 2048 is a well-known material (see, e.g., [85]). To the best of our knowledge, the compound CB15 is less known

(see, e.g., [83, 86, 87]). Planar aligned cells of 5 µm thickness were fabricated by using two antiparallel rubbed Polyimide (PI-150, from Nissan) coated substrates.

2.3 Spectral Characterization

The transmittance spectra of the above mentioned cells were measured by using a spectrophotometer (model Varian Cary 500 scan). There was no polarizer or wave plate used in this measurement. The probe light was thus almost non polarized (except the residual anisotropic influence of optical elements placed on the path of the probe beam of the spectrophotometer). The obtained results show that the resonant reflection band of the CLC mixture is in the range from $1450\,nm$ to $1650\,nm$ (Figure 2.1). However, the transmittance spectra of cells show also strong Fabry-Perot type oscillations in the spectral neighbourhood of the resonant reflection band of the CLC mixture (Figure 2.1). The application of a strong electrical field (SIN shaped AC voltage of $50V\ RMS$, at $1\,kHz$) destroys the CLC helix and we observe only the Fabry-Perot oscillations (Figure 2.1). Those oscillations are spectrally shifted because of the change of the effective refractive index of the unwound (homeotropic) molecular orientation.

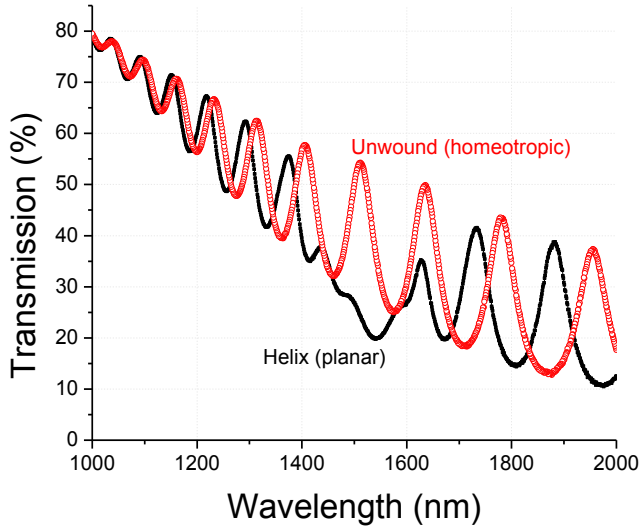

Figure 2.1: Transmittance spectrum of cholesteric liquid crystal cell (measured with non-polarized light, see text for details) with and without the unwinding electric field applied. Cell thickness is $5\,\mu m$, molecular orientation on the substrate surfaces is planar.

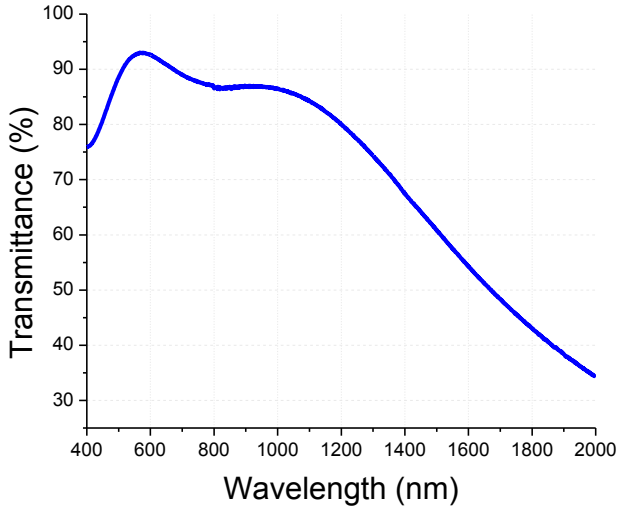

Figure 2.2: The transmittance spectrum of the ITO coated glass substrate, measured in air.

of the change of the effective refractive index of the unwound (homeotropic) molecular orientation.

The observed Fabry-Perot effect was the reason why the transmittance of the ITO coated glasses (used to build our cells) was characterized separately in the broad spectral range. The obtained results (see Figure 2.2) show that the light transmittance is significantly reduced in the near infra-red range of wavelengths. This is very likely because of both the ITO absorption as well as the index mismatch between various adjacent optical layers (We have measured the transmission and reflection coefficients (for $\lambda = 1481$ nm wavelength) of ITO coated glass we used. The following are the results: the reflectivity $R = 0.2$ and the transmittance $T = 0.61$. So, both are higher in the infrared region then in visible region. As we have already mentioned, the obtained cell is thus a rather complex element since it is characterized by two feedback mechanisms. The optical properties in such structure may be very complex, particularly the dependence of its transmittance upon wavelength and polarization. This is because both phenomena are wavelength dependent. In addition, the Fabry-Perot effect may be considered as polarization independent (for normal incidence and for a non gyrotropic material inside); in contrast, the CLC has strongly polarization dependent (gyrotropic) properties.

We proceeded to the experimental characterization of this structure and performed preliminary theoretical modeling of the cell. This modeling reproduces qualitatively the observed transmission of our structure in unpolarized white light (Figure 2.3). The corresponding details of the theoretical analysis will be presented later. For the moment, the values of parameters used for this modeling, are as follows: ordinary refractive index $n_o = 1.5$, extraordinary refractive index $n_e = 1.7$, helix pitch $p = 0.96\,\mu m$ (the distance in which the LC molecules to realise an entire rotation of 360^o) and the number of entire helixes $t = 6$. Since the Fabry – Perot effect is significant in this specific case, it is important to choose correct parameters conditioning all reflections (e.g., the effective refractive indexes n and the effective thicknesses d). Based on the observed transmittance spectrum of the ITO coated glass (Figure 2.2), where the curve is nearly linear in the range from 1000 nm to 2000 nm, we supposed that the effective refractive index n is also changing linearly. By varying these two parameters (n and d) we have chosen those which fit better with our experimental curve (Figure 2.3): $n = 1.4 + 2(\lambda - 1)/\lambda$, $d = 1\,\mu m$. We have obtained a rather qualitative agreement and we have used the above mentioned parameters in our further theoretical simulations.

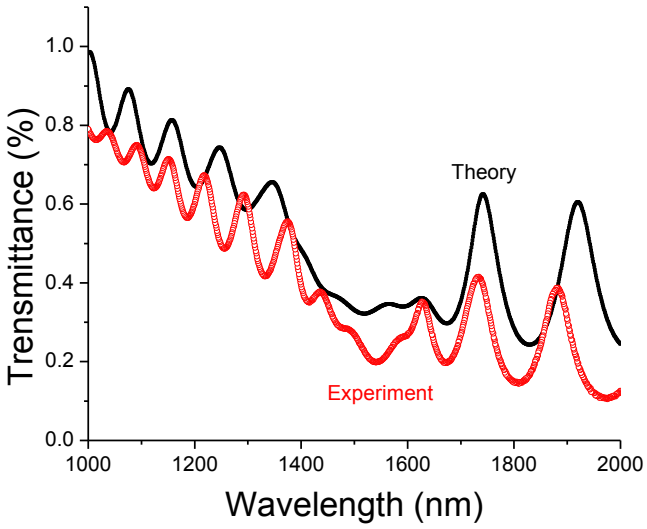

Figure 2.3: The CLC cell transmittance spectrum (theory and experiment) for unpolarized broadband (white light) probe beam.

2.4 Experimental Set-Up

The polarization dependence of the transmittance of our structure was studied in two different set-ups. First, we built a simple set-up (Figure 2.4) to study the transmittance dependence of the linearly polarized narrow band light upon the orientation of its polarization plane with respect to the input orientation of the CLC director (average orientation of long molecular axes, [5]), defined by the rubbing direction of the polyimide layers.

In this experiment, a HP 8155A laser diode source, operating between $1300\,nm$ and $1321\,nm$, was used. The source was coupled to a single mode SMF28 fiber. This wavelength is not exactly inside the resonant reflection band, but is near its short wavelength wing. The fiber output beam was collimated with a lens (Figure 2.4), passed through Polarizer 1, then through a planar aligned nematic liquid crystal (NLC) cell, which was used as an electrically variable retardation plate. In this case, the NLC cell rubbing direction was oriented to 45^o with respect to the first polarizer transmission axis. Thus, for an appropriate applied voltage U the NLC cell optical path difference (defined by the effective birefringence and the thickness of the cell) corresponds to a quarter wave plate. In this way one can convert the probe light into circular polarization. Keeping the voltage fixed during the experiment, Polarizer 2 was gradually rotated, thus changing the incident light polarization plane, while keeping its power constant. The power transmitted through the CLC cell was measured by photodetector PD.

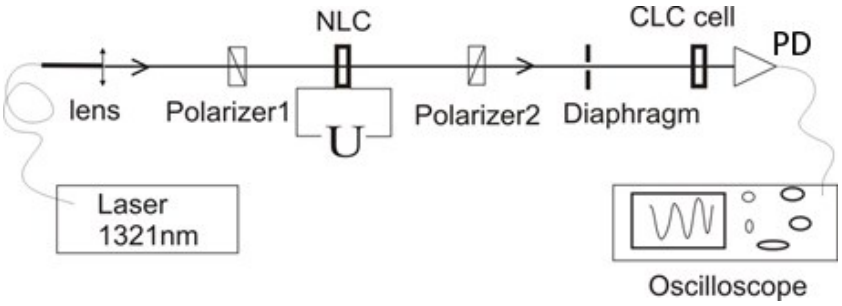

Figure 2.4: Schematic representation of the experimental setup for the study of a dependence of the cholesteric liquid crystal cell transmittance upon the plane polarized probe light electric field orientation with respect to the director orientation on the substrates.

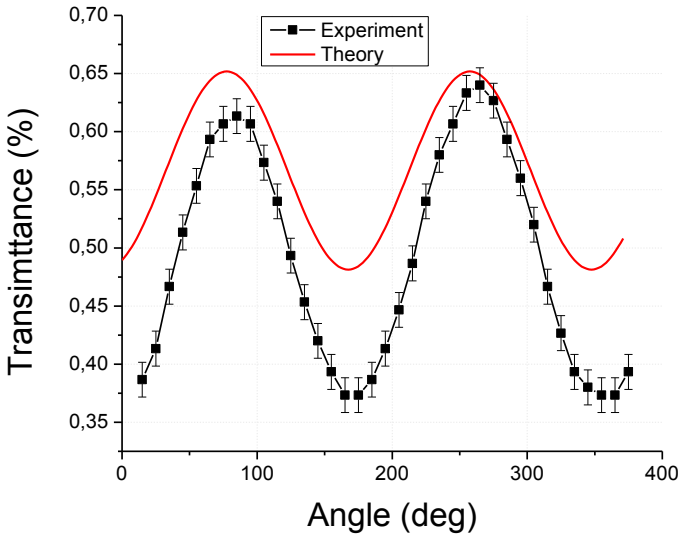

Figure 2.5: The CLC cell transmittance dependence upon the angle between the linearly polarized light polarization direction and the substrate rubbing direction (defining the director orientation on the surfaces).

2.5 Experimental and Simulation Results

Figure 2.5 shows the transmittance dependence upon the angle between the probe light polarization plane and the rubbing direction of the cell (theory end experiment). We see, in Figure 2.5, that the variation in transmittance with respect to the incident light polarization plane is periodic with a period of 180^o. This is to be expected since the incident beam polarization stays the same if Polarizer 2 is turned through 180^o. One sees also, that the transmittance is minimal for the 0^o angle, which corresponds to the incident beam of extraordinary type (polarized in the same plane as the rubbing direction defining the input orientation of the CLC director). In contrast, the transmittance is maximum for the input probe light of ordinary polarization (polarized perpendicular to the rubbing direction).

The transmittance dependence of the cell was also measured versus the polarization state of the incident beam. Namely, here we changed not only the angle of the polarisation plane of the probe light, but also its ellipticity (from circular left - elliptical - linear - elliptical - circular right, etc.). The previous experimental set-up was slightly changed to perform this experiment (Figure 2.6).We have added a glass beam splitter, a second Polarizer 2 and a second photodetector (PD2), to monitor, in real time, the incident light polarisation state.

Polariser 2 was always crossed with the Polarizer 1 and the NLC cell director was oriented at 45^o with respect to the first polarizer transmission axis (the transmission axis of Polarizer 1 was set vertical). The PD2 detected a "reference" signal having a minimum value that corresponds to linearly polarized probe light (incident on the CLC cell) oriented in the vertical plane. The maximum signal corresponds to linearly polarized light oriented in the horizontal plane (Figure 2.7). The CLC cell rubbing direction was set horizontal.

During the experiment we gradually increased the voltage U (applied to the NLC cell. This changed the NLC cell effective birefringence, and thus the probe light polarization state was gradually changed at the input of the CLC cell. We registered the dependence of the light power transmitted through the CLC cell upon the applied voltage.

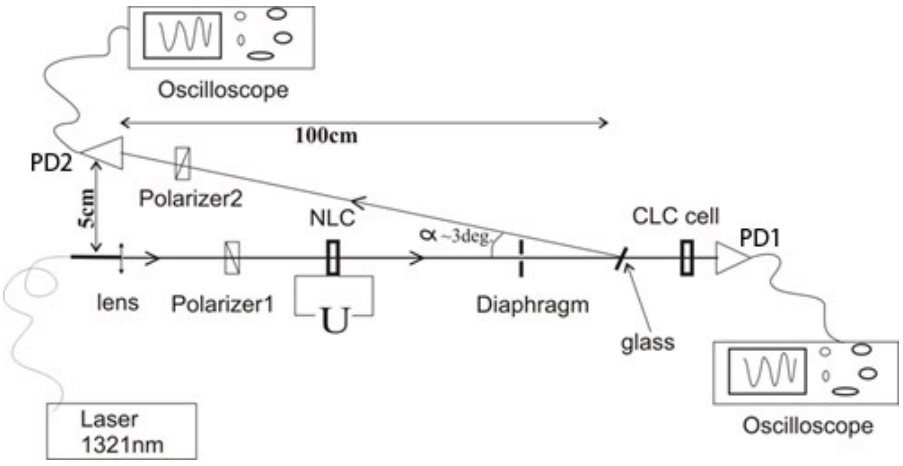

Figure 2.6: Schematic representation of the experimental setup to study of the cell transmittance dependence upon the probe light polarization state.

During these changes, the signal, detected by PD2 was also monitored to follow the dynamic change of the polarization state of the probe beam. This signal was used as reference (Figure 2.7).

The results obtained are shown in the Figure 2.7. As one can see, there are multiple cycles of changes in the polarization state of the probe beam with changes in the applied voltage (below $7.5\,V$). The transmittance shows oscillations correlated with the cycles. There is almost a 50% variation in the probe beam transmittance depending on the orientation of the plane of the input polarization. There is also a noticeable shift between the two oscillations (signal and reference).

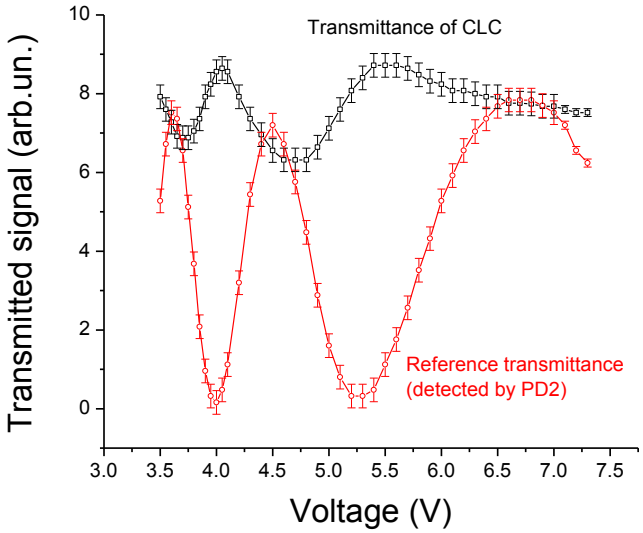

Figure 2.7: Voltage dependence of the CLC cell transmittance. The "reference transmittance" curve allows the monitoring of the corresponding polarization state of the probe beam. The minima and maxima of this curve correspond to the linearly polarized probe beam with its polarization plane being, respectively, perpendicular or parallel, to the cellrubbing direction (see the text for details). The first polarizer is aligned at 90º.

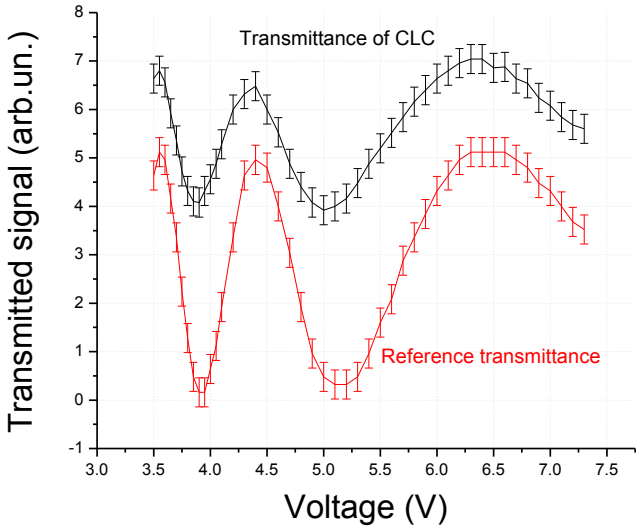

Figure 2.8: CLC cell transmittance dependence upon the voltage, applied on the variable retardation NLC cell (see the text for more details). The first polarizer is aligned at 30º.

Some additional experiments were also performed. We first turned the Polarizer 1, the NLC cell rubbing direction and Polarizer 2 by 60^o (Figure 2.8) and then by another 30^o (Figure

2.9), and repeated the above mentioned measurements. As we can see in Figure 2.8 and Figure 2.9, the transmittance changes significantly, depending on the incident azimuthal angle. Saying azimuthal angle we mean the angle between the probe beam (linear) polarization plane and the input orientation of the CLC director. The transmitted (through the CLC cell) power maximum and minimum conditions are changed, and also the amplitude of the transmitted light oscillation is changed significantly. Let us remind ourselves that, in Figure 2.8, the minimum of the reference curve corresponds to the linearly polarized probe light with an azimuthal angle of 30^o (with respect to the input orientation of the director), whereas in Figure 2.9 it corresponds to the azimuthal angle of 0^o (with respect to the input orientation of the director).

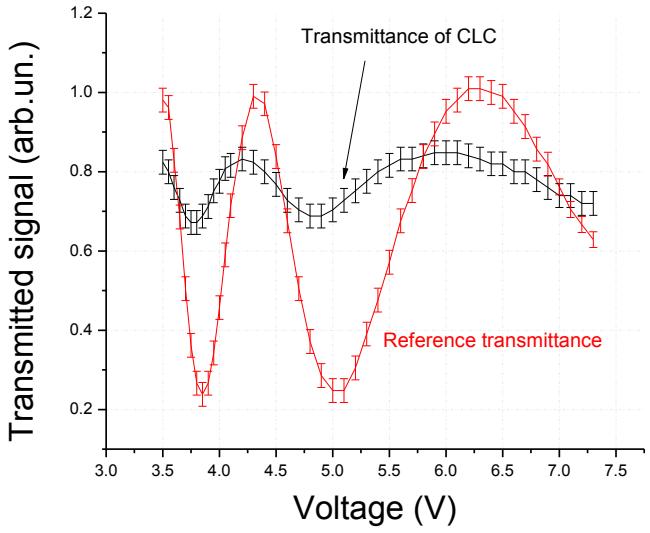

Figure 2.9: CLC cell transmittance dependence upon the voltage, applied on the variable retardation NLC cell. The "reference transmittance" curve allows the monitoring of the corresponding polarization state of the probe beam. The minima and maxima of this curve correspond to the linearly polarized probe beam with its polarization plane being, respectively parallel and perpendicular to, the cell rubbing direction (see the text for details). The first polarizer is aligned at 0º.

2.6 Theoretical Method of Analysis

The corresponding theoretical simulations have been done to reproduce the experimentally observed dependences of the probe light transmittance upon its state of polarization. The problem was solved by the Ambartsumian layer addition modified method [88, 89] adjusted

to the solution of such problems. Namely, let us represent the solution of the boundary problem of light transmission through the multi-layer system in the following form:

$$\vec{E}_r = \hat{R}\vec{E}_i\,, \quad \vec{E}_t = \hat{T}\vec{E}_i \tag{2. 1}$$

where the indices i, r and t denote the incident, reflected and transmitted wave fields, $\hat{R}$ and $\hat{T}$ are the reflection and transmission matrices, and $E^{p}_{i,r,t}$ and $E^{s}_{i,r,t}$ are corresponding amplitudes of the incident, reflected and transmitted waves:

$$\vec{E}_{i,r,t} = E^{\,p}_{i,r,t}\hat{n}_p + E^{\,s}_{i,r,t}\hat{n}_s = \begin{bmatrix} E^{\,p}_{i,r,t} \\ E^{\,s}_{i,r,t} \end{bmatrix},$$

where $\hat{n}_p$ and $\hat{n}_s$ are the unit vectors of orthogonal linear polarizations.

According to the Ambartsumian method, if there is a system consisting of two adjacent (from left to right) layers, A and B, then the reflection transmission matrices of the system, $A + B$, viz. $\hat{R}_{A+B}$ and $\hat{T}_{A+B}$, are determined in terms of similar matrices of its component layers by the matrix equations:

$$\begin{aligned} \hat{R}_{A+B} &= \hat{R}_A + \tilde{T}_A\hat{R}_B\left[\hat{I} - \tilde{R}_A\hat{R}_B\right]^{-1}\hat{T}_A, \\ \hat{T}_{A+B} &= \hat{T}_B\left[\hat{I} - \tilde{R}_A\hat{R}_B\right]^{-1}\hat{T}_A, \end{aligned} \tag{2. 2}$$

where the tilde denotes the corresponding reflection and transmission matrices for the reverse direction of light propagation, and $\hat{I}$ is the unit matrix. The exact reflection and transmission matrices for a finite CLC layer (at normal incidence) and an isotropic layer are well known [90, 91]. First, we attach the CLC layer to the isotropic layer (1) from the left side, using the matrix Eqs (2.2). In the second stage, we attach the isotropic layer (2) with the obtained CLC layer - isotropic layer (2) system. The ellipticity e and the azimuth ψ of the transmitted light are expressed as a function of $\chi = E^s_t/E^p_t$ through the following formulae:

$$\psi = \frac{1}{2}\tan^{-1}\frac{2Re(\chi)}{1-|\chi^2|}\,, \quad e = \tan\left(\frac{1}{2}\sin^{-1}\frac{2Im(\chi)}{1+|\chi^2|}\right). \tag{2. 3}$$

We have already mentioned the parameter values used for the theoretical fitting. Four different azimuthal angles of the incident light polarization are shown in Figure 2.10. We can see that all four curves are different, and that they coincide only when the ellipticity is equal to -1 or 1, i.e., when the probe polarization is circular.

Another interesting point is the transmittance dependence upon the ellipticity of the input probe polarization. None of the four curves is constant. Finally, transmittance modulations are different for different azimuthal angles and the maximum or/and minimum transmittance values are not obtained for the same ellipticity values. They also depend upon the azimuthal angle.

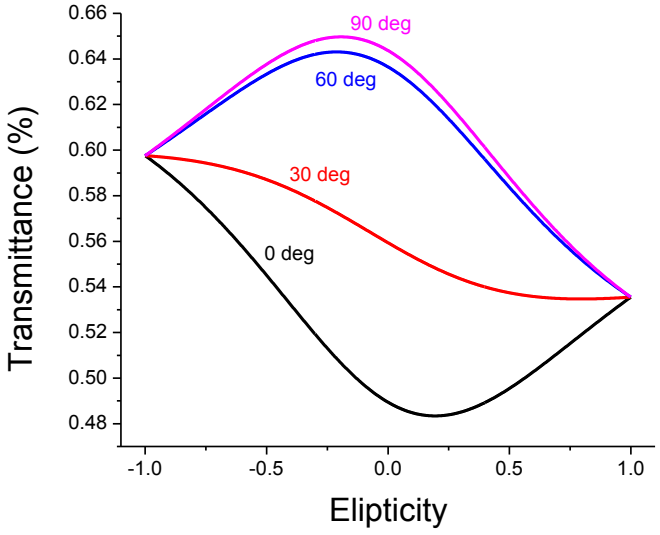

Figure 2.10: Theoretical simulation results for dependence of transmittance on the probe light polarization elipticity for four different fixed ellipse axes (The angles between the axis of the polarization ellipse and the rubbing direction are shown on each curve).

Figure 2.11 presents (plotted in 3D and 2D) the result of simulations of the dependence of the reflection spectra upon the refractive indexes of the cell substrates. It shows that the form of the spectra depends strongly upon the CLC cell substrate refractive index; thus the spectrum is "typical" (without Fabry-Perot oscillations, as we usually see in the literature) for refractive indexes near the refractive indexes of the CLC ($\sim 1 < n < \sim 2$). The Fabry-Perot effect appears for higher refractive index differences. This oscillation amplitude increases with increasing substrate refractive index.

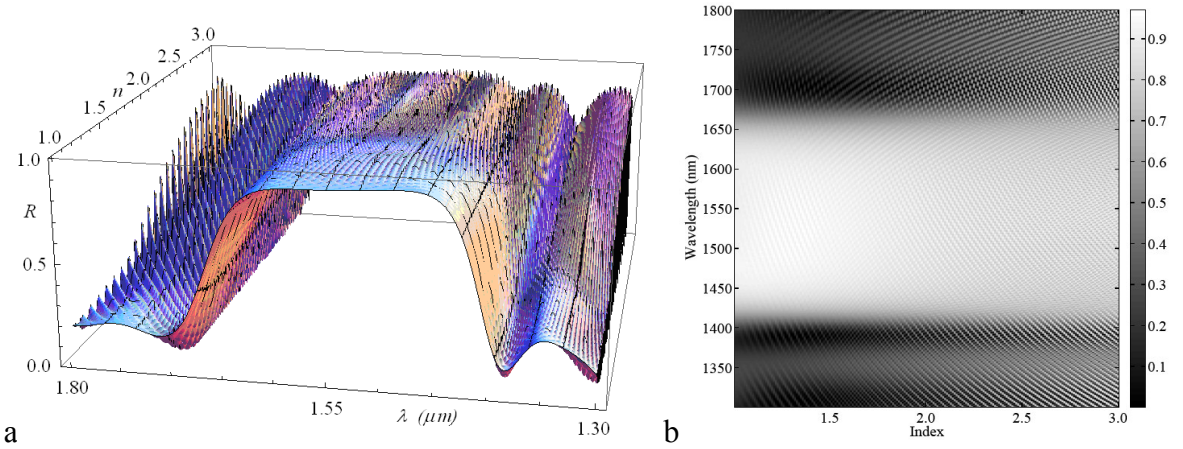

Figure 2.11: Simulation results for the dependence of the CLC cell reflection coefficient on the probe wavelength and upon the substrate refractive indexes for non-polarized probe light.

2.7 Summary and Conclusions

The experimental results confirm the complexity of polarization and spectral dependences of the double-feedback system composed of a Fabry-Perot cavity filled with planar oriented CLC. The corresponding simulations are in qualitative agreement with the experimental results. In fact, a closer look at the simulation results shows that, in some cases, there is quantitative agreement. This is evident, for example, in the case of the transmittance dependence upon the incidence azimuthal angle of the plane of the polarization of the probe beam (Figure 2.7 vs Figure 2.10). Here, both simulation and experiment show a ratio of 1.3 for the transmittance of the plane polarized probe beam with its polarization aligned in vertical and horizontal directions. However, the same comparison for the two opposed circularly polarized probe beams gives the experimental ratio of 1.3 (see Figure 2.7and Figure 2.8) against the theoretical ratio of 1.13 (which is closer to the experimental value of 1.15 obtained in the Figure 2.9).

The qualitative picture of spectral dependences is well represented by simulations. For example, the overlap of the Fabry-Perot effect with the resonant reflection of the CLC (Figure 2.3) and the gradual appearance of the Fabry-Perot effect when introducing an index mismatch at substrates of the CLC cell (Figure 2.11). However, the overall

agreement between experimental and theoretical results is should be viewed as qualitative and preliminary.

We have fabricated and characterized CLC cells exhibiting a double feedback phenomenon generated by the Fabry-Perot effect and the helicoidal structure of the CLC. We believe that this is a very interesting element and eventually it could be useful for various photonic applications (ie, fast switching). A preliminary study (experimental and theoretical) was conducted, which provided a qualitative agreement. Further study is required to better understand the key factors influencing the polarization and spectral properties of obtained elements.

Acknowledgment

We would like to thank Professor Beliakov (from Landau Institute for Theoretical Physics, Russia) for discussions. We also thank the financial support of Canadian Institute for Photonic Innovations (CIPI), Fonds Québécois de la Recherche sur la Nature et les Technologies (FQRNT) and Natural Sciences and Engineering Research Council of Canada (NSERC).

Chapter 3
Light Propagation through a Chiral Medium with Asymmetric Boundaries

We saw in chapter 2, that the optical boundaries can effectively change light propagation through a CLC layer. The transmittance spectrum changes significantly when we change the effective refractive index of the confining substrates (Figure 2.11). In Nature and in technological applications, such boundaries are not always symmetric. Different species of scarab beetle, for example, possess helicoidal textured cuticles (just as the CLC) surrounded by air on one side and by the scarab body on the other (Figure 3.1) [70]. The optical response of the cuticle is similar to that of a CLC layer: it reflects circularly polarized light with the same rotation direction as its helicoidal structure.

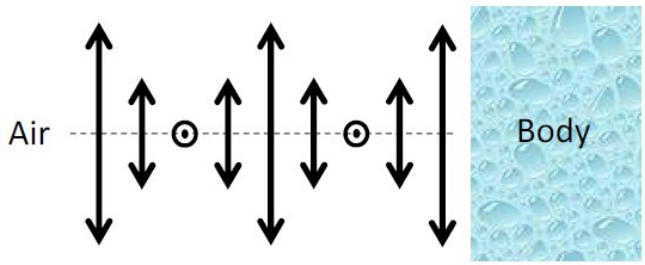

Figure 3.1: (After Ref. [70]) Schematic presentation of the helicoidal layer (only one period of molecular rotation is shown) and its asymmetric boundary conditions for the case of scarab beetle cuticle.

Hence those structures very often appear in Nature surrounded by different media (on different sides). It is interesting and important from a biological point of view to understand how the cuticle interacts with light. Particularly, it is important to know whether the asymmetric boundaries can be useful for those organisms or they are just consequences of nutrition without any advantage, as many believe [23, 67]. Among the scarabs, there are species exhibiting an exciting structure of cuticle: an anisotropic uniaxial layer between two helicoidal layers (such as the CLC). The anisotropic layer behaves as a half-wave retarding plate for wavelengths that resonantly reflect from the helicoidal chitin layer of the cuticle

[24]. This periodic patterning suggests a potential evolutionary advantage that might be lined to a structured colour response. Structured colour might offer camouflage, advantages in mating, thermoregulation [92, 93], and so on.

The subject of the present chapter is the breaking of light propagation reciprocity. This has been a topic of intense research for a few decades (see e.g. [94, 95] and the references therein) because it promises important applications ranging from experimental research in classical and quantum optics to the high-rate telecommunications and data interconnects.

The present chapter is based on a manuscript of a published article which investigates the optical characteristics of a helicoidal structure (mainly CLC) that has asymmetric optical boundaries. Particularly, the presence of non-reciprocal transmission is considered and confirmed both experimentally and theoretically.

Résumé de l'article inséré

Observation de d'effet de non réciprocité optique dans une simple couche de matière chirale linéaire et transparente avec des limites asymétriques

Nous présentons une observation de l'effet de non-réciprocité optique dans une matière qui ressemble beaucoup aux structures naturelles comme la carapace des insectes: une couche simple de la matière transparente linéaire dans son état fondamental. Comme la matière est dans son état fondamental, il n'y a pas la nécessité de champs externes pour obtenir la non-réciprocité de transmission de la lumière. L'effet est confirmé d'être défini par deux facteurs principaux: la chiralité de la matière et les conditions asymétrique aux surfaces limites. Nos analyses qualitatives et quantitatives préliminaires sont en accord avec les résultats expérimentaux.

Pis'ma v ZhETF, vol. 96, iss. 11, pp. 778-782

Observation of optical non reciprocity in a single layer of transparent linear chiral media with asymmetric boundaries

K. R. Allahverdyan[1], A. H. Gevorgyan[2], R. R. Hakopyan[2], T.V Galstian[1]*

[1]Center for Optics, Photonics and Laser, Department of Physics, Engineering Physics and Optics, Laval University,
Pav. d'Optique-Photonique, 2375 Rue de la Terrasse, Québec, Canada G1V 0A6

[2] Department of Physics, Yerevan State University, 1 Alex Manoogian, 0025 Yerevan, Armenia

* Corresponding author: galstian@phy.ulaval.ca

Submitted 26 september 2012

Abstract

We report the observation of optical non reciprocity in a material system that is very close to natural structures, such as insect skin: a single layer of linear transparent material in its ground state. The process is shown to be defined by two key parameters: the chirality of the material and its asymmetric boundary conditions. Our qualitative and preliminary quantitative analyses are in very good agreement with experimental results.

Main Text

Electromagnetic non-reciprocity has attracted significant attention both for fundamental (time reversal breakdown) and practical (unidirectional propagation) reasons. Apart from the traditional magnetic field excitation cases, very specific physical conditions must be satisfied by material systems to exhibit such behaviour (see Ref. [46, 96] and references therein). Thus, in one family of material systems, the use of external fields or optical nonlinearities is required [96, 97]. Multiple cells of gyroscopic media, such as cholesteric liquid crystals (CLC), containing defect layers [89] or combined with nematic liquid crystals (NLC), have been used in another family of material systems where the use of an external electric field allowed also their dynamic tuning [98]. Finally, lossy planar (two dimensional) CLC structures were also proven to exhibit optical non reciprocity [5].

In all above mentioned cases, the non-reciprocity is created artificially. We think that particularly interesting are the cases of using chiral materials, such as CLCs, which are frequently found in the nature. In fact, it is well known that a free-standing CLC layer does not change its handedness when observed from two opposed directions and its optical properties are reciprocal. This is the reason why additional "intervention" is required [5], [89], [98]. However, in the present work, we report the observation of optical non-reciprocity in a single layer of transparent (non-lossy) linear CLC without using additional layers or excitation fields. This material system thus represents a situation that may be readily found in many natural systems (see later). As it will be seen later, the transmission non-reciprocity here is "naturally" generated because of the asymmetric boundaries of the CLC.

Typical liquid crystal (LC) cells have symmetric geometry along the light propagation direction. Those cells are traditionally composed of two glass substrates (coated from one side by optically transparent conductive indium tin oxide (ITO) layers) that are sandwiching a thin layer of LC, with ITOs facing each other [3, 6, 99]. Usually, very thin (on the order of 50 nm) and unidirectionally rubbed polyimide (PI) layers are also added on the top of each ITO to align the LC [7]. However, some recent applications of LCs have generated the need for asymmetric cells, where the LC layer is still confined between two

PI coated substrates, but only one of them bears an ITO coating [83], providing thus optically asymmetric boundary conditions for the LC (see the top center inset of the Figure 3.2).

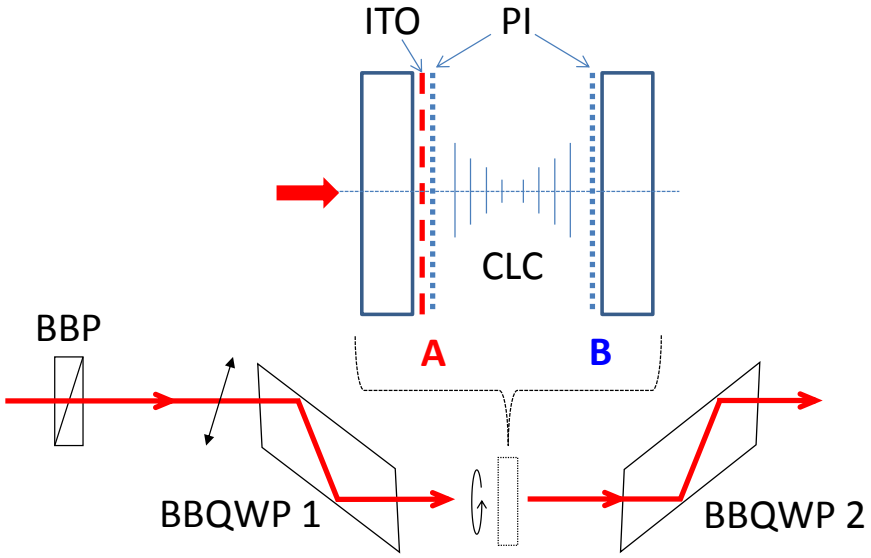

Figure 3.2: The schematic geometry (bottom) of the experimental scheme used for the study of light transmission through a layer (*top*) of CLC with optically asymmetric boundary conditions. *Top*: ITO – indium tin oxide, PI- polyimide layer, CLC – cholesteric liquid crystal. A and B are light incidence directions for two sequential experiments. *Bottom*: BBP – broad band polarizer, BB QWP1&2 – broad band quarter wave plates.

We used a cell of a planar aligned (on both substrates) CLC that was composed of 33 wt % of CB15 and 67 wt % of MLC 2048 (Merck). The original goal (not detailed here) of using this mixture was to create a fast switchable helical structure with a spectrally selective reflection band ("bandgap") in the 1350 nm – 1600 nm region. The first component (CB15) is a right handed CLC that provides an optical bandgap in the green spectral region (~520 nm – 560 nm) at room temperature. The average refractive index of CB15 was measured as n_{av}=1.567 ± 0.002 [85]. Its dielectric anisotropy is negative (tested from 100 Hz up to few 100 kHz). The second component (MLC2048) is a "dual frequency" NLC [90]. Its dielectric anisotropy is positive for "low" frequencies (~1 kHz) and is negative for "high" frequencies (~50 kHz, at room temperature).

We used two different glass substrates to build the sandwich-like cell containing the above mentioned mixture. The first one was made from a standard microscope glass of 1 mm of thickness, while the second one was ITO coated glass of 0.7 mm thickness (purchased from TFD). Cells were fabricated by spacing those two substrates at $8\ \mu m \pm 0.8\ \mu m$ distance by using spherical glass spacers (from Thermo Scientific) dispersed in the peripheral glue walls and by using the standard method of capillary injection of the CLC mixture.

We knew [6] that the above mentioned material mixture is simultaneously sensitive to the polarization state (or angular momentum) of light as well as to its wavelength (or linear momentum). We thus started our investigations by polarization dependent transmittance measurements by using Varian (Cary 500 scan) spectrophotometer. In order to obtain various polarization states (e.g., circularly polarized) of the broadband probe beam, we have built a simple setup inside the spectrometer (bottom of Figure 3.2). We used a broad band polarizer (BBP) that changed the original unpolarized beam into linear polarized one and a Fresnel rhomb, as broadband quarter wave plate (BBQWP1), which generated the circularly polarized probe beam. The polarizer axis direction was tilted at 45° relative to the horizontal direction and, when needed, we could turn it by 90° to change the circularity handedness (left - right) of the probe beam (after the BBQWP1). A second Fresnel rhomb (BBQWP2) transformed the probe polarization back to linear and also brought its propagation axis into the original direction. The CLC cell (with parallel but dissimilar interfaces, see the top inset of Figure 3.2) was placed between two BBQWPs, in the area where the probe beam was circularly polarized.

The experimental procedure was the following: we placed the sample of CLC between two BBQWPs and we measured the transmittance spectrum. Then we turned the sample by 180° (with respect to the vertical axis) and we measured the spectrum again (for the opposed direction of propagation of light through the cell). We repeated this procedure many times for various polarization states of the probe beam and for each position of the cell (the cells were also removed and placed back again multiple times to evaluate the contributions of various measurement errors).

The resulting transmittance spectra of our cells clearly show non-reciprocal behavior. Indeed, as one can see, from the Figure 3.3a, the transmittance of the cell in the spectral bandgap area is noticeably higher for the case when the left circularly polarized light (non-resonant with the CLC) is incident from side B (see the top inset of Figure 3.2). In fact, this non-reciprocity was observed for all key states of incident beam polarization (including for linear parallel and linear perpendicular to rubbing direction, both circularities, etc.) but the corresponding results will be detailed in a subsequent article (for the sake of the shortness of this communication).

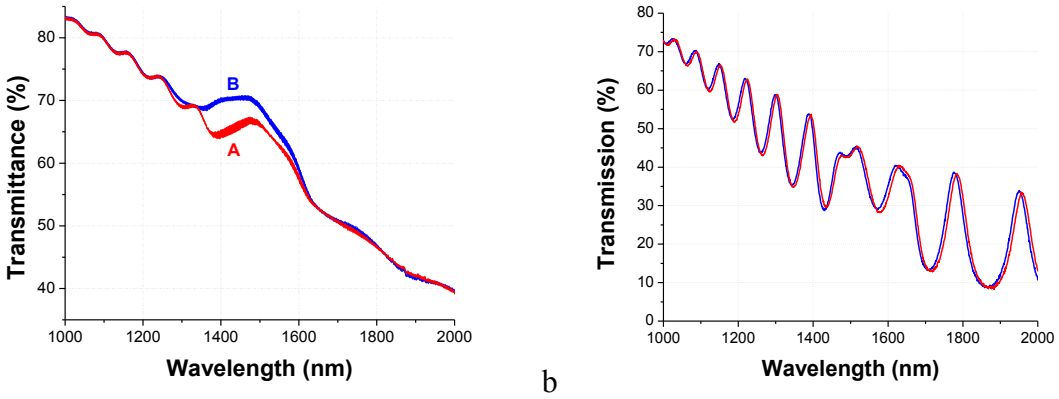

a b

Figure 3.3: Non resonant circularly polarized light transmittance spectra (through the planar CLC cell) detected for two opposite directions of light propagation through the cell that was built with (a) asymmetric and (b) symmetric optical boundary conditions (see Figure 3.2 for the definitions of a b cases).

The same measurement, performed with the same type of the cell of the same CLC mixture, but containing two ITO coated substrates (and thus with optically symmetric boundary conditions for the CLC), shows no such effect (Figure 3.3b). This emphasizes the key role of asymmetric boundary conditions in the observed non-reciprocity. Note that the lower transmittance and additional oscillations (Figure 3.3b) are caused by the presence of the second ITO layer causing a corresponding Fabry-Perrot effect. The factor of light source coherence can affect the final transmittance and reflectance of CLC cell. Given the non-coherence of the light source of the spectrophotometer used in our experiments, in the qualitative representation (see below) of light transmittance through the cell, we neglected the coherent effects of the final transmittance and reflectance. However, as the cell thickness is small, the coherent effects should be considered for more quantitative

estimations and they are considered in numerical simulations, presented at the end of the present chapter.

In addition, there was no such effect of non-reciprocity for the same asymmetric cells, which contained an NLC (non - gyroscopic LC), and for all individual elements of the used cells (ITO coated glass substrates, etc.). This confirms that the chirality of CLC layer is necessary for the observed non-reciprocal transmission effect.

Let us consider a layer of CLC with optically non-symmetrical boundary conditions to develop a simple qualitative analysis of the processes involved (Figure 3.4). Interface A of the CLC represents the boundary with the ITO, while interface B is the boundary with the ordinary glass (both are PI coated). Given that the experimentally observed non-reciprocity was presented (Figure 3.3) for the case of the probe beam having non-resonant circular polarization (designated as "-" in Figure 3.4), we shall consider this specific case only.

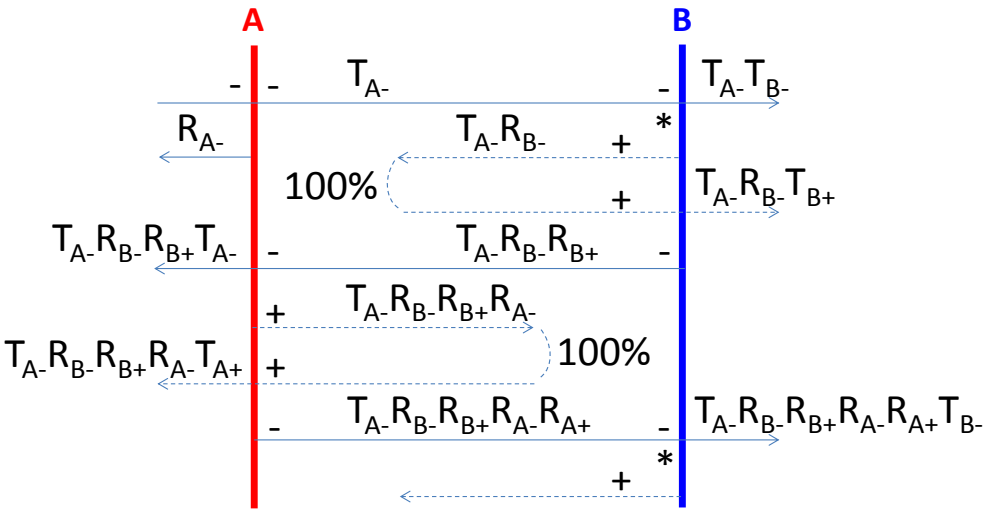

Figure 3.4: Qualitative description of the physical origins of the optical non reciprocity in the layer of CLC with asymmetric optical boundary conditions A and B (light is incident on the interface A).

Then, we can start by analyzing the probe beam transmission for incidence from the interface A (propagating from left to right). The coefficient T_{A-} represents the transmission coefficient (in intensity) of the probe (with "-" polarization) through the interface A. The coefficient T_{B-} represents the transmission coefficient of the probe (with "-" polarization)

through the interface B. Thus, for the first passage, the probe transmittance (through the interfaces A and B) may be expressed by the "aggregate" coefficient $T_{A-}T_{B-}$.

Furthermore, the coefficient R_{B-} represents the reflection coefficient of the probe (with "-" polarization) from interface B. As it is well known, the circular polarization state of light is inverted when it is reflected from a simple interface (since we have the same direction of rotation of the electric field of the light, but an opposed direction of its wave vector). Thus, given that the handedness of the CLC is not changed, we shall now have a resonantly polarized probe beam (designated as "+" in Figure 3.4), propagating from right to left, after its first reflection from the interface B. This light will be completely (100%) reflected from the bulk CLC [6] if the parameters of the CLC layer are appropriately chosen. In addition, it is also well known [6] that the polarization state of the resonantly reflected (from the CLC) light will remain the same (here "+"). This resonantly reflected beam will generate "another" transmitted beam in the second passage. However, given that the CLC is a gyrotropic media, the refractive indices (n_+ and n_-), seen by opposed circular polarizations ("+" and "-"), are different. Thus, the transmission and reflection coefficients of our interfaces (A and B) are not the same for two opposite circular polarizations. That is the reason why the transmittance term for the second passage will be expressed by the coefficient $T_{A-}T_{B-}T_{B+}$. This beam (with polarization "+") will be reflected from the interface B with the coefficient $T_{A-}T_{B-}R_{B+}$ and also with inversion of its polarization into the state "-". This beam will propagate across the CLC and will be reflected from the interface A with the coefficient $T_{A-}T_{B-}R_{B+}R_{A-}$ and with inversion of its polarization state (into "+"), which will be then 100% reflected from the bulk CLC, etc. The further analysis of light propagation (with another reflection from the interface A) shows that, after the third passage, the aggregate coefficient of transmission (from left to right) will be given as $T_{A-}T_{B-}R_{B+}R_{A-}R_{A+}T_{B-}$. We shall not continue further this consideration since it will simply repeat the same cycles (delimited by two star signs on the top right and bottom right of the Figure 3.4, near the interface B), but with smaller contributions. Given the non-coherent character of the light source used, we can estimate the total transmission coefficient (for the light's incidence from the interface A) as

$$T_{A\text{-}to\text{-}B} = T_{A-}T_{B-} + T_{A-}R_{B-}T_{B+} + T_{A-}R_{B-}R_{B+}R_{A-}R_{A+}T_{B-}\ldots \quad (3.1)$$

Similar analysis, conducted for light incident from the interface B (propagating from right to left), gives us an aggregate coefficient of transmission (for the first three passages) that may be presented as

$$T_{B\text{-}to\text{-}A} = T_{B-}T_{A-} + T_{B-}R_{A-}T_{A+} + T_{B-}R_{A-}R_{A+}R_{B-}R_{B+}T_{A-}\ldots \quad (3.2)$$

As one can see, the second and third terms of equations (3.1) and (3.2) are different. This difference disappears (confirming thus our observations) if the boundary conditions are the same

$$T_{A\pm} = T_{B\pm} \text{ and } R_{A\pm} = R_{B\pm} \quad (3.3)$$

Also, if the boundary asymmetry is still present, but the circular anisotropy of the CLC is very weak

$$T_{A-} \approx T_{A+} = T_A,\ R_{A-} \approx R_{A+} = R_A,\ T_{B-} \approx T_{B+} = T_B,\ R_{B-} \approx R_{B+} = R_B, \quad (3.4)$$

then we obtain a simple relation for the non-reciprocity

$$T_{A\text{-}to\text{-}B} / T_{B\text{-}to\text{-}A} \approx (1+R_B+R_B^2R_A^2)/(1+R_A+R_A^2R_B^2) \quad (3.5)$$

Thus, the difference in reflections R_A and R_B is the major contributor of non-reciprocity. However, the chiral character of the CLC is necessary for the non-reciprocity since, otherwise, the travel of light in the medium will be different and the ratio of transmittances in opposite directions will be expressed as

$$T_{A\text{-}to\text{-}B}/T_{B\text{-}to\text{-}A} = (1+R_BR_A+R_B^2R_A^2)/(1+R_AR_B+R_A^2R_B^2) = 1 \quad (3.6)$$

This again confirms our experimental results.

The above mentioned claim about the necessity of chiral character of the CLC layer for the non-reciprocal transmission is supported both theoretically and experimentally. Experimentally, we have shown that the non-reciprocal transmission vanishes if we replace the chiral layer with another (non-chiral layer). To do this, we prepared identical cells (together with the cell used in present work) and filled them with an NLC (non-chiral

anisotropic layer) or left them empty (that is, being filled with air – the isotropic layer). So, especially in the case of NLC, only the chiral character of the CLC was "eliminated".

There was not any non-reciprocal transmission observed in these cells (the results are presented in Appendix 1). Theoretically, Eq. 3.6 shows that if the structure is not periodic, there cannot be a non-reciprocal transmission. And if the cell is filled with a non-chiral periodic structure, the light will reflect from the periodic structure and the transmittance of the cell will vanish (in the ideal case). Simulation results also confirm the claim in question.

To further validate the hypothesis of the observed non-reciprocity as described in the Eq.(3.5), we have done additional experiments by measuring the coefficients of reflection and transmission for the microscope glass and ITO coated glass in air at normal incidence at a wavelength that was inside the spectral bandgap area (λ=1481 nm) of our CLC. The obtained values are as follows:

$T_{A(ITO\text{-}glass)} = 0.61\pm0.015$, $R_{A(ITO\text{-}glass)} = 0.2\pm0.015$, $T_{B(glass)} = 0.87\pm0.015$, $R_{B(glass)} = 0.07\pm0.015$.

Using these values we can estimate the effective refractive index values of the ITO and glass substrates, respectively as $n_{ITO} \approx 2.0 \pm 0.05$ and $n_G \approx 1.50 \pm 0.05$. Using the average refractive index of the CLC we can then estimate the values of $R_A \approx 0.019 \pm 0.002$ and $R_B \approx 0.0005 \pm 0.0001$. Obviously those reflection coefficients are smaller compared to the values obtained in air because of the smaller refractive index mismatch in the CLC cell. In this case, the expression (3.5) could be further simplified to yield

$$T_{A\text{-}to\text{-}B} / T_{B\text{-}to\text{-}A} \approx (1+R_B)/(1+R_A) \qquad (3.7)$$

We thus estimate that the non-reciprocity coefficient should be $T_{A\text{-}to\text{-}B} / T_{B\text{-}to\text{-}A} \approx 0.98 \pm 0.09$. The same ratio, calculated from Figure 3.3, is $\approx 0.953 \pm 0.008$. We think that, given the approximations made, this is a rather good agreement. In addition, this simple formula (3.7) also shows that the best ratio of non-reciprocity may achieve the factor of 2, when R_B=1 and R_A=0.

We have used the method described in Ref [89] to try to reproduce the experimentally observed non-reciprocal behavior. The system discussed here can be treated as a multi-

layer system: isotropic layer (1) - CLC layer - isotropic layer (2). According to the Ambartsumian layer addition modified method, if there is a system consisting of two adjacent (from left to right) layers, A and B, then the reflection / transmission matrices of the system, A + B, viz. $\hat{R}_{A+B}$ and $\hat{T}_{A+B}$ are determined in terms of similar matrices of its component layers by the matrix equations:

$$\hat{R}_{A+B} = \hat{R}_A + \tilde{T}_A \hat{R}_B \left[\hat{I} - \tilde{R}_A \hat{R}_B\right]^{-1} \hat{T}_A,$$
$$\hat{T}_{A+B} = \hat{T}_B \left[\hat{I} - \tilde{R}_A \hat{R}_B\right]^{-1} \hat{T}_A, \tag{3.8}$$

where the tilde denotes the corresponding reflection and transmission matrices for the reverse direction of light propagation, and is $\hat{I}$is the unit matrix. The exact reflection and transmission matrices for a finite CLC layer (at light normal incidence) and for an isotropic layer are well known [90, 91]. First, we represent the isotropic layer (2) with the CLC layer from the left side, using matrix equations Eq. (3.8). In the second stage, we represent the isotropic layer (1) with the obtained CLC Layer - isotropic layer (2) system, again from the left side.

Here we present (in Figure 3.5) one particular case corresponding to our experimental results (Figure 3.3a). The parameters used for simulation are as follows: the effective thickness of the ITO glass A is 1 mm and its effective refractive index is described by the equation: $n_A = 1.4 + 2(\lambda - 1)/\lambda$. The ordinary and extraordinary refractive indexes of the CLC are $n_o = 1.5$, $n_e = 1.7$ respectively. The helix pitch of the CLC is $p = 0.96\ \mu m$ (the distance at which the LC molecules rotate at 360°) and the number of entire helixes is $t = 6$. The thickness of glass B (ordinary glass) is 0.5 mm and its refractive index is 1.5. The use of above presented $n_A(\lambda)$ dependence is based on the best fit of measured (see Figure 2.2, 1000-2000 nm) and theoretically obtained (simulation) transmittance spectra of a free standing ITO coated glass, which was then used as substrate A (see Figure 3.3) . As one can see (Figure 3.5), we obtain very good agreement between the experimental and theoretical results for two opposed directions of light propagation through the CLC cell that was built with asymmetric optical boundary conditions.

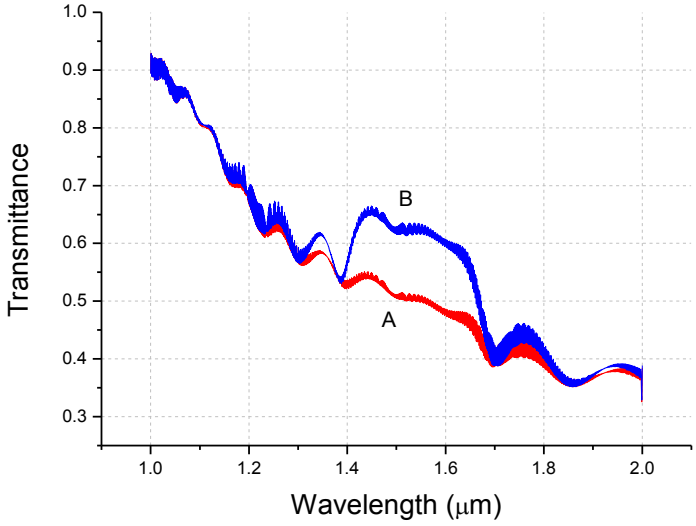

Figure 3.5: Theoretical description of light transmittance through the CLC cell with asymmetric boundary conditions in two opposed directions A and B (see Figure 3.2 and Figure 3.3a).

We have observed and explained, in the first approximation, an optical non reciprocity phenomenon in a linear and non-absorbing material layer without using excitation fields. We have shown that this non reciprocity is defined by two key parameters of the media: the chirality of the layer and the asymmetry of its boundary conditions. We believe that the described system is very simple (well suited for potential applications) and, at the same time, is rich since it has very specific dependence upon the angular and linear momentum of light. In addition, we think that the reported non-reciprocity might also have interesting implications in natural evolution given that such chiral material systems (with asymmetric boundary conditions) are present in the natural environment, such as some insect skins, that exhibit chirality and contain asymmetric boundaries (air and body tissue) [75, 98, 100].

We thank the Natural Sciences and Engineering Research Council of Canada (NSERC) for their financial support.

Chapter 4
Reconstruction of Chiral Structure

Orientational Defects in Cholesteric Liquid Crystals

Orientational deviations (defects) can occur in LC cells for different reasons. Having different origins, these defects are manifested differently under the polarizing optical microscope. The term "defect" comes from crystallography, where these deviations from the ideal crystalline network structure are observed either as empty points (point defects) or as deviations (line defects). A wide variety of defects exists in LC phases, many of which are not observed in solids. The investigation of properties of defects has academic and technological applications [101, 102]. Identifying the defects and their characteristics can help us to determine such different properties of LCs as, for instance, LC phases, viscoelastic properties and so on [18]. Usually the defects are regarded as obstacles for technological applications since they introduce undesired scattering of light. However, recently defective structures have found applications in many fields of optics and optoelectronics, in particular, in 3D photonic crystals and in bistable CLC displays.

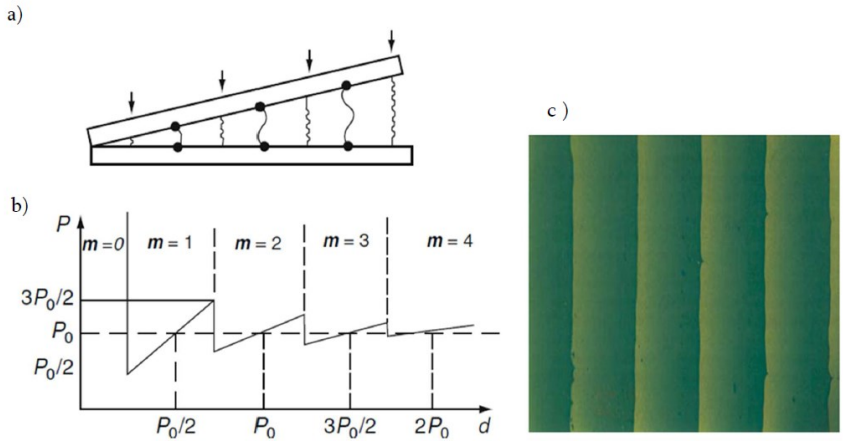

Figure 4.1(after Ref. [25]): a) Schematic of a wedge-shaped CLC cell. The flashes show the disclination lines between a uniform domain. b) The dependence of the CLC helix pitch on the cell thickness at a given point of the cell. *m* is the number of half-helixes at a given uniform domain. c) The image of the cell under a polarizing optical microscope.

The types and properties of orientational LC defects are discussed in [25]. Defects are usually manifested as disclination lines in CLC cells, especially in planar cells with strong

boundary conditions. In Figure 4.1b one can see the dependence of the CLC helix pitch in a wedge-shaped cell (Cano wedge [71, 103]) on the cell thickness. The schematic of the Cano-wedge cell is presented in Figure 4.1a. As one can see, the helix pitch undergoes multiple jumps with an increase of the cell thickness. These jumps are 'supported' by disclination lines: one disclination line corresponds to each jump (Figure 4.1c). The helix pitch undergoes an abrupt change in the left and right sides of these lines and the number of half-helixes is changed by one. So, in this case, the disclinations occur to provide abrupt changes of the LC director over a short distance. Another type of disclination lines in CLCs are the so called 'oily steaks' (Figure 4.2). They can

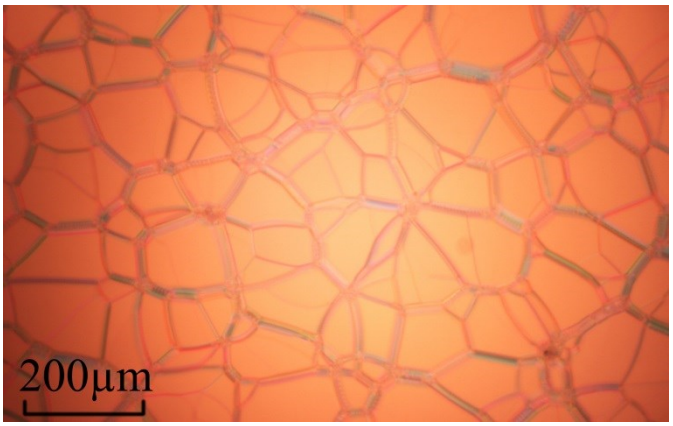

Figure 4.2: The disclination lines (oily steaks) in a 30 μm thick CLC (CB 15) cell, placed in the field of 'Zeiss' polarizing.

appear because of weak external forces such as mechanical deformation of the cell, thermal gradients over the cell or inhomogeneous electromagnetic fields. While the origins of the above-mentioned two disclinations are similar (the abrupt changes of the director), the 'oily steaks' remain there after the removal of external forces. Sometimes they take days to disappear. Different from NLCs – in which, depending on LC orientation, the disclination lines can pull or push one another – here the disclination lines do not interact.

There are very few works discussing the 'healing' of disclination lines in LC cells. One of those is [52] , which discusses the behaviour of open (4.3a) and closed (4.3b) disclination lines during time. The authors have first shown (by polarizing microscopy) that the separated open disclinations are healed linearly but the closed disclinations are healed logarithmically with time. The observations of the cell capacity (electric) changes in time

have shown that the overall length of disclination lines decreases logarithmically with time. It was also shown that the healing speed depends on the CLC temperature and the helix pitch: the higher the temperature and the longer the pitch, the faster they get healed.

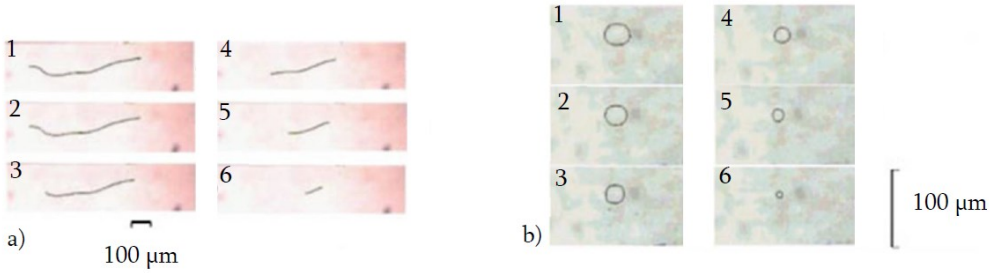

Figure 4.3 (after Ref. [52]): Healing of open (a) and closed (b) disclination lines with time in a CLC cell.

Quenching of Defects by External Electrical Field

If a thin layer of CLC is pure enough, it will possess a high degree of resistance to optical emission in visible region. However, undesirable scattering that usually occurs due to nonuniformities (orientational defects) in CLC layers, significantly reduces the sharpness of PBG boundaries and, thus, they represent an obstacle for applications of liquid crystal based thin film optical devices such as low-threshold lasers [104], light modulators [84], etc., [105]. Requirements are especially stringent in lasers and modulators (when used particularly in imaging systems), because minor scattering can significantly reduce the instrument quality factor.

The goal of the present work is the experimental investigation of the influence of an external electrical field on nonuniformities (disclinations and orientational defects) existing in CLCs with negative dielectric anisotropy and the possibility of quenching those nonuniformities. The influence of the external electric field on PBG has been also investigated.

Two types of nonuniformities were investigated. First are disclinations, which are rupture lines of optical homogeneity of the material. Molecules abruptly change (in space) their orientations within these lines. As in case of nematic liquid crystals (NLC), the molecules

conserve the direction of orientation on both the sides of disclinations, the rotation of director within the line cannot be random, but must be multiple of π. In NLC cells the disclinations usually arise when for some reason (inhomogeneity of the boundary conditions at the substrates, convective fluxes, thermal nonuniformities, etc.) the molecules, are forced to abruptly change (in space) their preferred sense along which their long axes (director) are directed [5], [106]. In the case of CLCs disclinations exist almost invariably (Figure 4.4, a and b). They exist even in case of the absence of above mentioned structural changes. The disclinations can move, unite or split with time [5, 52, 83]. The second type of nonuniformities is connected with bad orientation and they exist in the whole bulk of the cell.

Experiment. The discussed two types of nonuniformities are comparable in size to the wavelength of visible light and thus they cause undesirable optical scattering. In order to observe the feasibility of ‘‘clearing’’ these nonuniformities by application of electrical field, we have used planar and homeotropic cells filled with CLC having negative dielectric anisotropy characterized by $\Delta\varepsilon = \varepsilon_{\parallel} - \varepsilon_{\perp}$, where $\varepsilon_{\parallel}$ and $\varepsilon_{\perp}$, are dielectric constants of the material in directions parallel and perpendicular to the long molecular axis, respectively.

It is well known that the long axes of LC molecules with negative dielectric anisotropy are arranged perpendicular to the applied electric field. This means that instead of destroying the helicoidal periodic structure, the applied external electrical field stabilizes the structure. In the ideal case molecules forming a helicoidal structure are always parallel to the cell substrates. Molecules with different orientations (those located in the disclination lines) will reorient under the influence of electric field and be included in the helicoidal structure. Moreover, one can expect that the possibility of molecular fluctuations in the direction, perpendicular to the monomolecular layers, will decrease. So, one can suppose that under the influence of applied electric field the deviation inclinations of molecules from the periodic, helicoidal structure (defects) will decrease. Consequently, undesirable ligth scattering caused by director fluctuations will also decrease.

CB15 (purchased from ‘‘Merck’’ company) CLC with negative dielectric anisotropy, which possesses a PBG in the visible region of light ($\sim 520-560\,nm$) was used in experiments.

The situation is clearer for the case of planar aligning boundary conditions: the molecules in the layers which are in contact with the substrates are oriented parallel to substrates and point their axes in a certain (rubbing) direction. The molecules in the next layers also have a certain preferred direction that is also parallel to substrates, but it slightly twists from layer to layer forming thus a twisted (helicoidal) periodic structure [5] (Figure 4.5, a). However, in CLC cells some defects almost always exist in the form of disclinations [5] that usually cause undesired light scattering. Usually, the mentioned disclinations disappear in the course of time, but these time periods may be long enough (days, weeks…). Microscopic images of 5 μm thick cell are presented in Figure 4.4, when the cell is placed between crossed polarizers. The image in Figure 4.4a is taken immediately after the cell fabrication. One can see the disclination lines that gradually disappear over several days (Figure 4.4b). The disclinations disappear rapidly if we apply electric field (perpendicular to glass substrates). Indeed, as is seen in Figure 4.4c, which is taken 5 *s* after the application of field, the molecular structure is rather uniform without any disclination and does not change after switching off the electrical field.

Figure 4.4: Images of a 5 μm thick CLC cell with planar boundary conditions, placed in the field of "Zeiss" polarizing microscope. Images are taken: a) immediately; b) a few days after cell fabrication; c) about 10 *s* after applying U=20 V voltage.

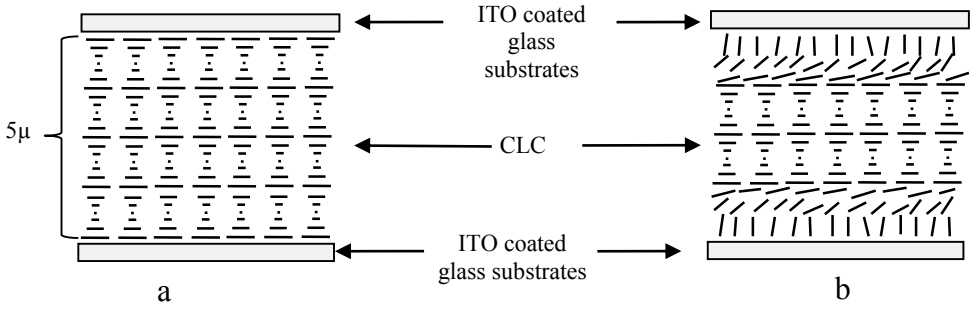

Figure 4.5: Schematic of molecular organization in CLC cells: a) planar and b) homeotropic boundary conditions on limiting substrates.

From the point of view of uniform molecular orientation, the situation becomes more complex in a CLC cell with homeotropic boundary conditions. The molecules of the near substrate layers, orient their long axes perpendicular to substrates and tend to transfer this direction to the layers in neighborhood. But as already mentioned, CLC molecules tend to form a helicoidal structure. Thus, the force created by a surfactant layer coated on the substrate and defining orientations of molecules oppose intermolecular interactions tending to form a helicoidal structure. As a result, an original arrangement of molecules is formed inside the cell. The molecules in direct contact with glass substrates align perpendicular to them. In the next layers, because of weakening of the influence of the surfactant layer, the director gradually turns up to parallel orientation (to substrates). Finally, a helicoidal periodic structure is formed, as is the case in planar cells (Figure 4.5 b).

As is seen from the polarizing microscope images (Figure 4.6a), the nonuniformities in homeotropic cell exceed in number those in planar cell (Figure 4.4). Here, along with the disclination lines there are also numerous little nonuniform domains that are dispersed in the whole volume of the cell. According to the experiments, the applied electrical field (20 V to 5 μm thick cell) quenches the disclinations and significantly reduces the dimensions of nonuniformities (Figure 4.6b). Usually, the disclination lines are not oriented but are dispersed in the CLC cell. In Figure 4.6a the lines have some preferred direction because of the flow of CLC during the filling of the cell with CLC (the image is taken immediately after the cell fabrication). The structure recovers from Figure 4.6a state to the Figure 4.6b state (but without any preferred direction of disclination lines formation) several days after switching off the electrical field.

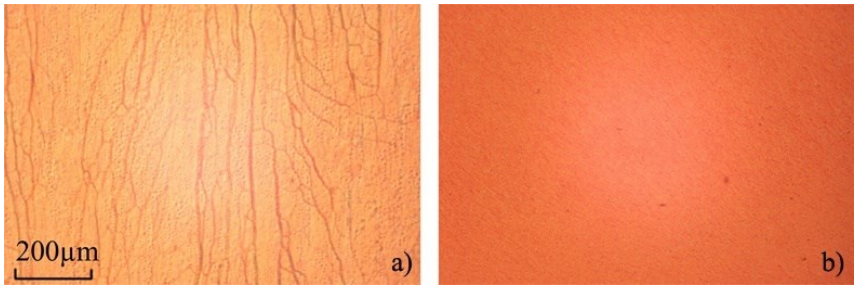

Figure 4.6: Images of the 5 μm thick CLC cell with homeotropic boundary conditions, placed in the field of Zeiss polarizing microscope: a) immediately after making the cell; b) about 10 s after applying $U = 20\ V$ voltage.

To study the variation (and the "correlation") of PBG to the quenching of disclinations (caused by external electric field), we have also realized a spectroscopic investigation of the cell. The transmittance spectra of homeotropic and planar cells for different applied voltages are presented in Figure 4.7. According to the experiments, the influence of an external electric field on the transmittance spectrum of the planar CLC cell is not significant despite the fact that the field eliminates the structural nonuniformities. The PBG is always clearly distinguished (Figure 4.4 a, b, c).

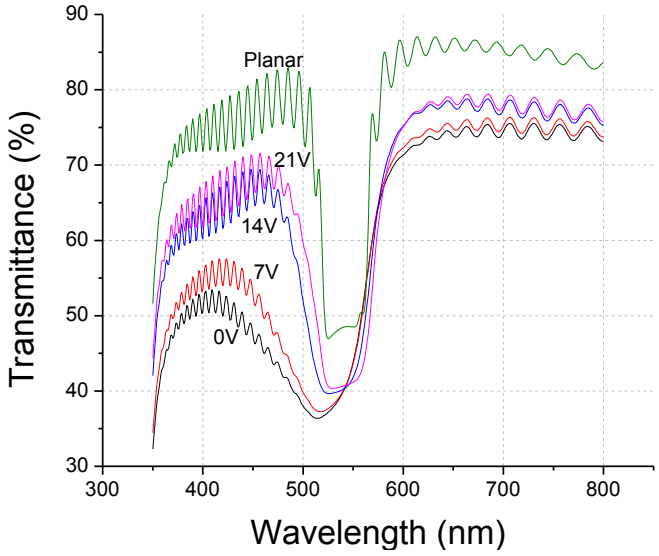

Figure 4.7: Spectroscopic observation of band gap of 5 μm thick planar and homeotropic CLC cells. Different voltages are applied between homeotropic cell substrates (0; 7; 14; 21 V).

The image is different in case of homeotropic cell. As is seen from Figure 4.7, the transmittance spectrum of the homeotropic cell void of the voltage ($U = 0$) differs from that of the planar cell. The PBG is warped and the wings are not sharp enough. It is important to mention that compared with the transmittance spectrum of an ''ideal'' helicoidal periodic structure (as that of the planar cell) the differences are clearer in the short wavelength region. The applied electrical field ''cleans'' the transmittance spectrum, thus bringing it towards the spectrum of ideal helicoidal structure. As is seen from Figure 4.7, the transmittance spectrum of the homeotropic cell for $U = 21\,V$ applied voltage is

close enough to that of the planar cell. In that case, one can clearly distinguish the PBG boundaries, which is symmetric, as in the case of the planar cell.

Discussion. The interaction forces of CLC molecules among themselves and the interaction forces of CLC molecules with the ones on the substrate surface are important for the orientational order of CLC molecules. With the application of an electric field on the CLC film, the forces exerted by this field also contribute to the rearrangement of CLC molecules. In the equilibrium state, the contributions of momenta produced by aforementioned three forces are balanced.

The interaction forces acting between CLC molecules tend to form a helicoidal (twisted) periodic structure. The interaction forces between CLC molecules and those on confining layers are usually short-range.

In the planar cell, these two interactions force the molecules to form a helicoidal structure, pointing their axes in planes parallel to the substrates. In case of homeotropic boundary conditions on the substrates the molecules that are in direct contact with them orient their long axes perpendicular to substrates, thus making the structure unstable. For this reason, sometimes the CLC forms a helicoidal periodic structure, the axis of which is parallel to the substrates confining the cell [2].

One can conclude thus that in case of positive dielectric anisotropy ($\Delta\varepsilon > 0$) the applied external field, which is perpendicular to glass substrates, disturbs the periodic structure of CLCs and starting from a certain value of electric field the CLC cell passes to the homeotropic state (chapter 1). As mentioned above, the situation is different when the cell is filled with negative dielectric anisotropy ($\Delta\varepsilon < 0$) CLC: under the applied external electric field the axes of CLC molecules arrange perpendicular to the direction of electric field contributing, thus to the formation of a helicoidal structure of CLC with axis perpendicular to the substrates (planar helicoidal structure).

The experiments show that even in the cell subject to planar boundary conditions, in the absence of electric field there arise some nonuniformities (Figure 4.4 a, b). This may be due to nonuniformities in the boundaries themselves when confining substrates, the presence of foreign particles in the CLC, hydrodynamic flow processes. As seen in the image taken

with the polarizing microscope (Figure 4.4, c), on the application of an electric field with $4\,V/\mu m$ intensity the causes of the disclinations are eliminated. As a result, a CLC cell with sufficiently uniform distribution of LC molecules is obtained.

In the case of a homeotropic cell, the aforementioned three forces acting on the CLC molecules are at variance from the viewpoint of helicoidal structure formation. The forces exerted by the substrates destabilize the structure of CLCs, the helical axes of which are oriented normal to the substrates. As a result, in the absence of electric field one can see in Figure 4.6a, some point defects spread over all the bulk of cell along with the disclination lines. Here also, as in the planar cell, the electric field tends to reorient the molecules that cause nonuniformities and drive them to the helicoidal structure. As we see in Figure 4.6b, the electric field eliminates the disclinations and reduces the size of point defects.

For a qualitative description of the above phenomenon we take advantage of the graphs of Figure 4.7. It is seen that prior to the application of the electric field the transmittance spectrum of the homeotropic cell differed significantly from that of the planar cell and the difference is larger in the short wavelength part of PBG. This can be explained by the presence inside the cell of small helicoidal formations (domains), the axes of which are not perpendicular to the cell walls. So, inside the cell there exist numerous little helices, the axes of which are not co-directed, but make different angles with the cell wall. As a result, a $1\,mm$ diameter beam will interrogate numerous little helices having different orientations. As a result one records the reflection of not only in the PBG range, but also a seemingly widening of PBG. The application of an electric field to CLC layer leads to reorientation of the little helixes that orient their axes perpendicular to the confining substrates. The deviation from normal incidence decreases the short wavelength part of PBG in the transmittance spectrum. As seen in Figure 4.7, after application of $E = 4.2\,V/\mu m$ electric field ($U = 21\,V$) the wings of spectrum are rather symmetric, which means that there are fewer tilted helices in the bulk of cell. On application of $U = 21\,V$, the depth and width of PBG increased by a factor of 1.8 or decreased by a factor of 1.4, respectively. However, experiments show that the transmittance spectrum of a homeotropic cell is still lower than that of a planar cell, which means that the orientations of molecules

are still homeotropic near the substrates because of strong anchoring of molecules to substrates.

Therefore, in the present section it was experimentally shown that the orientational order of CLCs is increased by using negative dielectric anisotropy CLCs and the application of an electric field. The nonuniformities in the director distribution decrease and the scattering of light in the CLC layer is reduced under the influence of an electric field. It was experimentally shown that the sharpness of the PBG edges is increased and its width decreased as the defects are quenched. The results can be used for numerous other investigations as well as in CLC devices, e.g., in CLC based light modulators, the CLC displays or the Smart Windows.

The above results suggest that an electric field can not only unwind the helicoidal structure, but by eliminating structural defects it can also help restore that structure.

Below, we present a published article discussing the dynamics of the transition processes. Microscopic and spectral observations are realized, in order to better understand the dynamics. Planar to homeotropic (helix unwinding) and homeotropic to planar (helix restoration) transitions are considered and a method for acceleration of helix restoration process is proposed and experimentally confirmed, as well.

Résumé de l'article inséré

Accélération de restauration de l'hélice cholestérique par un composant à deux fréquences

Nous présentons la création et l'utilisation d'un mélange de cristal liquide cholestérique à deux fréquences pour le 'déroulement' et la reconstruction dynamique de la structure hélicoïdale. L'ajout de cristal liquide nématique dans le mélange cholestérique a déplacé la bande interdite vers la région proche infra-rouge. Nous avons réalisé des mesures de transmission planimétrique pour évaluer le changement de biréfringence effective de la couche de cristal liquide et la réflexion résonante pour caractériser la dynamique des processus de 'déroulement' et de reconstruction de la structure hélicoïdale. Le processus de reconstruction est accéléré d'un ordre de grandeur par l'application de champs électriques modérés.

Mol. Cryst. Liq. Cryst., Vol. 560: pp. 35–48, 2012

Accelerating the cholesteric helix restoring by a dual frequency compound

*Karen Allahverdyan[1,2] and Tigran Galstian[1]**

[1] Center for Optics, Photonics and Laser, Department of Physics, Engineering Physics and Optics, Laval University, Pav. d'Optique-Photonique, 2375 Rue de la Terrasse, Québec, G1V 0A6, Canada
[2] Department of Physics, Yerevan State University,1 Alex Manoogian, 0025 Yerevan, Armenia

Abstract

We report the creation and the use of dual frequency cholesteric liquid crystal mixtures for the dynamic electrical unwinding and forced (accelerated) restoring of their molecular helix. The use of a cholesteric in a mixture with a dual frequency nematic shifts the resonant wavelength to the near infrared area. We use polarimetric transmission measurements (out of resonance) to check the effective birefringence of the cell as well as the resonant reflection (at near infrared) to characterize the dynamics of unwinding and restoring processes. The restoring process is accelerated almost by an order of magnitude for quite moderate voltages used.

KEYWORDS
Liquid crystals, cholesteric liquid crystals, dual frequency liquid crystal, frequency control, polarimetry, resonant reflection, electrooptic switch.

4.1 Introduction

Liquid crystal (LC) materials have been successfully used in various light modulation applications, [3, 6]. However, the inherent anisotropy operation of the majority of LCs requires the use of polarizers, which reduces light transmittance (increasing thus the power consumption), increases the cost of those modulators and reduces their long term stability.

One of the alternative (polarization-free) avenues, explored so far, was the use of cholesteric LCs (CLCs), which naturally form periodic helicoidal molecular structures reflecting light in a specific "resonant" wavelength band and having a circular polarization that is replicating the helix of the CLC [5, 73]. Several mechanisms have been explored so far to control the reflection properties of those materials (position of the bandgap, its strength and bandwidth, etc. (see, e.g., Ref. [28, 29, 53, 66, 79-83]). While the obtained results are very encouraging, there are however several drawbacks with the use of CLCs. First, the above-mentioned reflection band is relatively narrow (of the order of 50 nm) for broad band applications, such as solar filters or camera shutters. Second, the reflection of natural light (originating from a lamp, LED, sun, etc.) is only 50% since the resonant reflection happens only for the appropriate circular polarization [5]. Finally, the demonstrated so far dynamic modulations of the resonant reflection of CLCs (spectral shift, unwinding, etc.) are relatively slow to recover (sub-millisecond switching times would be needed for imaging or color TV applications). Significant efforts have been deployed to broaden the resonant reflection band and to increase the reflection coefficient [76-78], see also [107, 108] and references therein. To the best of our knowledge, the possibilities to accelerate the helix restoring were not explored as intensively as the two above mentioned directions. There are several reports of using CLCs with dual frequency functionality in light shutters (with photo curable materials), thin photonic band gap structures, etc. [109-114]. However, we were not able to find the details of material preparation and dynamic transition characterizations. In contrast, to the best of our knowledge, the possibilities to accelerate the response time, e.g., for the helix restoring were not explored as intensively as the two above mentioned directions [107].

In the present chapter, we were particularly interested by the electrical unwinding of the CLC helix in materials having positive dielectric anisotropy. We have thus focused our

efforts on the problem of slow restoring of the CLC helix in view of exploring the possible ways of its acceleration. The approach we have used here was based on a mixture of two LC materials, in a way to preserve the helical structure, while creating two frequency zones (for the electrical driving signals) for which the developed mixture has respectively positive and negative dielectric anisotropy allowing the fast "forced" recovery. Thus, we present below the preliminary results of the studies of the material composition developed as well as the electro-optical and morphological properties of cells containing this compound.

4.2 Materials Used

The material composition used was obtained by mixing two LCs: the CLC, called CB15, and the nematic LC, called MLC 2048 (both from Merck). These materials were mixed in two concentrations to obtain two mixtures, the first one containing 33 wt % of CB15 and 67 wt % of MLC 2048 (further referred as Mix 33) and the second one contained 41 wt % of CB15 and 59 wt % of MLC 2048 (further referred as Mix 41). The choice of those compounds was based on the desired dielectric parameters (see later) as well as the material availability. The CB15 is a right handed CLC with a resonant band gap in the green region of light spectra ($\sim 520\ nm - 560\ nm$) at room temperature. Unfortunately, Merck was not able to provide more data concerning the dielectric and optical parameters of the CB15. We have, however, recently measured and reported (Ref. [83]) some of its optical parameters at room temperature (see also Ref. [86]). Most importantly, it was shown that the dielectric anisotropy of the CB15 at low frequencies (1 kHz or so) is negative.

To prepare the current mixtures, we have proceeded to very approximate (qualitative) measurements of corresponding dielectric constants of each material component as well as those of the final mixture. Thus, planar aligned commercial cells ($L = 50\ \mu m$ thick) were used (filled with our materials) and subjected to capacitance measurements ("HP 4192" Impedance Analyzer was used) at different environmental temperatures. Figure 4.8 shows the driving electrical frequency dependence of measured dielectric constants. First we have measured (with very weak electrical excitation to avoid reorientation effects) the capacitance of the cell and thus the dielectric constants of materials at room temperature (20°C, squares) in their liquid crystalline phase. We attribute the obtained values to the

"ordinary" dielectric constant $\varepsilon_\perp$ thanks to the good planar alignment of the cell. Then we heated the cell to achieve the isotropic phase (60°C, triangles) of the material and measured it again to obtain (approximately) the average dielectric constant ε_{av}. Finally we calculated the parallel dielectric constant $\varepsilon_\parallel$ by the formula $\varepsilon_{av} \approx (\varepsilon_\parallel + 2\,\varepsilon_\perp)/2$. We must emphasize again that these data must be considered very qualitative. The main goal here was the rough identification of approximate concentrations that would allow us to obtain a "dual frequency" helicoidal mixture. To show the degree of imprecision of our estimations, we have used the same technique to do similar measurements also on the second component of our mixture (the MLC 2048), which is much better known and described in the literature. The results are shown in Figure 4.9. Its nematic-isotropic phase transition temperature is 106°C, the ordinary refractive index and anisotropy at 20°C are respectively $n_o = 1.4978$ and $\Delta n = 0.2214$ (both measured at $589\,nm$) [115]. This is a "dual frequency" nematic LC that was largely used to accelerate the "back" reorientation, e.g. in LC scatterers or retarders [116, 117]. Indeed, the dielectric anisotropy of this LC is positive for "low"

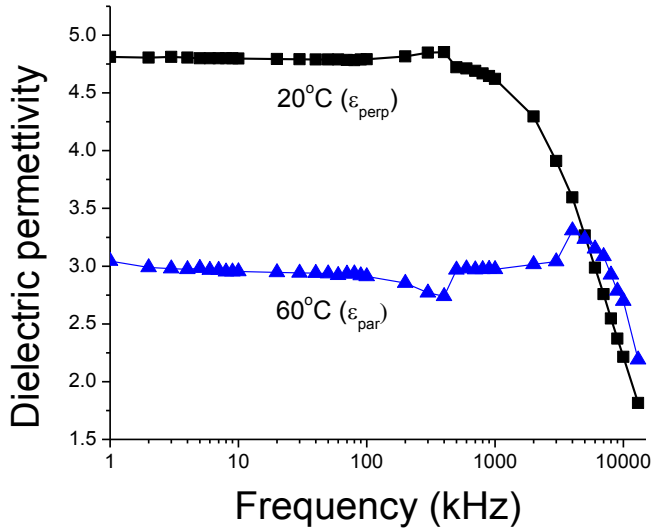

Figure 4.8: Qualitative dependence of CB15 parallel and perpendicular dielectric permittivities upon the electric field frequency, measured in CLC (20°C) and isotropy (60°C) phases.

frequencies (<10 kHz at 20°C) and is negative for "high" frequencies (>50 kHz at 20°C), as shown in Figure 4.9 [85]. The simple set-up and method we have used (to measure the

dielectric constants of our materials) provides rather similar qualitative values (compared to those reported elsewhere) when applied to the MLC 2048 (Figure 4.9). The difference in two graphs (a and b) could be caused by the high sensitivity of the cell capacity on various factors such as the wires that were used to connect the cell ITO electrodes to the impedance analyser or the incertitude of cell gap (capacitance thickness).

The final mixtures (Mix 33 and Mix 41) were thus made, taking into account the above mentioned measurements to have low-frequency positive dielectric anisotropy (to enable the electrical unwinding of the helix) and high frequency negative dielectric anisotropy (for forced restoring of the helix, see later).

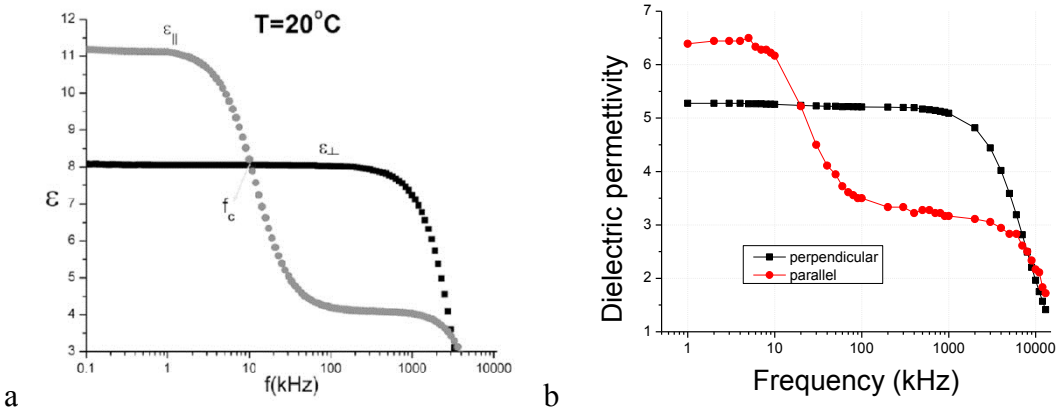

Figure 4.9: MLC 2048 parallel and perpendicular dielectric permittivity dependences upon the electric field frequency. a) from Ref. [110] and b) obtained by our approximate technique.

4.3 Cell Fabrication and Characterization

The cells were fabricated and filled by a standard capillarity method (filled at 20°C). First of all, the commercially purchased indium tin oxide (ITO) coated substrates were washed in an ultrasonic bath (for 8-10 minutes, in soap-water solution, 8-10 min. in water, 8-10 min. in acetone and 8-10 min. in isopropanol). Then they were lifted slowly from isopropanol and left in an oven to dry. The substrates were then spin coated (500 rpm during 5 seconds, then 3000 rpm during 20 seconds) with planar alignment Polyimide layer (PI 150, from Nissan) and heated in the oven ($T = 80^{o}C$, during $t = 15$ minutes and then heated again at $T = 280^{o}C$, during $t = 60$ minutes, then slowly cooled down to room

temperature). The obtained substrates were then unidirectionally rubbed to obtain planar alignment of LC mixtures. A UV sensitive adhesive NOA 65 mixed with glass spacers, see below was applied to seal the LC cell).

Immediately after the fabrication process was completed, some defect structures were initially observed, which then were gradually resorbed without further treatment. The application of electrical fields accelerated this process of defect healing. Three cells were fabricated for the initial comparative estimations. The first two cells were filled with the same mixture (Mix 33) but had different thicknesses (5 µm and 8 µm). These are identified, respectively, as cell 1 and cell 2. A third cell of thickness 5 µm and containing Mix 41, is identified as cell 3.

Spectral studies identified band gaps in the range $1400\,nm - 1600\,nm$ and $1000\,nm - 1200\,nm$, respectively, for compounds Mix 33 and Mix 41. The electrical excitation of the cells (AC, SIN shaped, at 1 kHz) have shown that the dielectric anisotropies of both mixtures are, in fact, positive since we were able to destroy their reflection resonances. Figure 4.10 demonstrates (polarizing optical microscope)

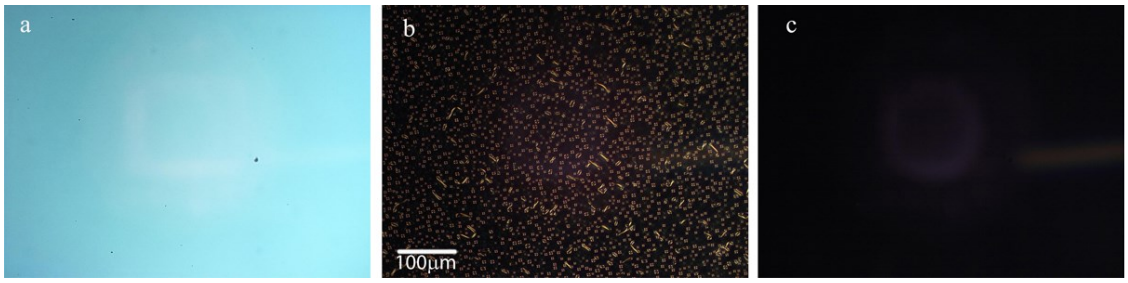

Figure 4.10: Polarizing microscope images of the cell 1 (placed between crossed polarizers) taken when the voltage, applied to the cell, is switched (increased step-wise and kept constant) from planar / helicoidal to homeotropic state; a) helicoidal state, b) transient state and c) homeotropic state.

the electrical unwinding of obtained helicoidal structures by using a low frequency field (the microscope polarizers are always crossed). Thus, at the beginning, the cell is in the planar state (helicoidal structure, Figure 4.10 a), then an excitation voltage (AC, SIN shaped, 50V RMS, 1 kHz) is applied to unwind the helix and to transfer it into homeotropic state (Figure 4.10 c). This happens through the generation of multiple transient

disclinations (Figure 4.10b). The speed of this "excitation" transition is easy to control by the applied voltage value.

Figure 4.11 demonstrates the "free-relaxation" (or natural restoration) of the cholesteric mixture when the voltage is simply switched off from the homeotropic (unwound) state (Figure 4.11 a). The various stages of this back transition may be seen in Figure 4.11 b)-f). The approximate time intervals between those pictures are as follows : b) is taken immediately after switching the field OFF, then c) and d) are taken with approximately 1-2 seconds of intervals, e) is taken after about a minute and f) is taken after several more minutes.

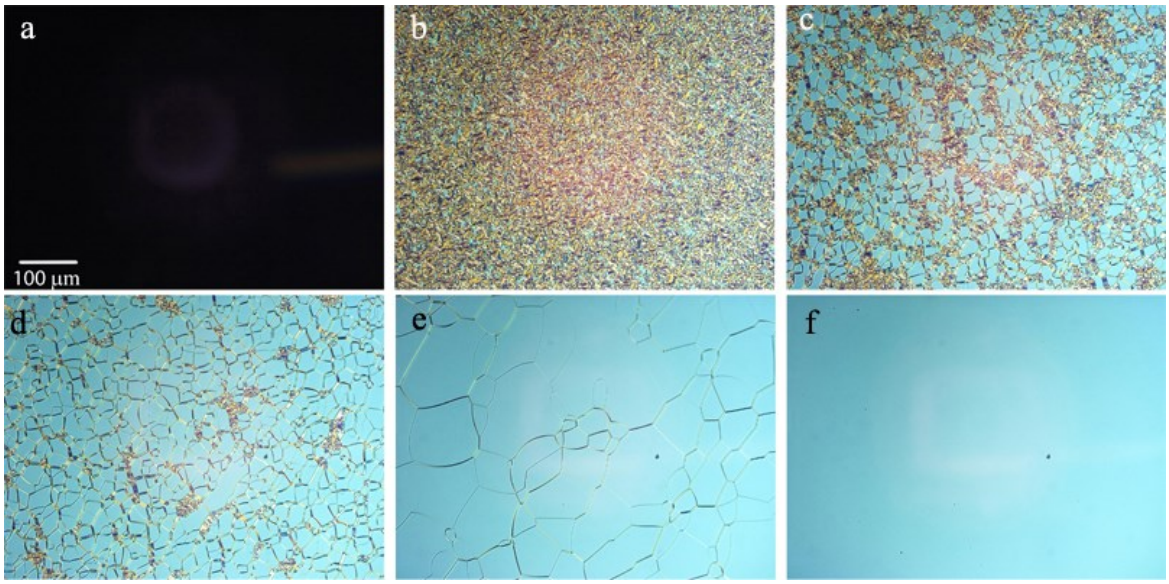

Figure 4.11: Polarizing optical microscope images of the cell 1 (placed between crossed polarizers) taken when the cell is relaxed from the unwound homeotropic state to planar (helicoidal) state, a) homeotropic state, b)-c)-d)-e) transient states, f) planar / helicoidal state.

The approximate thresholds of the electrical unwinding of the CLC helix for our three cells were measured to be $U_{th1} \approx 50V$, $U_{th2} \approx 80V$ and $U_{th3} \approx 100V$. Thus, the increase of the thickness of the cell (for the same mixture), e.g. by a factor of 1.6, increases the U_{th} by a factor of 2. In the same time, the decrease (e.g., by a factor of 1.3) of the concentration of the MLC 2048 increases the value of U_{th} by a factor of 1.6. This last effect is quite natural since the MLC2048 is responsible for the positive dielectric anisotropy at 1 kHz and, respectively, for the helix unwinding.

4.4 Time Resolved Measurements

To obtain quantitative data for the helix unwinding and restoring processes, we built the experimental set-up described in the Figure 4.12. A CW He–Ne laser (operating at 632.8 nm) provided the probe beam to observe the excitation and relaxation processes by monitoring the effective birefringence changes of the cell. The cell was placed between crossed polarizers and the CLC orientational state (homeotropic - planar) was changed by changing the voltage and frequency of the electrical signal applied to the ITO electrodes. The probe, passing through this polarimetric system was detected by a photodiode PD connected to the computer. Data were acquired every 50 ms).

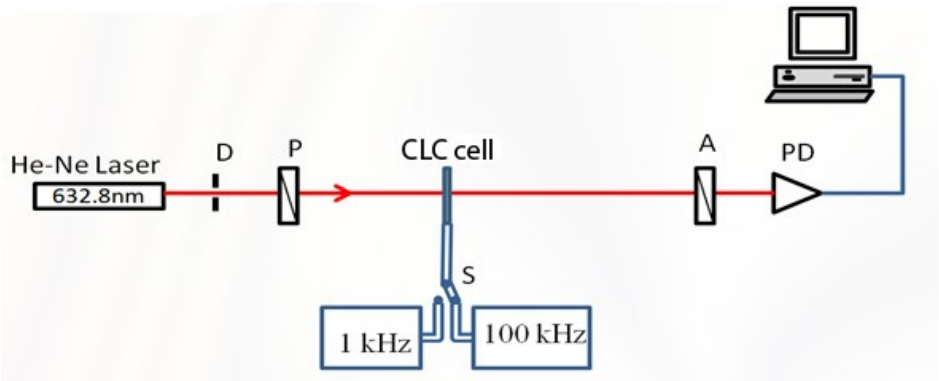

Figure 4.12: Schematic representation of the experimental setup used for time resolved transition measurements. D: diaphragm (1 mm), P: polarizer, A: analyzer (polymer film), PD: photodiode (at approximately 50 cm from the cell; active area diameter of the detector is d ≈ 2 mm), "1 kHz" and "100 kHz" designate generators of voltages at those frequencies.

The experimental procedure, used for our studies, was the following: the cell exhibited helicoidal (planar) alignment in the ground state ($U = 0V$, see Figure 4.13). Then, a nearly above-threshold voltage was applied to the cell (at $t \approx 3\ sec$) with 1 kHz frequency (AC, SIN shaped). The transition of the CLC was then monitored (approximately during 2 sec) up to the stabilization of the transmitted signal. Then, at $t \approx 5\ sec$, the frequency of the electrical signal was switched from 1 kHz to 100 kHz.

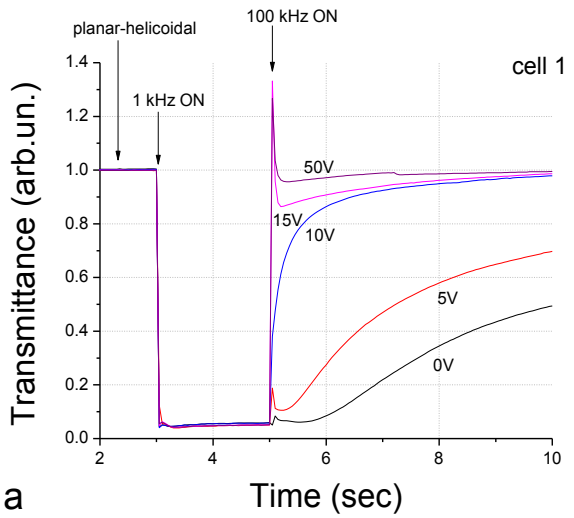

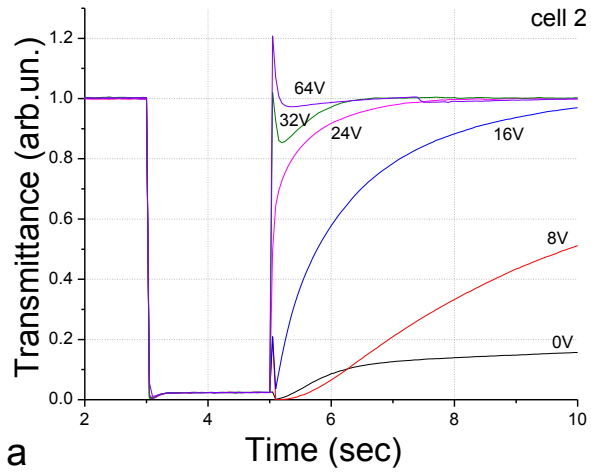

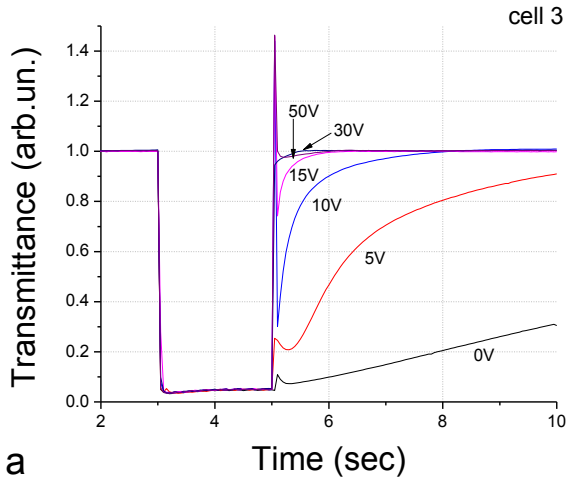

Figure 4.13: Variations of the polarimetric system transmittance during the excitation and relaxation processes for a) Cell 1 b) Cell 2 and c) Cell 3. The high transmittance corresponds to the blue state at Figure 4.10a), the low transmittance to the dark state at Figure 4.10c). There was no voltage applied up to ~ 3 sec. Then the helix unwinding voltage (U=50V RMS, AC, sine - shaped, at 1 kHz) was applied from ~ 3 sec to ~ 5 sec and finally, the restoring voltage (AC, SIN shaped at 100 kHz) was applied starting from ~ 5 sec up to ~ 10 sec. (Voltage RMS values are shown next to curves).

The restoring of the initial state was then monitored again up to the stabilization of the signal.

The experimental results are qualitatively similar for all three cells and may be summarized as follows. The transmittance of the probe is initially high (in the CLC ground state), as shown in Figure 4.13. Then this transmittance drops drastically with the application of the voltage at 1 kHz. The simple switch-off of the voltage results in a very slow free-relaxation process (see the curve $U = 0V$). The natural recovery of the cholesteric helix is faster for a thinner cell of the same LC mixture. However, this recovery is very slow for the thin cell containing smaller quantity of the CB15 compound, probably because of the smaller elastic constants of the MLC2048 compared to those of CB15.

The recovery of transmittance is accelerated if the voltage is maintained, but the frequency of the electric field is changed to 100 kHz. This acceleration is more pronounced when the voltage (at 100 kHz) was higher. Another feature that is common for all three cells is that there is a saturation voltage value (at 100 kHz) after which, a further increase of the voltage does not change the restoration process noticeably. This value corresponds to an electric field strength $\sim 8V/\mu m$. Figure 4.14 shows the recovery processes of the three cells under the action of different voltages, but the same electric field strength ($2V/\mu m$).

Although the recovery process is not the fastest in the case of cell 1, we continued our investigations with that cell. The reason for this choice is that cell 1 has the lowest helix unwinding voltage ($U_{th1} \approx 50V$). To quantify the restoring speed in an approximate way, we fit our experimental curves (Figure 4.13) with an exponential function $T = A - B \times \exp(-t/\tau)$, where T is light transmittance across the polarimetric system, A and B are constants defining the maximum and minimum values of transmittance, t is the time and τ is the restoring characteristic time. We present, in table 1, the fitting results, which show qualitatively the change of the recovery process under the action of the electric field, oscillating at 100 kHz frequency.

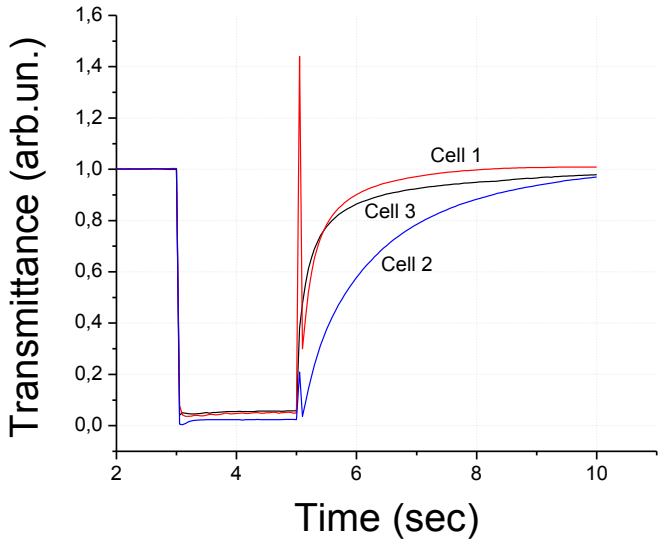

Figure 4.14: Variations of the polarimetric system (the CLC cell placed between crossed polarizers) transmittance during the excitation and restoration processes for three cells under the action of the same restoration electric field, E=2V/μm: U=10V (cell 1), U=16V (cell 2) and U=10V (cell 3).

Table 1: Helix restoration characteristic times for diferent restoration voltages.

Restoring voltage (RMS Volts)	0	5	10	15
Restoring characteristic time τ (sec.)	>10	2	0.35	<0.2

To observe directly the helix restoration process, we used another experimental setup where a fiber-output laser diode was used, operating at $1481\ nm$, lying in the stop band of the CLC mixture (see Figure 4.15) . The laser beam was collimated by a microlens, then passed through the diaphragm (D), polarizer (P) and quarter wave plate ($\lambda/4$). Thus the probe beam became circularly polarized. We measured (at every 0.1 sec) the reflected beam from the CLC cell by using the photodetector (PD) connected to a PC. The cell was very slightly tilted so that the incidence angle was approximately 0.75° off normal.

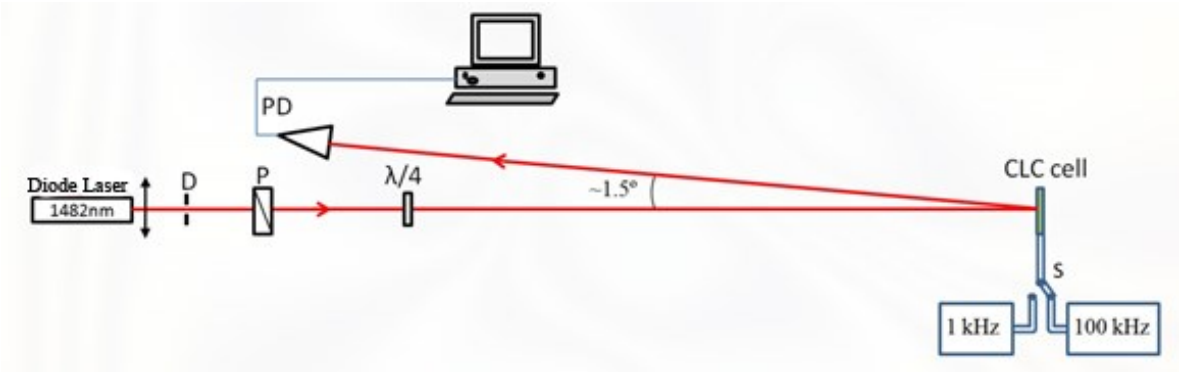

Figure 4.15: Schematic representation of the experimental setup used for observing the helix restoration process. D: diaphragm (~ 1mm diameter), P: polarizer, PD: photodiode, 1 kHz and 100 kHz: voltage sources at different frequencies.

The experimental procedure was similar to the first experiment, where the applied voltage frequency was changed and the photodetector signal changes were monitored during the excitation and relaxation processes. The CLC had planar (helicoidal) alignment in the ground state ($U = 0V$) (see Figure 4.16a). Then, a nearly above-threshold voltage ($U = 50V$) was applied to the cell (at $t \approx 3.4\ sec$) with 1 kHz frequency (AC, SIN shaped). The transition of the cell was monitored (approximately

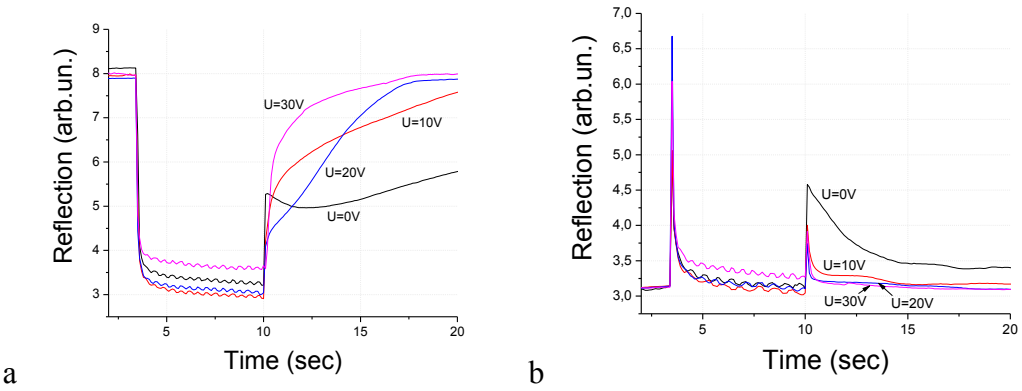

Figure 4.16: a) Right and b) Left circularly polarized ligth's reflectance (from the right handed CLC cell 1) variations in time during the excitation (helix unwinding) and relaxation (helix restoring) processes. There is no voltage applied up to ~ 3.4 sec. The helix unwinding voltage (U=50V RMS, AC, SIN shaped, at 1 kHz) was applied from ~ 3.4 to ~ 10 sec. The restoring voltage (AC, SIN shaped, at 100kHz) was applied from ~ 10 sec up to 20 sec (relaxation voltage RMS values are shown next to curves) .

during 6.6 sec) up to the stabilization of the signal. Then, at $t \approx 10\ sec$, the frequency of the electrical signal was switched (by using a homemade mechanical switch with a typical switching time significantly less than 0.1 sec) from 1 kHz to 100 kHz and the restoring of the initial state was monitored, again up to the stabilization of the signal. Let's emphasize again the three differences from the first experiment: the probe wavelength is inside the cholesteric mixture's bandgap, the probe beam is polarized circularly and we monitor the reflected (from the CLC cell) beam.

4.5 Results

First right and then left circularly polarized probe beams were used. We see, in Figure 4.16 a), that the application (at $t \approx 3.4$ sec) of the unwinding electrical field (oscillating at 1 kHz) decreases the reflected beam's power abruptly. When we switch off the applied voltage, the reflection starts to increase but very slowly. Other curves (in the Figure 4.16 a)) show that the application and the increase of restoring voltage (at frequency of 100 kHz) accelerates the recovery process (curves $U = 10V, U = 20V$ and $U = 30V$). If, in the case of $U = 0V$, the recovery process is much longer than 15 seconds, in the case of $U = 30V$ ($\sim 6\ V/\mu m$), the reflection is restored in approximately 7 seconds. Figure 4.16 b) presents the results of a similar measurement but performed for the opposite circular polarization (probe is left circularly polarized and the helix is right – handed). We see, that the probe beam reflection is the same (at least the same order of magnitude) after stabilisation in all three time intervals: 0 – 3.4 sec (planar / helicoidal), 3.4 – 10 sec (homeotropic) and from 10 sec to the end (restoring the planar / helicoidal structure).

To obtain some approximate characterization data for the acceleration of the forced restoring, we used a similar fit with the equation $T = A - B \times \exp(-t/\tau)$. From each fitting we have taken a value of τ (the time during which the transmittance changes e times). Fitting has been done for the right (resonant) circularly polarized light, Figure 4.16 a). Figure 4.17 shows the results of the fitting. It is clear that the application of the restoring electric field makes the relaxation process faster. The electric field U=30V (oscilating at 100 kHz of frequency), makes the process faster by a factor of 20 compared with the case of free relaxation.

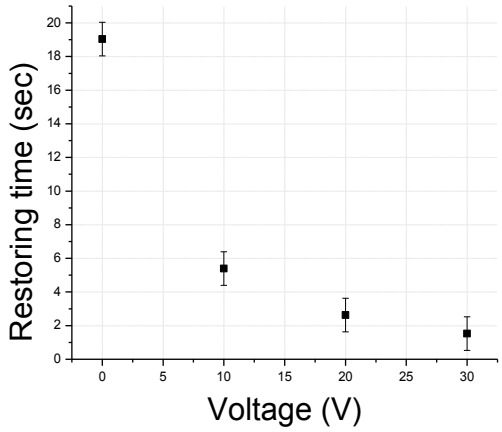

Figure 4.17: The helix restoring characteristic time's dependence upon the applied voltage at 100 kHz for the 5µm thick cell filled with the Mix3.

4.6 Summary and Conclusions

We have shown that the helix restoring process of a cholesteric mixture may be accelerated (by approximately an order of magnitude) by the use of high frequency electrical field where the dielectric anisotropy of the mixture is negative. Thus, the applied field helps to restore and to stabilize the helix. We have also studied the process of electrical unwinding to show that the process takes place through the simultaneous generation of multiple defects. In contrast, the free relaxation process of the helix restoring involves the formation of long disclination walls and their merges.

Despite the good acceleration obtained, the restoring process is still not fast enough, e.g., for telecommunication or imaging applications. Further optimization of composition, thicknesses and driving voltages and frequencies must be done before a practical use of the composition.

Acknowledgment

We thank the financial support of Canadian Institute for Photonic Innovations (CIPI), Fonds Québécois de la Recherche sur la Nature et les Technologies (FQRNT) and Natural Sciences and Engineering Research Council of Canada (NSERC).

Additional spectral experiments, completing the subject, in the visible region of light are realized and are presented in appendix 2.

Chapter 5
Band Gap Tuning

Almost all the observations of CLCs are connected with the PBG. That is natural, because this is the presence of PBG that gives unique properties to CLCs (at least among other LC types). The uniqueness of CLCs among other PBG materials is the possibility to tune its properties which gives them the possibilities to be used in various tunable devices (see introduction). So the tuning of the PBG of CLCs is one of the most interesting subjects of CLCs. Different approaches have been adopted to tune CLC pitch, thus, the spectral position of BG. As we already discussed in the introduction chapter (chapter 1) it can be tuned by temperature, by electric or magnetic fields, etc.

In the current chapter we present another method for tuning the PBG of CLCs which is based on electro-mechanical deformation of cell substrates and the collective self-adaptability (to external conditions) of CLC molecules.

So, the present chapter is based on article manuscript that discusses the electromechanical tuning of the BG CLCs. Accompanied with monotone decrease of PBG central wavelength, drastic changes of the wavelength are observed and discussed.

Résumé de l'article inséré

Sauts électro-optiques dans des structures hélicoïdales naturelles à bande interdite

Un effet électromécanique fort est utilisé pour générer et étudier l'auto-adaptation du pas d'hélice formé naturellement dans une couche de cristal liquide cholestérique. L'anisotropie négative diélectrique a permis d'assurer la stabilisation de la structure hélicoïdale de la couche pendant l'application du champ électrique qui a aussi changé l'épaisseur de la couche de cristal liquide en pliant le substrat mince de la cellule. Cette déformation de la couche a généré un accord (et des sauts) de longueurs d'onde de la bande interdite. Les études spectrales et morphologiques de la matière durant ces sauts sont présentées.

Optics Express, Vol. 19, Issue 5, pp. 4611-4617 (2011)

Electrooptic Jumps in Natural Helicoidal Photonic Bandgap Structures

Karen Allahverdyan and Tigran Galstian*

Center for Optics, Photonics and Laser,Department of Physics, Engineering Physics and Optics, Laval University,Pav. d'Optique-Photonique, 2375 Rue de la Terrasse, Québec, G1V 0A6, Canada

* galstian@phy.ulaval.ca

Abstract

Strong electro mechanical effect was used to generate and study self-adaptation and pitch jumps in a helicoidal photonic bandgap structure naturally formed by a cholesteric liquid crystal. The negative dielectric anisotropy of the material allowed its stabilization by the electric field and important thickness changes, achieved thanks to the use of a very thin substrate, allowed the observation of multiple dynamic jumps at fixed deformation conditions. Spectral and morphological studies of the material during those jumps were performed too.

OCIS codes: (160.3710) Liquid crystals; (160.5293) Photonic bandgap materials.

Helicoidal periodic structures, such as cholesteric liquid crystals (CLCs) [5], are one-dimensional photonic band gap (PBG) materials, which are present in nature in different forms [74]. Those are very promising systems for tunable distributed feedback lasing [28], [29, 79], large band reflection [76], tunable filtering [77, 78, 80], etc. In addition to their spatial periodic character, CLCs have unique vectorial properties, which are related to their helicoidal nature and which affect significantly the character of modes of the PBG [5]. Thus, for example, the eigenmodes of such a PBG are circularly polarized waves and the momentum conservation requirement prohibits the existence of higher order Bragg reflections at normal incidence [5, 73]. This well-known phenomenon is demonstrated in Figure 5.1, where we can see the transmittance spectra of a mono domain cell filled with a CLC mixture, composed of 46 wt % of CB15 (from Merck) and 54 wt. % of a homemade nematic liquid crystal 1756-6: the absence of the second order Bragg reflection is shown by the vertical arrow. Another unique property of those structures is their 'spatial adaptivity'.

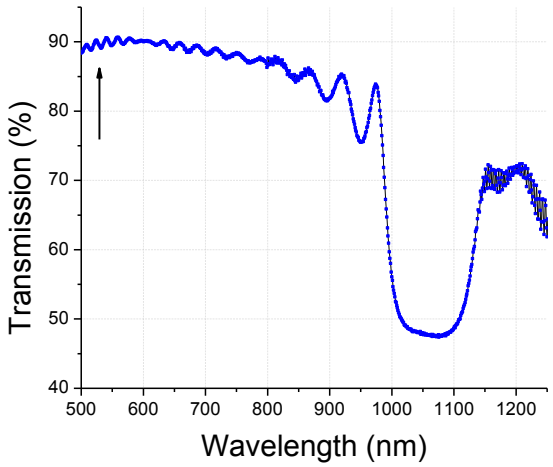

Figure 5.1: Transmittance spectra of a CLC mixture, measured with an unpolarized probe beam, demonstrating the key characteristics of a CLC: the absence of the second order Bragg reflection (shown by the vertical arrow) and the large bandwidth of the resonance defined by the local anisotropy of the CLC.

That is, the chemical composition and the molecular chirality of the CLC define the natural period, P_N, of the complete helical molecular rotation ($by\ 2\pi$) for 'free' boundary conditions only. In reality, there are always given boundary conditions, which define the 'adjusted' period, P_A, of the helix depending on the distance, L, of substrates of the cell that

contains the CLC, and on the molecular anchoring conditions on those substrates. Thus, if the alignment angle of the director, $\vec{n}$ (the average alignment of molecular axes [5]) on two opposite substrates (at $Z = 0$ and $Z = L$) of the cell is fixed by strong boundary conditions – say providing a total rotation of $\theta(L)$ – then the P_A of the CLC will naturally be 'self-adjusted' to provide a constant rate of the spatial rotation, $Q \equiv \partial\theta/\partial z = 2\pi/P_A$, of its director in a way to satisfy the above mentioned boundary conditions with $\theta(L) = 2\pi L/P_A$. The associated (to this adjustment) energy of the director's deformation will be counter-balanced by the anchoring energy of substrates. This total rotation angle may be split into N_C complete rotations (of 2π) and some additional rotation $\theta(L) = 2\pi N_c + \delta\theta$. Thus, we have $N_c = L/P_A$ for $\delta\theta = 0$, which is the case of the present experiment (see below). It must also be noticed that, given the local equivalence of the directions $\vec{n}$ and $(-\vec{n})$, the optical periodicity and corresponding resonance wavelength, λ_R, of the CLC are defined by the half period, $P_R = P_A/2$, of the helix (corresponding to director rotation by the angle, π [5]) as $\lambda_R = 2n_{av}P_R$, where $n_{av} = \frac{n_o+n_e}{2}$ is the average refractive index of the CLC. That is why the number of those half-helixes (or pitches) $N = 2N_c$, is often used for the analyses of the CLC behaviour.

Finally, the value of P_R depends also on various external stimuli, such as temperature, electric and magnetic fields [5, 28, 29, 73, 74, 76-79, 81, 118]. This dependence has attracted significant interest in the view of possible applications in dynamic electro-optic modulation devices (also see Ref [3]). In particular, the behaviour of CLC under the action of electric field has been intensely studied for CLCs having positive and negative dielectric anisotropies, $\Delta\varepsilon$ (see Ref [66] and references therein). So far various mechanisms of P_R modulation have been considered, but finally the electromechanical deformation induced by DC voltage was clearly identified as the dominating mechanism in CLCs with negative $\Delta\varepsilon$ [66]. This work reported very interesting data and analyses, including the detailed description of smooth variations of λ_R upon the electric field induced deformation of cell substrates. The possibility of dynamic breaking of the boundary condition, to change the number of pitches by jumps, was briefly mentioned in the stationary excitation regime and also was demonstrated when the clamp holding the sample was periodically tightened and loosened [66].

In the present work, we investigate this phenomenon but in much stronger excitation regime. This was achieved using a very thin cell substrate under AC voltage. We showed that those CLCs can demonstrate multiple abrupt transient pitch changes even at a stationary regime of excitation, for certain predetermined values of the fixed electric field (without tightening and loosening the clamp) and that this "jumping" process happens through formation of a transient disclination (the line of the abrupt change of the director orientation) while the other helical characteristics are unchanged.

The material composition used in the present work was the mixture, CB15, purchased from Merck and used without modifications. It is a CLC with a negative $\Delta\varepsilon$. Consequently, the applied electric field stabilized the helix. The cell was built using an ITO coated glass substrate of thickness 0.7 mm, which was additionally coated by a uniformly rubbed planar alignment Polyimide (PI 150, from Nissan). An adhesive wall was dispensed on the periphery of this substrate providing a square shaped working area (an optical window) of $\approx 6.5 \text{ x } 6.5 \text{ mm}^2$ size. The adhesive contained spacers to provide the desired thickness of the cell, $L = 5$ μm (± 0.5 μm). Then a second substrate, similar to the first one, but with thickness of 0.1 mm, was pressed on the first one and the peripheral adhesive was photo-polymerized using a UV lamp exposure. The CLC mixture was then injected into the obtained sandwich-like cell by capillary action at room temperature. All our experiments were carried out at room temperature (the isotropic phase transition of the CB15 taking place approximately at $37.5℃ \pm 0.5℃$).

We started our experiments with spectral studies, using a Sciencetech spectrophotometer with THI Halogen lamp and LDA 2000 monochromator. It is interesting to note that the transmittance spectra (Figure 5.2) of obtained cells were not perfectly symmetric, which could be related to the imperfections of the helix (the tilted domains could generate an effective 'blue shift' of reflection) as well as to the non-ideal collimation of the probe beam (which creates an artificial 'apodization' effect of the grating structure). However, it is also important to mention that even in perfect experimental conditions the resonance of a CLC has a certain width, $\Delta\lambda$, which is defined as $\Delta\lambda = \Delta n P_a$, where $\Delta n = n_e - n_o$ is the local optical anisotropy of the CLC [5].

We analyzed the spectral characteristics of the cell for different voltages applied to ITOs (waiting 5-10 minutes after each voltage change, before taking the data) through the Avtech power supply (AV-151 B-C) generating sine-shaped AC signals of 1 kHz frequency.

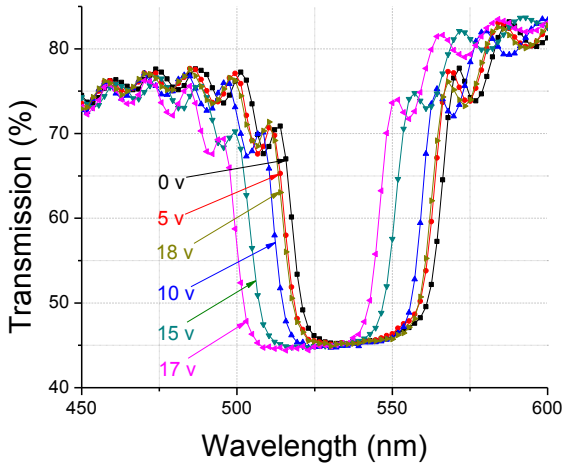

Figure 5.2: The transmittance spectra of the CLC cell for unpolarized input light at different RMS voltages applied to the cell up to the first jump of the pitch (voltages are growing from 0 to 18 RMS Volts; low excitation regime).

As one can see in Figure 5.2 and Figure 5.3, the moderate increase of the voltage leads to smooth changes of λ_R, as already reported in Ref [66]. One of the noticeable differences (apart of the material and AC excitation) here is the slope of this variation, which is very high in our case; approximately 18 nm for 17 V (applied to the 5 μm thick cell), providing thus a shift coefficient $\approx 5.3\, nm/V/\mu m$, which is more than twice the maximum value reported so far [53], due to the thin cell substrate used here.

As we also can see in Figure 5.2, the value of λ_R of the CLC is approximately equal to 0.542 μm in the ground state ($U = 0$). Surprisingly, in spite of the rather large use of the CB15 mixture (from Merck), to the best of our knowledge, there is no information about its optical properties. Therefore, we carried out measurements of its average refractive index, which gave us the following value: $n_{av} \approx 1.567 \pm 0.002$. We can thus estimate the room temperature ($T \approx 21°C$) value of $P_A = 0.542\mu m/01.567 \approx 0.35\mu m$. Thus, for the initial thickness, $L = 5\mu m$, we got for the number of helixes $N = 5/0.35 \approx 14$ (hence, 28 half helixes). In the same time, we could also use the corresponding width of the resonance,

$\Delta\lambda = 40\text{nm}$ (from Figure 5.2) to evaluate the local anisotropy of that compound, $\Delta n = \Delta\lambda/P_A \approx 40\text{nm}/0.35\mu\text{m}$, and this is rather a high value for CLC materials.

The further increase of the voltage shows an abrupt 'return jump' of λ_R,, U $\approx 17V_{RMS}$, see Figure 5.2, the curve for 18 V; and Figure 5.3, the open squares. This jump happens within approximately 3 min at a fixed voltage (observed with a probe beam of the diameter, $\approx$ 1 mm).

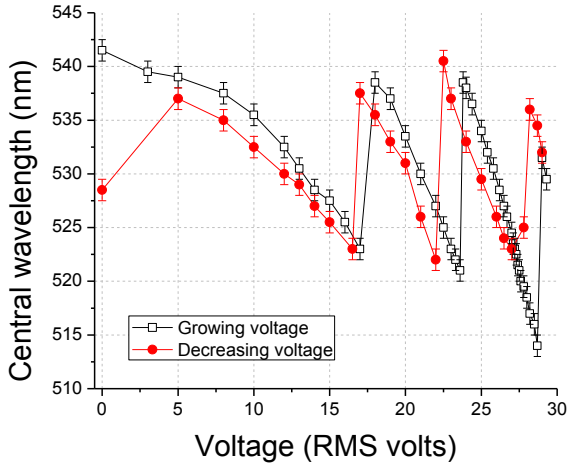

Figure 5.3: The dependence of the resonance wavelength of the CLC on the RMS voltage applied to the cell (growing voltage: the open squares and decreasing voltage: the filled circles).

In fact, with the continued increase of the voltage, we observe multiple zones of such smooth modulations followed by abrupt changes of λ_R. The decrease of the voltage then leads to the inverse transformation (Figure 5.3, the filled circles) with some variations of the positions of the jumps and also of the depth of modulations of λ_R,. This hysteresis-like difference may be related to the mechanical movement of the substrate, which in addition, is coupled with the mechanical movement of the CLC, as well as with a deformation of its director. Thus, the starting point during our experiments was the value, $\lambda_R = 0.528$ µm, or $\lambda_R = 0.542$ µm in a non-regular manner. One needs more studies to better understand the origins of such bistability. It is to be noted that similar phenomena have also been described in [103, 119].

It is clear that the use of a thin (0.1 mm) substrate allowed us to obtain significantly stronger electro-mechanical effect compared to those in [66] (more deformation is obtained at much lower voltages). As we can see in 5.4, the bending of the thin substrate is easily observed (at room temperature) for the light reflected from the cell, after filling it with the CLC (the cell was illuminated by a broadband light of the ambient illumination, and its reflection is observed at the optimal angle to visualize the periodic transverse modulation of the reflection).

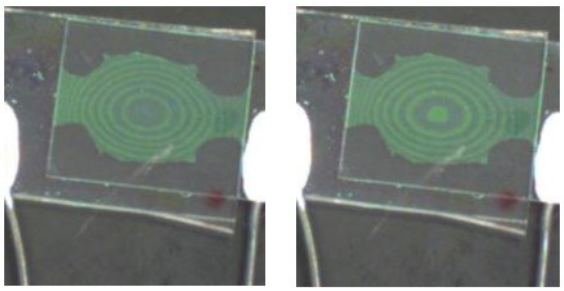

Figure 5.4: The ring structure observed in the reflected from the CLC-filled cell for various voltages. 20 V (the left picture) and 10 V (the right picture). Vertically aligned half ellipsoidal white zones (on the right and left sides of each picture) are the conductive adhesive zones with vertical wires in the bottom zones of the figure.

In fact, the electro-mechanical modulation of the cell thickness, L, is so strong that the energy of director deformation (needed to adapt the value of P_R) is overcoming the energy necessary to create a transient disclination of the director. This disclination is the transition mechanism, which allows the re-adjustment of the P_R for the given value of L, while preserving the overall helical structure of the CLC, as demonstrated in Figure 5.5. In fact, the spectral monitoring of the cell during this transition was done when the applied voltage was set just above the critical voltage, U_c (that was necessary to cause the jump of λ_R). The consecutive moments of the same jump are represented by curves 1 (squares), 2 (circles) and 3 (triangles), taken with approximately 1 min of delay. This monitoring confirms that the spectral and vector characteristics of the resonance do not change significantly during those jumps (obviously, averaged on the area covered by the probe beam, approximately of 1 mm^2) the second order Bragg reflection always being non-observable (not shown here).

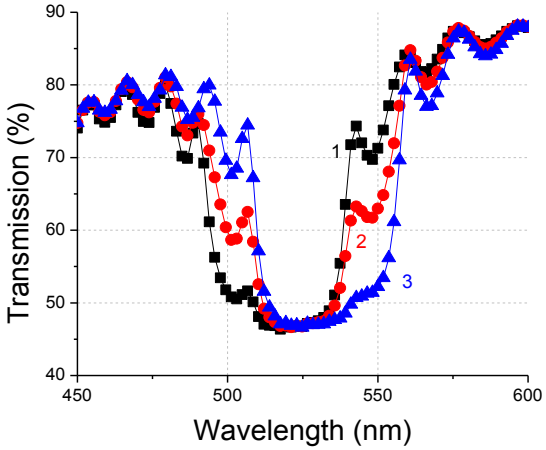

Figure 5.5: Spectral modifications of the cell during the evolution of the disclination (at a fixed voltage, slightly above the jumping threshold voltage) allowing the re-adjustment of the helix pitch. The consequent spectra (labelled 1, 2 and 3) are taken with approximately 1 min of delay.

Observations of the same transition, using Zeiss polarizing microscope, allowed the confirmation of the above-mentioned scenario. As it can be seen in Figure 5.6 (bottom left), in this particular case, the disclination is generated almost simultaneously in the top right corner and the left side of the picture, when the voltage exceeds the threshold value, 20V (which, by the way, differs from cell to cell, but also can be slightly different for the same cell from experiment to experiment, on approximately by $\pm 10\%$). Then, for a fixed voltage (20 V), the left-side disclination wall propagates faster and merges with the top right corner zone, providing a stabilized CLC with a new P_R. It must be emphasized, however, that this picture shows only the central part of the cell where the disclination walls usually appear. From cell to cell, various surface or volume defects were at the origin of those disclinations.

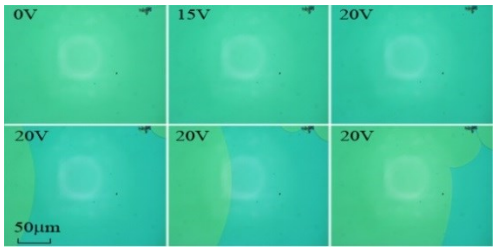

Figure 5.6: The microscope observation of the transient propagation of the disclination wall allowing the establishement of a self-adjusted (to the new value of L) period of the director rotation. Consequent pictures (at 20 V) were taken with about 0.5 min of delay.

Discussion

One can notice (from Figure 5.3) that the slope of the dependence, $\lambda_R(U)$, in the first zone (for voltages below 17 V) is relatively smaller and the corresponding voltage range of smooth changes (before the first jump) is rather broad. In contrast, the slope increases and the smooth zone width decreases for further zones. This is consistent with the hypothesis of periodic generation of transient disclination lines allowing the jumps of P_A. In fact, for a given value of cell thickness, L, its reduction, ΔL, must be redistributed equally on the number of the pitches and the director rotation rate, Q (between the jumps) must then be increased consequently: $Q + \Delta Q = \frac{2\pi}{P_{A0} - \Delta L/N_c}$, to reduce the initial period, P_{A0}, of the helix on the amount, $\Delta L/N_c$. In the same time, the appearance and propagation of the disclination wall is rather a complex phenomenon [5, 103, 119, 120]. The situation here is further complicated due to the presence of the mechanical movement and stabilizing electrical field (since $\Delta\varepsilon < 0$). Qualitatively, we can imagine the process of observed pitch jumps as the transient analogy of structures observed in the stationary Cano wedge cell [121, 71]. This analogy however is limited to the role of disclination wall splitting two neighboring zones with clearly distinguishable pitches. Closer analysis of the disclination wall, dynamically propagating from the left corner, shows that its width is of the order of $l \sim 3$ μm with some 'fine structure' (not shown here) of the light transmittance modulation (across the wall) with characteristic sizes of ≤ 0.5 μm. In the same time, the character (and structure) of the disclination line, which started from the top right corner, is different, which perhaps could explain its lower spatial mobility. More studies must be conducted to understand this difference, but the possibility of generating singularity lines of different forces has been already discussed in the literature [5]. For the moment, in a very rough approximation, we could imagine that the additional density of free energy (due to the additional rotation rate, ΔQ, allowing the pitch adaptation) could be estimated to be of the order of $F_A \sim 0.5 K_2 \Delta Q^2$, where K_2 is the twist elasticity constant, typically of the order of 10^{-6} erg/cm [5]. Given the complexity of the disclination wall (including various types of deformation), we could consider the so called one-constant elasticity approximation ($K_1 = K_2 = K_3 \equiv K$) to evaluate the corresponding energy very roughly. Thus, with the scale of this deformation, l, the corresponding energy, $F_{d,}$ might have been estimated by the following expression, $F_d \approx$

K/l^2 [5]. Thus, the generation of the disclination wall will be energetically justified for voltage values (and corresponding deformations) satisfying the condition, $F_A \geq F_d + \Delta F_s$, where ΔF_s is the difference of anchoring energies before and after generation of the disclination. In the framework of the present approximation, we considered the ΔF_s to be independent on the cell thickness (it could be interesting to use the experimental technique described here to estimate the surface anchoring potential. Thus, for approximately the same value of F_d, the pitch jumps should happen when the thickness reduction, ΔL, would generate the critical change of rotation rate, $\Delta Q^2 \approx 2(Kl^2 + \Delta F_s)/K_2$. Given the definition of $\Delta Q = 2\pi\Delta L/P_{A0}(N_c P_{A0} - \Delta L)$, we obtain, for small deformations ($\Delta L \ll L$), that the critical values of ΔQ (and the corresponding pitch jumps, too) would be achieved for larger values of ΔL if the number of pitches, N_c, was initially high. In the same way, the slopes of both dependences, $\Delta Q(\Delta L)$ and $\lambda_R(\Delta L)$, would be higher for lower values of N_c. Both the above-mentioned hypotheses are in agreement with our experimental observations (Figure 5.3).

In conclusion, we believe that using a thin cell substrate the present work allowed us to observe a significantly higher electro-optic effect. The combination of two conditions (more flexibility and the helix stabilizing field) allowed us to generate multiple pitch jumps. The spectral and polarizing microscope observations confirmed that the key features of the helix were preserved and the self-adaptation proceeded via transient disclination propagation. This work, however, also shows that the modulation range of λ_R in these self-adaptive CLCs is limited (in our case, to approximately $\pm$ 5%) due to the self-adaptivity of the CLC, which generates transient disclination and re-adjusts its period when the deformation of the pitch becomes energetically 'unfavorable'.

Acknowledgments

We acknowledge the financial support of Canadian Institute for Photonic Innovations (CIPI), Fonds Québécois de la Recherche sur la Nature et les Technologies (FQRNT) and Natural Sciences and Engineering Research Council of Canada (NSERC). We also thank TLCL Research Optics inc for the material support.

Chapter 6
Summary and Conclusion

The main results of the present thesis are included in four chapters (2-5). Each chapter is based on a published work (in reviewed scientific periodicals). We can divide those four chapters into two branches, one of which concerns the optical and the other the electro-optical investigations of CLCs.

The first part, chapter 2 and chapter 3, is devoted to the optical properties of CLC layers. The subject of these investigations is the influence of optical boundaries on light propagation. Some interesting phenomena were observed and discussed, the key factors of which are the helicoidal periodic structure of CLCs and mismatched boundary conditions. Symmetric (chapter 2) and asymmetric (chapter 3) boundaries are considered. It is experimentally shown that the light propagation through a Fabry-Perot resonator filled with CLC (gyrotropic media) can effectively change the CLC layer optical properties, depending on optical properties (the refractive index) of limiting materials and on the input polarization of the probe beam. Theoretical simulations (conducted by collaborators) are in good agreement with the presented results.

The investigations of the CLC layer surrounded by asymmetric optical boundaries led us to a non-reciprocal light transmission effect in those materials. This effect was explained (in the first approximation) and it is in a good qualitative agreement with results of theoretical simulations (conducted by collaborators). It is important to mention here that the non-reciprocal transmission occurs in the cells having negligible absorption, and without any non-linear interaction or any kind of external field. The observed non-reciprocity is caused by the combination of a helicoidal BG material and asymmetric boundaries.

The second part, chapter 4 and chapter 5, mainly concern the electro-optical properties of CLC layers, discussing the PBG changes under the influence of external electric fields.

A dual frequency NLC was used in a CLC mixture that let us obtain a dual frequency CLC. Then, applying electric fields of different frequencies, we carried out transitions between

the planar (helicoidal) and homeotropic states of the CLC cell. Different authors (see chapter 1) reported switching between the planar (helicoidal) and focal conic (scattering) states or between the homeotropic and focal conic states. The novelty we introduced was the fast restoration of the helicoidal structure and the switching between the transparent and semitransparent states (the two non-scattering states). The polarizer free electro-optical light modulators working in IR region are demonstrated in chapter 4, and the modulators working in the visible region are demonstrated in appendix 2. Dynamics of transitions were investigated under a polarizing microscope. Dynamic spectral observations were conducted as well.

A CLC with a negative dielectric anisotropy is used in chapter 5. Consequently, the field did not realign the CLC molecules, moreover, it quenched the orientational defects. The influences of electric-field induced deformation of the cell substrates are investigated. The collective self-adapting effect of the CLC layer with strong (mechanical) boundary conditions allowed us to tune the spectral position of the PBG. The helicoidal structure of CLC responded like a spring and readjusted its pitch with deformations of the cell (a slight change in the CLC layer thickness). Finally, the change of the CLC pitch resulted in a change of the BG central wavelength.

In conclusion, we present the main achievements and results of the thesis:

- We experimentally demonstrated that the transmittance of a plane polarized probe beam through a CLC Fabry-Perot slab can be modulated by varying the incident beam polarization angle (respected to the cell rubbing direction). An experimental ratio (the modulation depth) of 1.3 was achieved. It was shown that the ratio can be increased by simply increasing the refractive index mismatch between the CLC and limiting materials.
- Non-reciprocal transmission of the probe beam through a CLC cell with asymmetric boundaries was experimentally demonstrated. A non-reciprocity coefficient of 0.98 was achieved experimentally. The phenomenon was schematically explained and a value of 0.95 was estimated for the non-reciprocity coefficient. Again, the non-reciprocity coefficient can be increased by increasing the asymmetry of boundary conditions (the difference in refractive indexes).

- It is shown that the key peculiarities of the non-reciprocal transmission are the asymmetric boundaries of the CLC cell and the helicoidal BG structure of CLC. It was experimentally demonstrated that those factors are both crucial and the absence of any of them leads to the absence of non-reciprocity.
- The use of the CLC with a negative dielectric anisotropy allows quenching the orientational defects in the layer of CLC and an increase of abruptness of the BG of the CLC layer with homeotropic aligned boundaries.
- The use of a dual frequency CLC allows accelerating the restoration of helix (from homeotropic to planar - helicoidal state) and realise switches between semi-reflecting and all-transparent states. The helix restoration rate was accelerated by a factor of ~20.
- A thin cell substrate was used to build a cell and electromechanical tuning is realised due to deformation of cell substrates caused by electric field: ~20nm blue shift of BG is acheaved for applied voltage of 17V RMS.

The obtained results can be used in different applications and can serve for other academic investigations. For example, the reported effect of non-reciprocal transmission has promises of different applications such as the high - rate telecommunications. The further optimisation of reported structure (especially the optimisation of limiting optical conditions) can lead to technological applications in the field of data interconnects. The further investigation of the phenomena and its association with similar structures in Nature can reveal the role of those structures in Nature.

The results concerning to PBG control of CLC layers have diverse potential technological applications, as well. The most promising applications are the reflective CLC displays and the “smart windows”. Still, further investigations and optimisation are needed. These are especially the decrease of operational voltages and the response times.

Appendix

Appendix 1: Non-Reciprocal Transmission of Light

Below, we present some additional measurements that confirm (once again) some statements made in chapter 3 (these results were not included in the article because of its shortness). To do that we first obtained additional transmittance spectra of the same asymmetric cell, as in chapter 3. This time, the probe beam was linearly polarized. Two orthogonal polarizations and an opposed propagation directions were considered.

In the Figure A.1 we can clearly see that the non-reciprocal transmission appears for linear polarized beams, too. Thus, non-reciprocity was observed for all the (considered) polarizations of the probe beam. In both circular (Figure 3.3) and linear (Figure A.1) cases, the non-reciprocities of opposed (or orthogonal) polarizations have different signs and equal absolute values. By non-reciprocity we mean: $\Delta T = T_A - T_B$, where T_A and T_B are the transmittance values for any fixed wavelength (inside the BG) in the directions from A to B and from B to A, respectively.

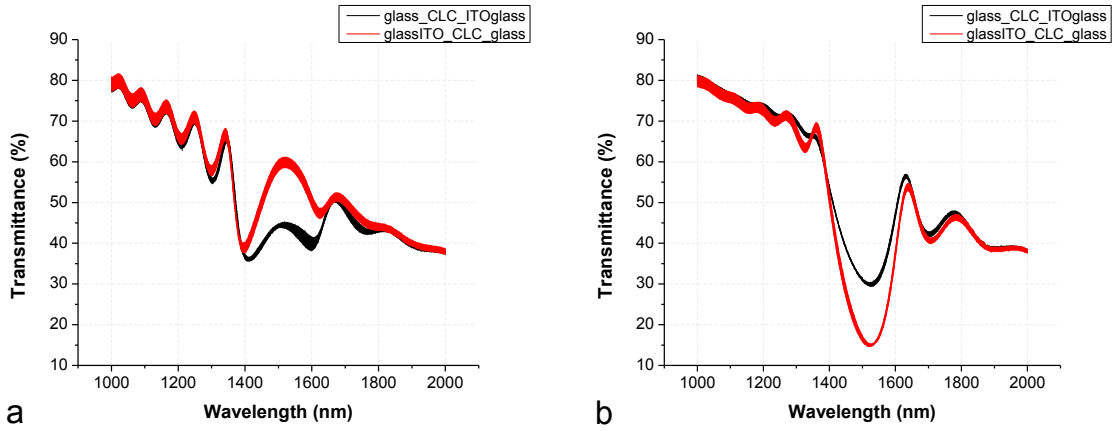

Figure A.1: The transmittance spectra of the parallel (a) and perpendicular (b) polarized (respected to the rubbing direction) probe beams through the CLC cell for two opposite directions of propagations.

The above mentioned equivalence of the absolute values comes to confirm the theoretical result that there is no non-reciprocal transmission for an un-polarized probe beam. For the un-polarized beam, the non-reciprocity can appear only in the reflection and absorption if there is some absorption in the cell. We did not carry out experiments with the un-polarized beam, because the used spectrometer beam was slightly polarized (elliptically), probably caused by multiple reflections inside the device.

To confirm that the CLC layer has a major role in the non-reciprocal transmission effect, we built two extra cells, having exactly the same characteristics (same thickness, same substrates etc) except for the layer between the glass substrates. One of the cells was filled with a NLC (the anisotropic, non gyrotropic media) and the other one was empty (the isotropic, non gyrotropic media). Then we repeated the measurements (using the linearly polarized probe beam) and we can see in the next graphs (Figure A.2b and Figure A.3) that there is not any non-reciprocal effect observed in these cells which do not possess any helical structure.

In Figure A.2a the transmittance spectra of the glass substrates that were used for cell fabrication (an ITO coated glass and a polyimide coated ordinary microscope glass) are presented. We can see that there is not any non-reciprocal behaviour in the glasses, too.

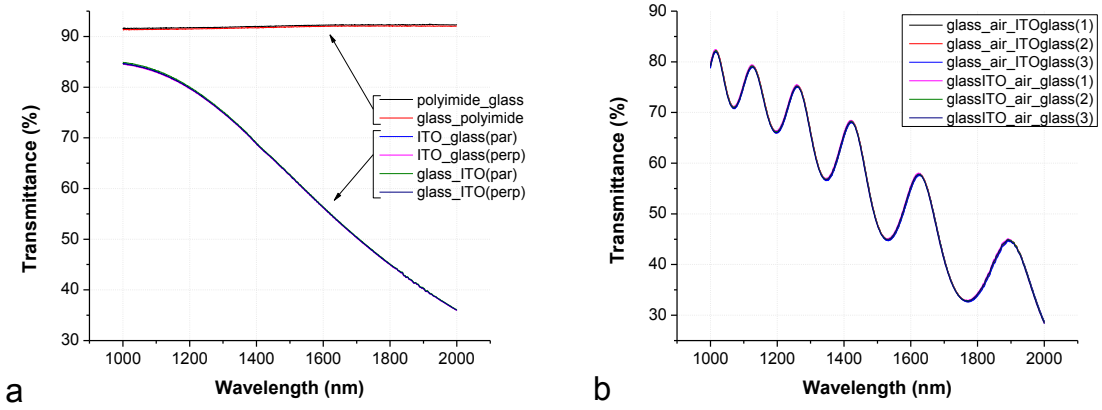

Figure A.2: The transmittance spectra of the glass substrates used for the cells (a) and for the empty cell which was then filled and used in the experiments (b). The spectrometer beam was polarized linearly

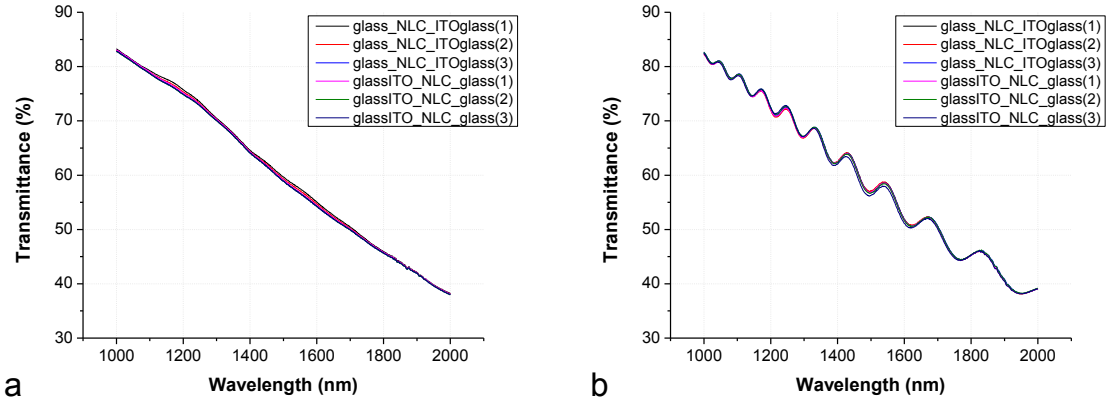

Figure A.3: The transmittance spectra of the asymmetric NLC cell for the two opposite directions of propagation of the probe beam. The spectrometer beam was polarized linearly, parallel (a) and perpendicular (b) to the rubbing direction.

Once again, Figure A.2b and Figure A.3) show the absence of non-reciprocity in the cells with asymmetric boundary conditions but filled with NLC (anisotropic) or air (isotropic). The Figure A.4 shows the absence of non-reciprocity in the symmetric cell filled with the same CLC mixture we had used in the experiments where non-reciprocity was observed.

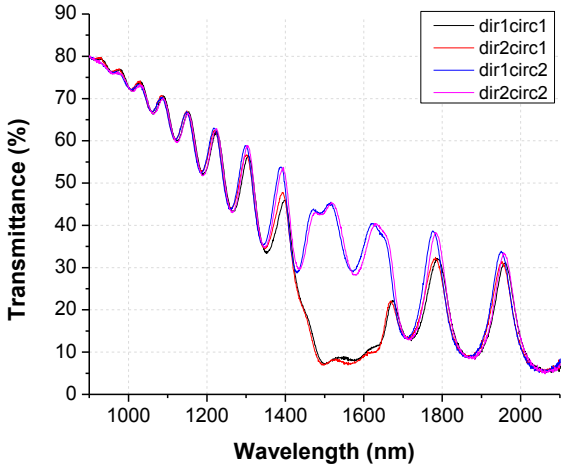

Figure A.4: The transmittance spectra of an ordinary (symmetric) CLC cell: the CLC layer was sandwiched between two identical glass substrates) for the right and left circularly polarized probe beams and for two opposite directions of propagations.

Combining the results of Chapter 3 and these measurements we can conclude that the observed non-reciprocal transmission is resulted by gyrotropic properties (by the helicoidal structure) of the CLC, as well as by the asymmetric boundary conditions (by the difference of the refractive indexes). They both are essential, and the absence of one of them leads to the absence of the non-reciprocal transmission.

Appendix 2: Reconstruction of Chiral Structure with Visible Band Gap

Below, we continue the investigation of the planar-homeotropic and homeotropic-planar transitions of the CLC cell as it was carried out in chapter 4. Here the difference is in the use of another CLC mixture with a BG lying in the visible range of light. In contrast to chapter 4, here we concentrate on the spectral investigations of processes. Both transmittance and reflectance spectral measurements were realized.

Materials & cell fabrication

The dual frequency NLC (MLC 2048, purchased from Merck) with the ordinary ($n_o = 1.5$) and extraordinary ($n_e = 1.72$) refractive indexes was mixed with the chiral dopant (1-phenyl-1,2-bis4-(trans-4-pentylcyclohexylbenzenecarbonyl) ethane, from AWAT Co. Ltd), in order to obtain a dual frequency CLC. Several mixtures with different concentrations were prepared but the results obtained for only one of them are reported in the present work. We did all the experiments using the same mixture with the following compound proportions: 90.4 wt. % of NLC and 9.6 wt. % of chiral dopant. The choice of the mixture was based on its Bragg reflection band, lying in the range of 560nm - 630nm. As it is well known, the period and, consequently, the BG position in the transmittance (or reflectance) spectrum of a thin layer of a CLC, among other parameters (temperature, external fields, etc.) depends on the concentration of chiral molecules in the cholesteric mixture [73]. Thus, we chose the concentration that best corresponded to our requirement, which was: to have a BG in the visible range of light. As it is already mentioned in chapter 4, the dielectric anisotropy of the NLC we used (MLC 2048) is positive for the frequency range of ~1-50kHz and is negative for ~50kHz-1MHz (see Figure 4.9). The molecules of the NLC with a positive dielectric anisotropy ($\Delta\varepsilon > 0$) tend to point their long axes parallel to the

applied electric field and the molecules of the NLC with a negative dielectric anisotropy ($\Delta\varepsilon < 0$) tend to point their long axes in the plane that is perpendicular to the applied electric field. Consequently, the orientation of molecules (with respect to the external electric field) of the dual frequency NLC depends on the frequency of the electric field, and the use of the dual frequency NLC as a host compound in the cholesteric mixture made possible to obtain a dual frequency CLC.

A standard LC cell was assembled and filled with the above mentioned CLC. The cell assemblage procedure was the following. The ITO (indium tin oxide) coated glasses were first coated with a thin surfactant layer of Polyimide (PI 150) and unidirectionally rubbed in order to give the LC molecules the preferred direction for their planar orientation. The glass substrates were then glued one to the other taking care that their ITO coated sides and rubbing directions were faced to each other. An adhesive NOA 65 was used as the glue and the spherical glass spacers with 5 μm of diameter were dispersed. Due to the glass spacers, the glass substrates were separated from each other by the 5 μm thick gap. Initially empty (filled with air), the above-mentioned gap was then filled with the CLC mixture, using the standard capillarity method.

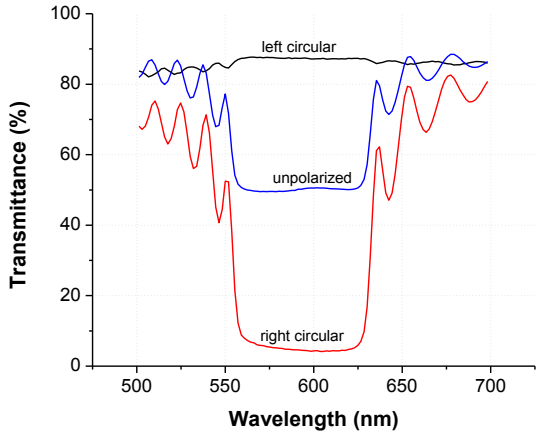

Figure A.5: The transmittance spectra of the planar aligned CLC cell for un-polarized, resonant circularly polarized (right) and non – resonant (left) circularly polarized probe beams.

In Figure A.5 the transmittance spectra of the assembled cell for three (the right, left circular and natural) polarizations of the normal incident white beam are presented. As we

can see, the right circularly polarized light is almost totally reflected from the CLC cell (only ≈ 5% of transmittance) in the BG region while the left circularly polarized light is transmitted without 'feeling' the periodic structure and without producing a BG. We can also see, that the BG limits are not perfect but rather abrupt. So we can consider that we have a good helicoidal structure which does not have major orientational or non - orientational defects such as disclination lines or impurities in the LC material.

Transmittance: the Experimental Setup

A.6 shows the scheme of the experimental setup that was used for measurements of the transmittance spectra of the CLC cell in different states. The ScienceTech spectrometer was used which consisted of the white light halogen source (1) and the monochromator (ScienceTech LDA 2000). The system recorded the spectra at every 50ms.

The diaphragm aperture, D, was ~1 mm, so the incident white probe beam had 1 mm diameter. The light polarization was set to be circular by the polarizer (P) and the broadband quarter-wave (λ/4) plate. The following experiments were done using right and left circularly polarized probe beams. The quarter-wave plate axis was inclined at +45° or – 45° with respect to the polarizer axis in order to make the beam circular polarization right-handed or left-handed. The CLC cell was placed close (~1cm) to the monochromator aperture. The aperture being thin enough (~ 100 μm), let pass almost only the directly transmitted light, i.e. the scattered light was not detected.

We used two voltage sources to apply voltage between the ITO layers of the cell. Each of those sources was fixed at one specific frequency (1 kHz and 100 kHz) and these frequencies were not changed during the experiments. To apply (or change) the desired electric field (frequency) we used a mechanical switch (3) that activated the action of the desired source and deactivated the other one. The switching characteristic time was of the order of 10 ms.

As we have already mentioned, we have used the so-called dual frequency CLC mixture, having a dielectric anisotropy sign depending on the frequency of the applied electric field. This is why one of the voltage source frequencies was fixed at 1 kHz, which was in the

positive zone of the dielectric anisotropy and, consequently, the LC molecules tended to point their axes along the electric field. The other source frequency was fixed at 100 kHz, which was in the negative zone and the LC molecules tended to point their axes perpendicular to the electric field direction.

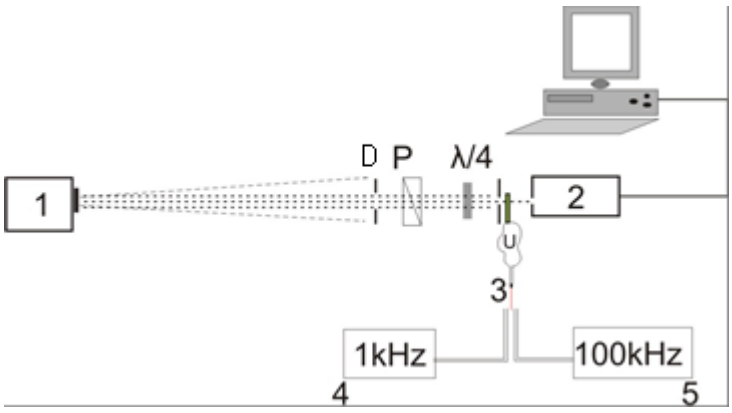

Figure A.6: The experimental setup. 1: light source, 2: monochromator, 3: switch, 4: source of voltage (oscillating at 1 kHz frequency), 5: source of voltage (oscillating at 100 kHz frequency), D: diaphragm, P: polarizer, λ/4: large-band quarter-wave plate.

The Experimental Procedure

The experimental procedure was the following. At the beginning, there was nothing applied to the cell. As the cell glasses were treated for the planar orientation, the CLC formed a planar- helical structure and, as the state was a cell equilibrium one, it would not change if there was no external action applied. Then, to unwind the helical structure, we applied the low frequency (1 kHz) voltage between the ITO layers of the cell. The unwinding voltage for our cell was $U = 80\ V$, i.e. $E = 16\ V/\mu m$. Below we call it 'excitation voltage' and we never changed its value or frequency.

When we applied the excitation voltage, the cell always passed from the planar-helical arrangement to the homeotropic arrangement, where almost all the molecules pointed their long axes perpendicular to cell glass substrates.

In the next step, we changed the frequency of the applied voltage (as well as the voltage value) switching the other voltage source, having a higher frequency (100 kHz). As it was already mentioned, the CLC mixture dielectric anisotropy was negative for the field of 100 kHz. That is why in this case the applied electric field (having a voltage between the ITO

layers) was supposed to help the helix restoration process, because the molecules tended to point their axes in the plane that was perpendicular to the electric field (i.e. parallel to the glass substrates). From now on, we call the voltage frequency, 100 kHz, 'restoration voltage.' Its frequency always was 100 kHz and the voltage value was changed to evaluate the influence of the restoration field on the helix restoration dynamics. We observed the restoration dynamics, observing the changes in the transmittance spectrum during the helix restoration.

Results

The process of transformation of the cell from the planar- helicoidal state to the homeotropic one is illustrated in Figure A.7, where one can see three consequent transmittance spectra of the CLC cell with 50ms of intervals. The 'planar 0 ms' curve corresponds to the moment before the excitation voltage (80V RMS, AC, at 1 kHz) was switched on. As we can see, this process is fast enough: in about 100 ms the helix was completely unwound and almost all the light (~ 80-85%) transmitted through the cell. The difference from the perfect transparency (100%) was partly because of the Fresnel reflections from the interfaces: from the air-glass, glass-CLC, CLC-glass and Glass-air. We can see a transient state (50 ms) appearing between the two key (the planar and homeotropic) states. That state did not last long; its maximum duration was 50ms. Taking into account the fact that the transmittances of both the resonant (Figure A.7a) and

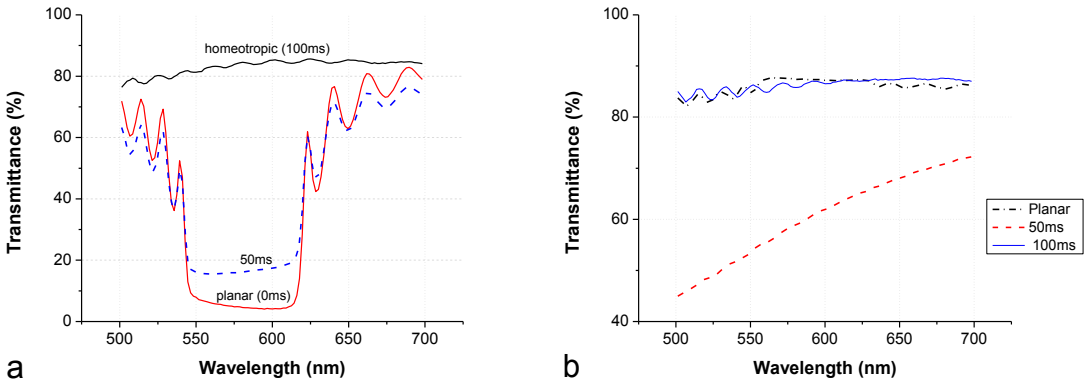

Figure A.7: The helix unwinding process under the action of 80V excitation voltage applied between the ITO layers. The resonant (a) and non-resonant (b) circularly polarized probe beams.

non-resonant (Figure A.7b) circularly polarized beams adapted their final states in less than 100 ms (which meant that the CLC cell was completely transparent), we could take that the helix unwinding times were less than 100ms.

In Figure A.8a we see the transmittance spectra of the CLC cell during the process of the natural (not forced by external fields) helix restoration. Here the cell passes from the homeotropic state to the planar - helicoidal-helical state. The excitation voltage was applied at the beginning which was switched off at the 0 sec instant. As we can see, there is a transient scattering state (of 50 ms) that follows the homeotropic state and that endures less than 100 ms. Starting from 100 ms (or earlier) after switching off the excitation field, the BG started to form which indicates that the helix (the periodic structure) was restoring. The spectra were taken with 50 ms of intervals but here we present only some of them to demonstrate the tendencies. The curve 'planar' is the spectrum of the cell in the planar-helicoidal state, i.e. this would have been the transmittance spectrum if we had waited long enough (about an hour). The complete natural restoration times for the same mixture depend strongly on the cell thickness, that is, the thickness of the LC layer. The thicker the cell, the longer the restoration time.

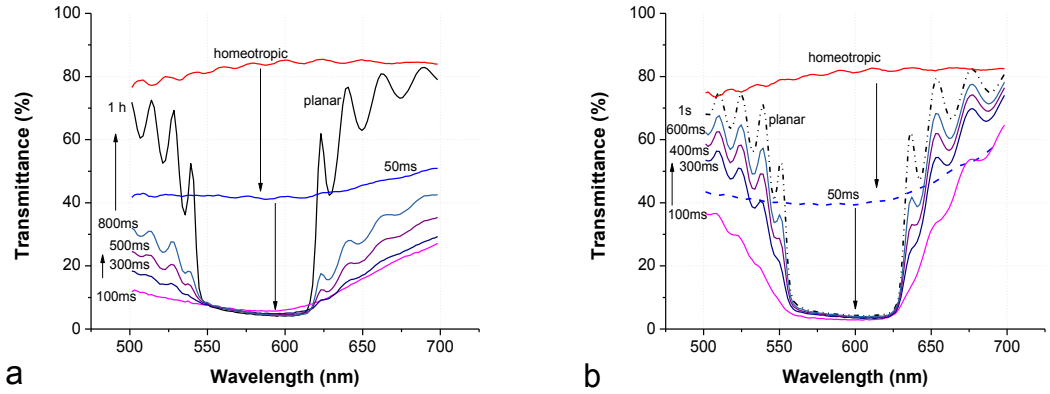

Figure A.8: The helix free relaxation (a) and forced restoration under the electric field U=40V RMS, 100 kHz, AC, Sin (b) the processes (from the homeotropic to the planar). The incident light is resonant and circularly polarized.

The Figure A.8b illustrates the same process as Figure A.8a, but here, instead of switching the voltage OFF and observing the free restoring process, we switched on the "restoration" voltage and observed the forced restoration process. The restoration voltage oscillating at 100 kHz frequency was supposed to 'help' and fasten the helix restoration. Comparing

Figure A.8a with Figure A.8b we can see that there is not a significant change inside the BG. In both cases the transmittance adapts its final value enough rapidly. The important difference we can see in these two figures (Figure A.8 a and b) is that in Figure A.8b the BG wings adapt their final value faster than in Figure A.8a, where there was not any external action during the helix restoration process. There always exists a transient state at 50 ms; its existence does not depend on the fact whether there is an external field applied to system or not. Also, the BG adapts its final value fast enough in both cases. The process does not take more than 100 ms.

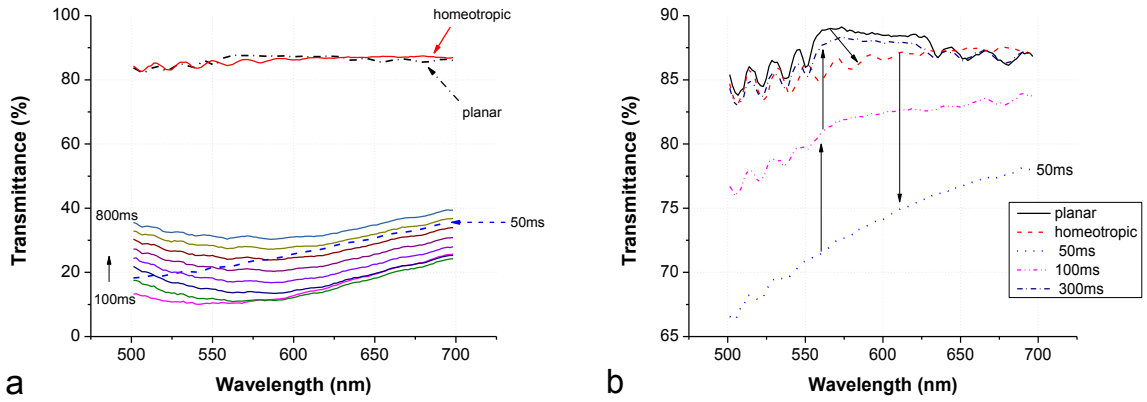

Figure A.9: The helix free relaxation (a) and forced restoration under electric field U=40V RMS, 100 kHz, AC, Sin (b) processes (from Homeotropic to Planar). The incident light is non - resonantly circular polarized.

Comparing Figure A.9 with Figure A.8, and representing the helix free relaxation (a) and forced restoration (b) for the resonant (Figure A.8) and non-resonant (Figure A.9) circularly polarized beams, we notice that the spectrum 'returns back' to its initial state more quickly for the non-resonantly polarized light than that for the resonantly polarized light if the helix restoration voltage is applied. Whereas there is no significant difference in restoration dynamics for those two opposed polarizations if there is no external restoration voltage applied: they both are slow. We will see this in a more detailed way and more evidently in the next graphs.

We can also notice that unlike the resonantly polarized light, in the last two graphs (Figure A.9a and Figure A.9b: the non-resonantly polarized probe beam) the transmittances in both regions (inside and outside the band gap) return to their initial states simultaneously.

In the next two graphs (Figure A.10) the dependences of the transmittance on the time for the resonant and circularly polarized light beam outside (a) and inside (b) the BG are

shown. In each figure we can see the process for different helix restoration voltages. We chose $\lambda = 628\,\text{nm}$ outside the BG, which is the nearest (to the BG) minimum of the oscillations in the transmittance spectrum. And we chose $\lambda = 570\,\text{nm}$ inside the BG, which is the approximate central wavelength of the BG.

At the beginning, there was no voltage applied to the cell. Then, at 360 ms, we applied the excitation voltage (which always was 1 kHz, 80V RMS, AC and a sine-shaped one). For the next step (at 860 ms), we switched the applied voltage to the restoration voltage (which always was 100 kHz, AC and sine-shaped). The voltage values shown in the figure are the restoration voltage values and they are in RMS. (The described process repeats for next two figures, Figure A.10 and Figure A.11).

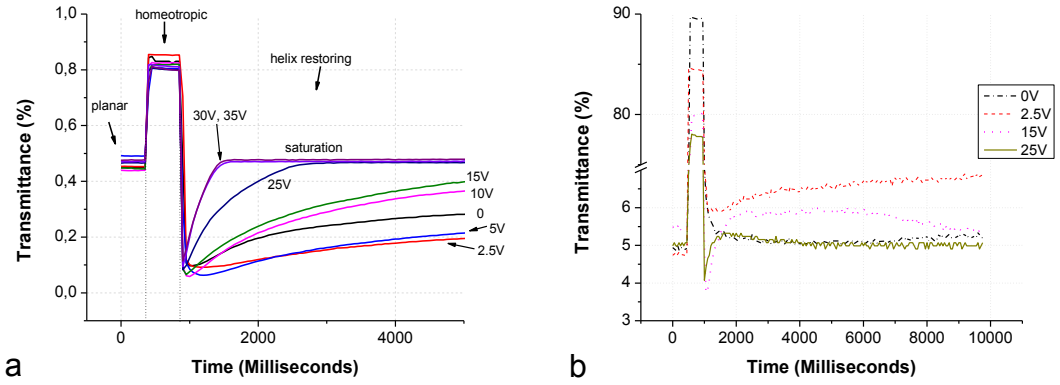

Figure A.10: **The transmittance** dependencies on time during the helix excitation and restoration processes, for various restoration voltages. The probe wavelength is outside (a: 638nm) and inside (b: 570nm) the BG. The light is resonant and circularly polarized**.**

The tendencies in Figure A.10a are a little confusing. As we can see, contrary to expectations, the applied restoration voltages that have low amplitude (2.5V and 5V), make the restoration slower than the same process when there is no external action (0V). Only the voltages oscillating with 10V of the amplitude or higher make the restoration process faster than at the '0V'. We can also see that the voltages above 30-35V do not change the helix restoration dynamics significantly.

We can see in Figure A.10 that the restoration process inside the BG is fast enough even if we do not apply any restoration voltage and the restoration voltage does not change the dynamic significantly. But if we look closer, we can notice that the tendencies in the Figure

A.10a are repeated: the low voltages make the process slower (the differences are minor, but they exist). The voltages higher than 25V do not change the dynamics of the restoration.

The Figure A.11 shows that there is no 'surprise' from the expectations for a non-resonantly polarized probe beam: The higher the restoration voltage, the faster the transmittance value. The voltages above 25V do not change the restoration dynamics. We notice that in the last three graphs (Figure A.10 and Figure A.11) we observe the same process; the difference is the probe beam polarization and the wavelength on which we concentrated our attention. The non-resonant polarized probe does not 'feel' the helical domains, so its transmittance increases or decreases only because of scattering (that is why the transmittances of all the wavelengths change in the same way without manifesting any difference for the BG wavelengths, as seen in Figure A.9). So we can suppose that the low voltages 'disturb' the helix formation but, however, they 'help' the quenching of non-uniformities. These non-uniformities are the so called disclination [25] lines, which cause scattering. Another difference between Figure A.10a and Figure A.11 is that the transmittances for the same voltages (say 15V) reach their final values faster in Figure A.11 (the non-resonant polarization). Consequently, there is a difference (from the viewpoint of BG restoration dynamics) whether the beam 'feels' the periodic structure or not. But this difference is 'artificial'; it does not mean a difference in the dynamics of the structure restoration.

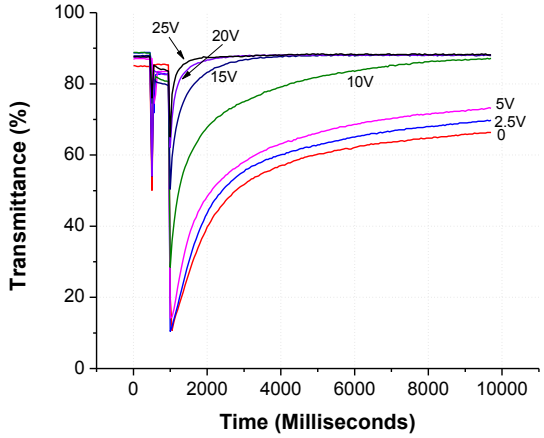

Figure A.11: The transmittance dependence on time during the excitation and relaxation (restoration) for various restoration voltages. The light is non-resonant and circularly polarized.

Reflection Measurements: the Experimental Setup and Procedure

As the helix restoration process in question is a restoration of the periodic structure, assuming Bragg reflection in the visible range of light, it is interesting to observe the dynamics of the reflection spectra of the CLC cell during the helix restoration. If in the case of the transmittance spectra, we cannot be sure whether the decrease of transmittance value is because of diffusion, absorption or reflection of light, in the case of the reflectance spectra we do not have this ambiguity. The increase of the reflectance value (which in this case is the equivalent of the decrease in the transmittance) directly indicates the formation of a periodic structure. We used the experimental setup shown in the Figure A.12 to study the influence of the external restoration electric field on the reflection of the light beam from the same CLC cell. The light beam from the supercontiniuum laser source (SuperK COMPACT, from NKT photonics) was collimated and then it passed through the polarizer, P, and the wide-band quarter wave plate (WBQWP, λ/4). Orienting the WBQWP's optical axis at "+" or "–" 45 degrees respected to the polarizer transmission axis, we changed the light polarization from the circularly right one to the left. Then, after splitting by the polarization non-dependent beam splitter, the beam reaches the CLC sample. The reflected (or back diffused) light was collected by an integrating sphere (IS: FIOS-1, from Ocean Optics) with 9.5 mm of aperture, which was connected with the Ocean Optics spectrometer (USB 2000) by an optical fiber. The spectrometer, connected with the PC, returns the

spectra of the reflected (or back diffused) light. The IS detects not only the direct reflected light, but it collects back the diffused light at a certain solid angle, Ω.

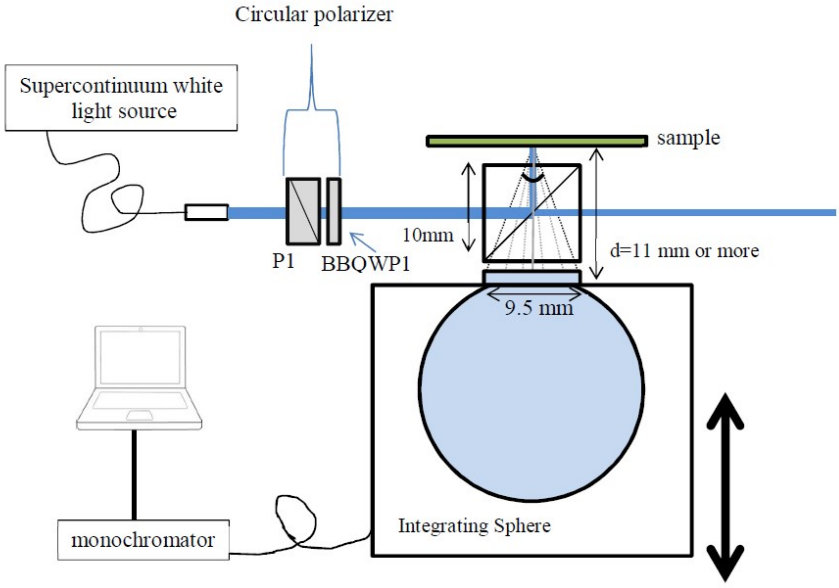

Figure A.12: The schematic illustration of the experimental setup of the reflection spectra measurements.

Results

In Figure A.13 the reflection spectra changes during the helix restoration process for the applied U = 20V (100 kHz) restoration voltage are presented. All the experimental conditions for those two observations are the same, but the positions of the IS (detector). In Figure A.13a the distance, *d,* between the CLC cell and the IS aperture was 11mm, so it collected the light reflected (back diffused) inside the cone with a total opening angle of ~ 46°. And in the next figure (Figure A.13a) the distance, *d,* is 90 mm, so that it collected the reflected (back diffused) light inside the cone with a total opening angle of ~ 6°. In Figure A.13 (*a* and *b*), the consequent spectra were taken at following instants: 0 corresponds to the homeotropic state of the CLC cell which was obtained applying the excitation voltage of U = 80V (1 kHz), then 50 ms, 100 ms, 250 ms and 7 s after applying the restoration voltage U = 20V (100 kHz). As we can see, the reflection band restores faster if the sphere is placed closer to the CLC cell (collecting the light diffused in wider angles). We can also conclude from these two graphs that the important changes were produced inside the BG, i.e. there was no any significant back scattering outside the band gap during the restoration process.

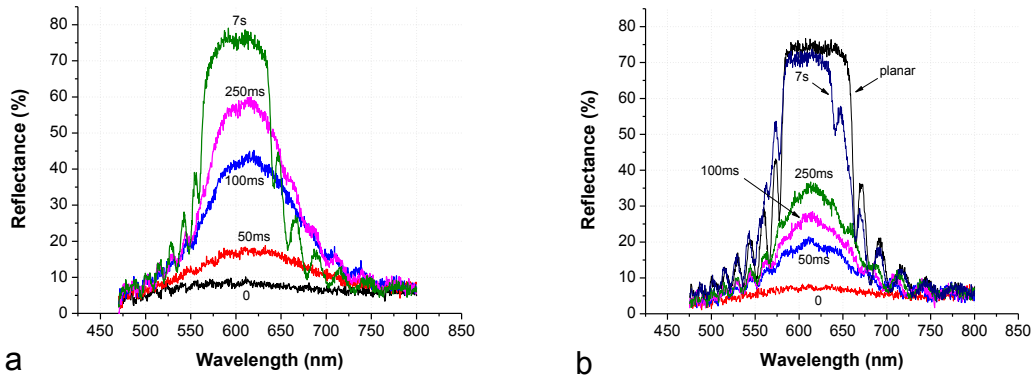

Figure A.13: The consequent reflectance spectra of the CLC cell during the forced helix restoration under the action of the electric field (U=20V RMS, 100 kHz, AC, Sin). The probe beam is resonant circularly polarized and the distance, d, between the IS aperture and the CLC (see Figure A.12) was 11 mm (a) and 90 mm (b).

We repeated this measurements for different restoration voltages: U=0, 10V and 20V (100 kHz, sine-shaped) and for two positions of the IS: d=11 mm and 90 mm (not presented here). They all showed that the stronger the restoration voltage, and the closer the sphere to the CLC cell, the faster the reflection band restoration. We think it important to mention again that in the both cases we observed the same process in the same conditions, the only difference being the distance between the sample and the IS aperture. So the helix restoration times were the same (in Figure A.13 a and b), but the reflection band restoration times were different because of the light scattering: If (apparently this was the case) the helixes were formed in little domains and there still were orientation defects in the structure, the BG wavelengths would reflect but not directly (back scattering). In that case the closer the IS, the more collected light and the more the transmittance value inside the BG.

As we can see and as it was mentioned above, the significant change during the restoration takes place inside the BG. For a more detailed observation of the influence of applied external electric field on the reflection restoration we took a wavelength (600 nm) situated inside the band gap and we observed its evolution during time. The reflection values were obtained from the reflection spectra taken at every 50 ms.

We can see in Figure A.14a that the reflection coefficient restoration is faster if there is an applied restoration voltage. In this case, the detector (the integration sphere) was placed as close to the simple as it was possible (11 mm). It is limited by the dimensions of the side of

the beam splitter (a cube) that was 10 mm, and 1 mm space, total between the cube and the sample and between the cube and the integration sphere. As it was mentioned above, in this case the detecting system collected the light reflected (back scattered) inside the cone with a total opening angle of ~ 46°. In Figure A.14b the reflection restoration is presented when the sphere was placed relatively far (90 mm) from the CLC cell where it collected the light reflected (back scattered) inside the cone with a total opening angle of ~ 6° (with a rough approximation, we can call it a direct reflection).

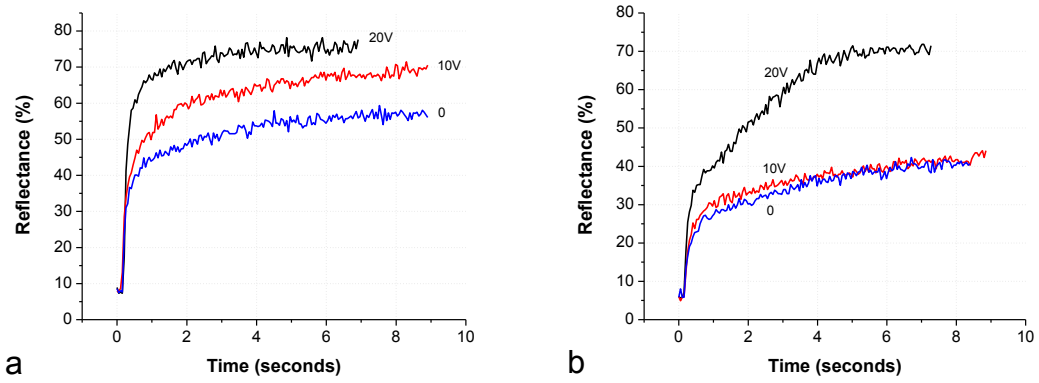

Figure A.14: the reflectance dependence on time during the helix relaxation (restoration) for various restoration voltages. The probe beam was resonant circularly polarized, the wavelength is 600 nm and the distance, d, between the IS aperture and the CLC (see Figure A.12) is 11 mm (a) and 90 mm (b).

Comparing Figure A.14a and Figure A.14b we can see that the corresponding curves (the same restoration voltages in the two figures) are always lower in Figure A.14b but this difference decreases during the time. For example, the difference is minor after 4 seconds, and it becomes about 5% between the curves with U=20V (when the scattering becomes less important).

In Figure A.15 we have the same configuration as in Figure A.14a, i.e. the distance between the sphere and the CLC cell is 11 mm, but the probe beam had non-resonant circular polarization. So the beam could principally pass through the cell and the signal detected by the sphere could be minimal for the both cases, when the cell was in a planar-helical state or in a homeotropic one. We see (the curve U=0) that after switching off the excitation voltage, the reflection (back scattering) increases and after that it starts to decrease slowly enough, while the reflection (under a restoration voltage; the curves

U=10V, U=20V) it decreases (for a few seconds) once the field frequency is changed from the excitation frequency to the restoration one.

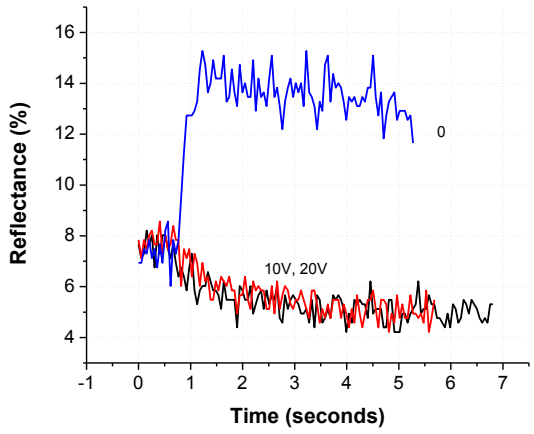

Figure A.15: The reflectance dependence on time during the helix relaxation (restoration) for various restoration voltages. The probe beam was non-resonant and circularly polarized, the wavelength is 600 nm and the distance between the IS aperture and the CLC (see A.12) was 11 mm.

In conclusion, we investigated the electric field induced transitions of the CLC cell in chapter 4. Particularly, the planar to homeotropic transitions and the reverse ones were investigated under a optically-polarizing microscope which confirmed the initial idea, i.e. the use of a dual-frequency NLC compound in the CLC mixture can help to quench the orientation defects in the CLC layer and that it can accelerate the process of the helix restoration. Further experiments of measurements of the variation of the effective birefringence of the CLC layer during the homeotropic-planar transition showed that the application of the electric field (at frequency lying in the zone of the negative dielectric anisotropy of the LC) accelerated the helix restoration by a factor of ~ 20. Spectral investigations (the present appendix) of the same transitions assured us once again that the use of the dual frequency CLC and electric fields of different frequencies let us carry out fast switches between planar – helicoidal and homeotropic states. They also showed us that during the transitions, the scattering of light occurs because of the orientational defects in the LC layer. Those defects introduce both forward and backward scatterings. It is to be mentioned that the forward scattering appears for all the wavelengths, while the backward scattering is mainly reserved for the BG wavelengths. This means that little helicoidal

domains are formed in the LC layer and they back-scatter the light as these domains are randomly oriented.

We believe that the investigations of chapter 4 and appendix 2 can be useful for CLCs to be used as polarizer free light modulators. Using our results, it is also possible to design elements that control light scattering and the energy flow. We would like to stress that a possible branch of application is designing of CLC films in greenhouses and in 'smart windows' where electric field could be used to control the energy flow into the building. They also could optimize the energy consumption for air conditioning of buildings.

Bibliography

[1] C. Kittel, Introduction to Solid State Physics, 8th edition ed., John Wiley & Sons, 2005.

[2] I.-C. Khoo and S.-T. Wu, Optics and Nonlinear Optics of Liquid Crystals, vol. 1, Singapore: World Scientific, 1993, p. 425.

[3] L. Blinov and V.G.Chigrinov, Electrooptic Effects in Liquid Crystal Materials, New York: Springer, 1994, p. 464.

[4] P. J. Collings and M. Hird, Introduction To Liquid Crystals, London: Taylor & Francis, 1997.

[5] P. De Gennes and J. Prost, The Physics of Liquid Crystals, 2nd ed., Oxford: Oxford University Press, 1995, p. 597 .

[6] P. Yeh and C. Gu, Optics of Liquid Crystal Displays, 2 ed., New Jersey: Wiley, 2010.

[7] K. Asatryan, V. Presnyakov, A. Tork, A. Zohrabyan, A. Bagramyan and T. Galstian, "Optical lens with electrically variable focus using an optically hidden dielectric structure," *Optics Express,* vol. 18, no. 13, pp. 13981-13992, 2010.

[8] V. V. Presnyakov, K. E. Asatryan, T. Galstian and A. Tork, "Tunable polymer-stabilized liquid crystal microlens," *Optics Express,* vol. 10, no. 17, p. 865–870 , 2002.

[9] T. V. Galstian, Smart Mini-Cameras, CRC Press, 2013.

[10] T. Scarf, Polarized Ligth In Liquid Crystals And Polymers, New Jersey: Wiley, 2007, p. 400.

[11] C. Gähwiller, "Temperature dependence of flow alignment in nematic liquid crystals," *Phys. Rev. Lett.,* vol. 28, no. 24, pp. 1554-1556, 1972.

[12] L. A. Archer and R. G. Larson, "A molecular theory of flow alignment and tumbling in sheared nematic liquid crystals," *J. Chem. Phys.,* no. 103, pp. 3108-3111, 1995.

[13] E. Dubois-Violette, P. d. Gennes and O. Parodi, "Hydrodynamic instabilities of nematic liquid crystals under A. C. electric fields," *J. Phys. France,* vol. 32, no. 4, pp. 305-317, 1971.

[14] S. Sarman and A. Laaksonen, "Flow alignment phenomena in liquid crystals studied by molecular dynamics simulation," *J. Chem. Phys.,* vol. 131, p. 144904, 2009.

[15] G. H. Vegnière, On Chirality and the Universal Asymmetry, Zurich: WILLEY-VCH, 2007, p. 247.

[16] B. Aryal, S. R. Acharya and W. Saurer, "Chiral property of spiral and barred spiral galaxies in the local supercluster," *Astrophys Space Sci ence,* no. 307, p. 369–383, 2007.

[17] S.P. Palto, *Usp. Fiz. Nauk,,* vol. 175, p. 784, 2005.

[18] L. M. Blinov, Structure and Properties of Liquid Crystals, New York: Springer, 2011, p. 439.

[19] M. Born and E. Wolf, Principles of Optics, New York: Pergamon, 1980, p. 808.

[20] C. Elliot, The molecular basis of optical activity : optical rotatory dispersion and circular dichroism, New York: Wiley, 1979, p. 364.

[21] H. Kimura, M. Hosino and H. Nakano, "Temperature dependent pitch in cholesteric Phase," *Journal de Physique,* vol. C3, no. 4, pp. 174- 177, 1979.

[22] E. Sackmann, S. Meiboom, L. C. Snyder, A. E. Meixner and R. E. Dietz, "Structure of the liquid crystalline state of cholesterol derivatives," *J. Am. Chem. Soc.,* vol. 90,

no. 13, p. 3567–3569, 1968.

[23] M. Srinivasarao, "Nano-Optics in the biological world: beetles, butterflies, birds, and moths," *Chemical Reviews,* vol. 99, no. 7, pp. 1935-1961, 1999.

[24] S. Caveney, "Cuticle reflectivity and optical activity in scarab beetles: The role of uric acid," *Proceedings of the Royal Society of London. Series B,* vol. 178, pp. 205-225, 1971.

[25] I. Dierking, Textures of Liquid Crystals, Weinheim: WIELEY-VCH, 2003, p. 218.

[26] D. W. Prather, S. Shi, A. Sharkawy, J. Murakowski and G. J. Schneider, Photonic Crystals: Theory, Application and Fabrication, New Jersey: Wiley, 2009.

[27] J. D. Joannopoulos, S. G. Johnson, J. N. Winn and R. D. Meade, Photonic Crystals:Molding the Flow of Light, 2nd edition ed., Princeton: Princeton University Press, 2008.

[28] H. Finkelmann, S. Kim, A. Muæoz, P. Palffy-Muhoray and B. Taheri, "Tunable mirrorless lasing in cholesteric liquid crystalline elastomers," *Adv. Mater,* vol. 13, no. 14, pp. 1069-1072, 2001.

[29] G. Chilaya, A. Chanishvili, G. Petriashvili, R. Barberi, R. Bartolino, G. Cipparrone, A. Mazzulla and P. Shibaev, " Reversible tuning of lasing in cholesteric liquid crystals controlled by light-emitting diodes," *Adv. Mater,* vol. 19, p. 565–568, 2007.

[30] *Liquid crystal Bragg filters.* [Sound Recording]. SPIE 7955. 2011.

[31] I. J. Hodgkinson, Q. h. Wu, M. Arnold, M. W. McCall and A. Lakhtakia, "Chiral mirror and optical resonator designs for circularly polarized light: suppression of cross-polarized reflectances and transmittances," *Optics Communications,* vol. 210, no. 3-6, pp. 201-211, 2002.

[32] W. F. Liu, P. S. J. Russell and L. Dong, "Acousto-optic superlattice modulator using

a fiber Bragg grating," *Optics Letters,* vol. 22, no. 19, pp. 1515-1517, 1997.

[33] E. Yablonovitch, "Inhabited spontaneous emission in solid-state physics and electronics," *Phys. Rev. Lett,* vol. 58, no. 20, p. 2059–2062, 1987.

[34] S. John, "Strong localization of photons in certain disordered dielectric superlattices," *Phys. Rev. Lett,* vol. 58, no. 23, p. 2486–2489, 1987.

[35] V. I. Kopp, B. Fan, H. K. M. Vithana and A. Z. Genack, "Low-threshold lasing at the edge of a photonic stop band in cholesteric liquid crystals," *Optics Letters,* vol. 23, no. 21, pp. 1707-1709 , 1998.

[36] W. L. Bragg, "The specular reflection of X-rays.," *Nature,* vol. 90, no. 2250, p. 410, 1912.

[37] R. Kashyap, Fiber Bragg Gratings, San Diego: Academic Press, 1999.

[38] V. I. Kopp and A. Z. Genack, "Twist Defect in Chiral Photonic Structures," *PhysRevLett,* vol. 89, no. 3, p. 033901.

[39] E. Yablonovitch, T. J. Gmitter, R. D. Meade, A. M. Rappe, K. D. Brommer and J. D. Joannopoulos, "Donor and acceptor modes in photonic band structure," *PhysRevLett,* vol. 67, no. 24, pp. 3380-3383, 1991.

[40] V. A. Belyakov, "Defect Modes in Chiral Liquid Crystals: An Analytic Approach," *Molecular Crystals and Liquid Crystals,* vol. 494, no. 1, pp. 127-152, 2008.

[41] T. Matsui, M. Ozaki and K. Yoshino, "Tunable photonic defect modes in a cholesteric liquid crystal induced by optical deformation of helix," *Phys. Rev. E,* vol. 69, no. 6, p. 061715, 2004.

[42] O. Ryotaro, M. Tatsunosuke, O. Masanori and Y. Katsumi, "Electro-Tunable Defect Mode in One-Dimensional Periodic Structure Containing Nematic Liquid Crystal as a Defect Layer," *Jpn. J. Appl. Phys.,* vol. 41, no. 2-12b, p. L1482, 2002.

[43] B. Maune, M. Lončar, J. Witzens, M. Hochberg, T. Baehr-Jones, D. Psaltis, A. Scherer and Y. Qiu, "Liquid-crystal electric tuning of a photonic crystal laser," *Appl. Phys. Lett.,* vol. 85, no. 3, pp. 360-362, 2004.

[44] H.-G. Park, S.-H. Kim, S.-H. Kwon, Y.-G. Ju, J.-K. Yang, J.-H. Baek, S.-B. Kim and Y.-H. Lee, "Electrically Driven Single-Cell Photonic Crystal Laser," *Science 3,* vol. 305, no. 5689, pp. 1444-1447 , 2004.

[45] T.-H. Lin, Y. Huang, Y. Zhou, A. Y. G. Fuh and S.-T. Wu, "Photo-patterning micro-mirror devices using azo dye-doped cholesteric liquid crystals," *Optics Express,* vol. 14, no. 10, pp. 4479-4485, 2006.

[46] J. Hwang, M. H. Song, B. Park, S. Nishimura, T. Toyooka, J. W. Wu, Y. Takanishi, K. Ishikawa and H. Takezoe, "Electro-tunable optical diode based on photonic bandgap liquid-crystal heterojunctions," *Nature Materials,* vol. 4, pp. 383 - 387, 2005.

[47] M. H. Song, B. Park, Y. Takanish, K. Ishikawa, S. Nishimura, T. Toyooka and H. Takezoe, "Simple electro-tunable optical diode using photonic and anisotropic liquid crystal films," *Thin Solid Films,* vol. 509, no. 1-2, pp. 49-52, 2006.

[48] G. Petriashvili, M. A. Matranga, M. P. D. Santo, G. Chilaya and R. Barberi, "Wide band gap materials as a new tuning strategy for dye doped cholesteric liquid crystals laser," *Optics Express,* vol. 17, no. 6, pp. 4553-4558, 2009.

[49] M. Belalia, M. Mitov, C. Bourgerette, A. Krallafa, M. Belhakem and D. Bormann, "Cholesteric liquid crystals with a helical pitch gradient: Spatial distribution of the concentration of chiral groups by Raman mapping in relation with the optical response and the microstructure," *Phys. Rev. E,* vol. 74, no. 5, p. 051704, 2006.

[50] V. Belyakov and A. Sonin, Optika kholestericheskikh zhidkikh kristallov, Moscow: Nauka, 1982.

[51] M. Kurik and O. Lavrentovich, "Topological defects in cholesteric liquid crystals," *JETP LETTERS,* vol. 33, no. 10, pp. 528-531, 1981.

[52] F. Zhang and D. Yang, "Evolution of disclinations in cholesteric liquid crystals," *Phys. Rev. E,* vol. 66, no. 4, p. 041701, 2002.

[53] L. Natarajan, J. Wofford, V. Tondiglia, R. Sutherland, H. Koerner, R. Vaia and T. Bunning, "Electro-thermal tuning in a negative dielectric cholesteric liquid crystal material," *Journal of Applied Physics,* vol. 103, p. 093107, 2008.

[54] S. K. Tang, L. Zhang, W. J. Zheng and e. all, "Cholesteric liquid crystal system used for precision measurement of body temperature," *Polymer Materials Science and Engineering,* vol. 25, pp. 128-130, 2008.

[55] M. Luban, D. Mukamel and S. Shtrikman, "Transition from the cholesteric storage mode to the nematic phase in critical restricted geometries," *Phys. Rev. A,* vol. 10, no. 1, pp. 360-367.

[56] V. Fréderiksz and V. Zolina, "Forces Causing the Orientation of an Anisotropic Liquid," *Trans. Faraday Soc.,* vol. 29, pp. 919-930, 1933.

[57] R. J. Witonsky and J. W. Scarantino, "Method for preparing an improved liquid crystal clinical thermometer". USA Patent US6284078 B1, 22 Nov 1994.

[58] P. J. Collings, Liquid crystals : nature's delicate phase of matter, 2nd ed. ed., Princeton: Princeton University Press, 2002.

[59] Y. Watanabe, M. Uchimura, F. Araoka, G.-i. Konishi, J. Watanabe and H. Takezoe, "Extremely low threshold in a pyrene-doped distributed feedback cholesteric liquid crystal laser," *Appl. Phys. Express,* vol. 2, no. 10, p. 102501, 2009.

[60] G. P. Crawford and S. Zumer, Liquid Crystals in Confined Geometries Formed by Polymer and Porous Networks, London: Taylor & Francis, 1996.

[61] M.-H. Lua, "Bistable reflective cholesteric liquid crystal display," *J. Appl. Phys,* vol. 81, no. 3, pp. 1063-1066, 1997.

[62] M. Ji, S. Lei and Y. Deng-Ke, "Bistable Polymer Stabilized Cholesteric Texture Light Shutter," *Appl. Phys. Express,* vol. 3, no. 2, p. 021702, 2010.

[63] H.-H. Liang, C.-C. Wu, P.-H. Wang and J.-Y. Lee, "Electro-thermal switchable bistable reverse mode polymer stabilized cholesteric texture light shutter," *Optical Materials,* vol. 33, no. 8, p. 1195–1202, 2011.

[64] P.-T. Lin, S.-T. Wu, C.-Y. Chang and C.-S. Hsu, "Molecular Crystals and Liquid," *Mol. Cryst. Liq. Cryst,* vol. 411, no. 1, pp. 243-253,, 2004.

[65] C.-H. Wen, S. Gauza and S.-T. Wu, "Photostability of liquid crystals and alignment layers," *Journal of the SID,* vol. 13, no. 9, pp. 805-811, 2005.

[66] C. A. Bailey, V. P. Tondiglia, L. V. Natarajan, M. M. Duning, R. L. Bricker, R. L. Sutherland, T. J. White, M. F. Durstock and T. J. Bunning, "Electromechanical tuning of cholesteric liquid crystals," *J. Appl. Phys.,* vol. 107, no. 1, p. 013105, 2010.

[67] M. Blahó, Á. Egri, R. Hegedüs, J. Jósvai, M. Tóth, K. Kertész, L. P. Biró, G. Kriska and G. Horváth, "No evidence for behavioral responses to circularly polarized light in four scarab beetle species with circularly polarizing exocuticle," *Physiology & Behavior,* vol. 105, no. 4, p. 1067–1075, 2012.

[68] J. Li, S.-T. Wu, S. Brugioni, R. Meucci and S. Faetti, "Infrared refractive indices of liquid crystals," *J. Appl. Phys.,* vol. 97, no. 6, p. 073501 , 2005.

[69] S. M. Arakelyan, O. S. Eritsyan, A. S. Karayan and Y. S. Chilingaryan, "Optical characteristics of a layer of cholesteric liquid crystal between dielectric plates of finite thickness and analysis for a filled Fabry–Perot resonator," *Sov. J. Quantum Electron.,* vol. 10, no. 5, pp. 547-554, 1980.

[70] K. Allahverdyan, T. Galstian, A. Gevorgyan and R. Hakobyan, "Could the Cuticle of Beetles Serve Also for Their Radiative Thermoregulation?," *OPJ,* vol. 3, no. 7A, pp. 12-17, 2013.

[71] R. Cano and B. S. Fr, *Mineral. Cristallogr,* vol. 90, p. 333, 90.

[72] D.-K. Yang, X.-Y. Huang and Y.-M. Zhu, "BISTABLE CHOLESTERIC REFLECTIVE DISPLAYS:Materials and Drive Schemes," *Annu. Rev. Mater. Sci.,* vol. 27, no. 1, pp. 117-146, 1997..

[73] V. A. Belyakov, V. E. Dmitrienko and V. P. Orlov, "Optics of cholesteric liquid crystals," *Sov. Phys. Usp.,* vol. 22, no. 2, p. 64, 1979.

[74] A.C, Naville and S. Caveney, "Scarabaeid beetle exocuticle as an optical analogue of cholesteric liquid crystals," *Bio.l Rev. Camb. Philos. Soc.,* vol. 44, no. 4, pp. 531-62, 1969.

[75] V. Sharma, M. Crne, J. O. Park and M. Srinivasarao, "Structural origin of crcularly polarized iridescence in jeweled beetles," *Science,* vol. 325, no. 5939, pp. 449-451 , 2009.

[76] D. J. Broer, J. Lub and G. N. Mol, "Wide-band reflective polarizers from cholesteric polymer networks with a pitch gradient," *Nature,* vol. 378, pp. 467 - 469, 1995.

[77] M. Mitov, E. Nouvet and N. Dessaud, "Polymer-stabilized cholesteric liquid crystals as switchable photonic broad bandgaps," *The European Physical Journal E,* vol. 15, no. 4, pp. 413-419, 2004.

[78] S.-Y. Lu and L.-C. Chien, "A polymer-stabilized single-layer color cholesteric liquid crystal display with anisotropic reflection," vol. 91, no. 13, p. 131119 , 2007.

[79] Y. Huang, Y. Zhou, C. Doyle and S.-T. Wu, "Tuning the photonic band gap in cholesteric liquid crystals by temperature-dependent dopant solubility," vol. 14, no. 3, pp. 1236-1242 , 2006.

[80] W. C. Yip and H. S. Kwok, "Helix unwinding of doped cholesteric liquid crystals," *Appl. Phys. Lett.,* vol. 78, no. 4, pp. 425-427, 2001.

[81] V. A. Belyakov, "Untwisting of the helical structure in a plane layer of chiral liquid crystal," *JETP Letters,* vol. 76, no. 2, pp. 88-92, 2002.

[82] U. A. Hrozhyk, S. V. Serak, N. V. Tabiryan, T. J. White and T. J. Bunning, "Nonlinear optical properties of fast, photoswitchable cholesteric liquid crystal bandgaps," *Optical Materials Express,* vol. 1, no. 5, pp. 943-952 , 2011.

[83] K. Allahverdyan and T. Galstian, "Electrooptic jumps in natural helicoidal photonic bandgap structures," *Optics Express,* vol. 19, no. 5, pp. 4611-4617 , 2011.

[84] K. Allahverdyan and T. Galstian, "Accelerating the cholesteric helix restoring by a dual frequency compound," *Mol. Cryst. & Liq. Cryst,* vol. 560, no. 1, pp. 35-48, 2012.

[85] Y. Yin, M. Gu, A. Golovin, S. Shiyanovskii and O. Lavrentovich, "fast switching optical modulator based on dual frequency nematic cell," vol. 421, no. 1, pp. 133-144, 2004.

[86] W. Li, H. Zhang, L. Wang, C. Ouyang, X. Ding, H. Cao and H. Yang, "Effect of a chiral dopant on the electro-optical properties of polymer-dispersed liquid-crystal films," *Journal of Applied Polymer Science,* vol. 105, no. 4, p. 2185–2189, 2007.

[87] "Merck Ltd. http.//www.merck-chemicals.com/lcd-emerging-thechnologies," [Online].

[88] A. A. Gevorgyan, K. V. Papoyan and O. V. Pikichyan, "Reflection and transmission of light by cholesteric liquid crystal-glass-cholesteric liquid crystal and cholesteric liquid crystal(1)-cholesteric crystal(2) systems," *Optics and Spectroscopy,* vol. 88, no. 4, pp. 586-593, 2000.

[89] A. H. Gevorgyan, "Tunable reflectance of a two-defect-layer cholesteric liquid crystal," *Phys. Rev. E,* vol. 83, no. 1, p. 011702, 2011.

[90] A. A. Gevorgyan, "Reflection and Transmission of Light for a Layer with Dielectric and Magnetic Helicities. I. Jones Matrices. Natural Polarizations," *Optics and Spectroscopy,* vol. 89, no. 4, pp. 631-638, 2000.

[91] R. Azzam and N. Bashara, Ellipsometry and Polarized Light, New York: North-Holland, 1997.

[92] A. T. D. Bennett, I. C. Cuthill and K. J. Norris, "Sexual selection and the mismeasure of color," *The American Naturalist,* vol. 144, no. 5, pp. 848-860, 1994.

[93] J. Mappes, N. Marples and J. A. Endler, "The complex business of survival by aposematism," *Trends in Ecology & Evolution,* vol. 20, no. 11, pp. 598-603, 2005.

[94] C. Galland, R. Ding, N. C. Harris, T. Baehr-Jones and H. Michael. [Online]. Available: http://arxiv.org/ftp/arxiv/papers/1405/1405.1169.pdf.

[95] N. A. Estep, D. L. Sounas, J. Soric and A. Alù, "Magnetic-free non-reciprocity and isolation based on parametrically modulated coupled-resonator loops," *Nature Physics,* vol. 10, no. 12, p. 923–927, 2014.

[96] A. E. Miroshnichenko, E. Brasselet and Y. S. Kivshar, "Reversible optical nonreciprocity in periodic structures with liquid crystals," *Appl. Phys. Lett.,* vol. 96, no. 6, p. 063302 , 2010.

[97] F. Jonsson and C. Flytzanis, "polarization state controlled multistability of a nonlinear magneto-optic cavity," *Phys. Rev. Lett.,* vol. 82, no. 7, pp. 1426-1429, 1999.

[98] V. A. Fedotov, P. L. Mladyonov, S. L. R. A. V. Prosvirnin, Y. Chen and N. I. Zheludev, "asymmetric propagation of electromagnetic waves through a planar chiral structure," *Phys. Rev. Lett.,* vol. 97, no. 16, p. 167401, 2006.

[99] K. Takatoh, M. Sakamoto, R. Hasegawa, M. Koden, N. Itoh and M. Hasegawa, Alignment Technology and Applications of Liquid Crystal Devices, New York: Taylor & Francis, 2005.

[100] G. Agez, R. Bitara and M. Mitov, "Color selectivity lent to a cholesteric liquid crystal by monitoring interface-induced deformations," *Soft Matter,* vol. 7, no. 6, pp. 2841-2847, 2011.

[101] F. F.C., "On theory of Liquid crystals," New York, 1958, pp. 19-28.

[102] M. Kleman and O. Lavrentovich, Soft Matter Physics, New York : Springer, 2003.

[103] V. A. Belyakov, "Cano-Grandjean Wedge at Weak Surface Anchoring," *Mol. Cryst. & Liq. Cryst,* vol. 480, no. 1, pp. 262-277, 2008.

[104] V. I. Koppa, Z.-Q. Zhangb and A. Z. Genacka, "Lasing in chiral photonic structures," *Progress in Quantum Electronics,* vol. 27, no. 6, pp. 369-416, 2003.

[105] R. B. Alaverdyan, K. R. Allakhverdyan (Allahverdyan), A. H. Gevorgyan, A. D. Chilingaryan and Y. S. Chilingaryan, "Chiral photonic crystals with an electrically tunable anisotropic defect. Experiment and theory," *Technical Physics,* vol. 55, no. 9, pp. 1317-1323, 2010.

[106] N. Osterman, J. Kotar, E. M. Terentjev and P. Cicuta, "Relaxation kinetics of stretched disclination lines in a nematic liquid crystal," *Phys. Rev. E,* vol. 81, no. 6, p. 061701 , 2010.

[107] S. Relaix and M. Mitov, "Polymer-Stabilized Cholesteric Liquid Crystals with a double helical handedness: influence of an ultraviolet light absorber on the characteristics of the circularly polarized light reflection band," *Liq. Cryst.,* vol. 35, no. 8, pp. 1037-1042, 2008.

[108] G. Agez and M. Mitov, "Cholesteric Liquid Crystalline Materials with a Dual Circularly Polarized Light Reflection Band Fixed at Room Temperature," *J. Phys.*

Chem., vol. 115, no. 20, p. 6421–6426, 2011.

[109] Y.-C. Hsiao, C.-Y. Tang and W. Lee, "Fast-switching bistable cholesteric intensity modulator," *Optics Express,* vol. 19, no. 10, pp. 9744-9749 , 2011.

[110] S. A. Jewell and J. R. Sambles, "Measurement of Azimuthal Backflow in a Dual-Frequency Chiral HAN Cell," *Mol. Cryst. Liq. Cryst.,* vol. 477, p. 57/[551]–65/[559, 2007.

[111] S. A. Jewell and J. R. Sambles, "Dynamic response of a dual-frequency chiral hybrid aligned nematic liquid-crystal cell," *Phys. Rev. E,* vol. 73, no. 1, p. 011706, 2006.

[112] C. -Y. Huang, K. -Y. Fu, K.-Y. Lo and M. -S. Tsai, "Bistable transflective cholesteric light shutters," *Optics Express,* vol. 11, no. 6, pp. 560-565, 2003.

[113] M. Xu and D.-K. Yang, "electrooptical properties of dual-frequency cholesteric liquid crystal reflective display and drive scheme," *Japanese Journal of Applied Physics,* vol. 38 part 1, no. 12A, p. 6827 .

[114] M. Xu and D.-K. Yang, "Dual frequency cholesteric light shutters," *Appl. Phys. Lett.,* vol. 70, no. 6, pp. 720-722, 1997.

[115] E. C. Inc., "http://www.edmchemicals.com," [Online].

[116] Y.-H. Fan, H. Ren, X. Liang, Y.-H. Lin and S.-T. Wu, "Dual-frequency liquid crystal gels with submillisecond response time," *Appl. Phys. Lett.,* vol. 85, no. 13, pp. 2451-2453, 2004.

[117] A. B. Golovin, S. V. Shiyanovskii and O. D. Lavrentovich, "Fast Switching Dual-Frequency Liquid Crystal Optical Retarder, Driven by an Amplitude and Frequency Modulated Voltage," *SID International Symposium Digest of Technical Papers,* vol. 34, no. 2, pp. 1472-1475, 2003.

[118] S.P. Palto, "On Mechanisms of the helix pitch variations in a thin cholesteric layer

confined between two surfaces," *J. Exp. Theor. Phys,* vol. 94, no. 2, pp. 260-269, 2002.

[119] A. Belyakov and W. Kuczynski, "motion of nonsingular walls in plane layer of twisted nematics," *Mol. Cryst. & Liq. Cryst.,* vol. 480, no. 1, pp. 243-261, 2008.

[120] D. V. Shmeliova and V. A. Belyakov, "non-singular walls in cano-grandjean wedge," M*ol. Cryst. & Liq. Cryst,* vol. 527, no. 1, pp. 53/[209]-58/[214], 2010.

[121] E. P. Raynes, "Twisted wedges for the measurement of long pitch lengths in chiral nematic liquid crystals," *Liquid Crystals,* vol. 34, no. 6, pp. 697-699, 2007.

[122] A. H. Gevorgyan, "Anomalies of radiation absorption and superluminal propagation of light: II. A layer of a periodic medium with a helical structure," *Opt. Spectrosc.,* vol. 96, no. 6, pp. 887-893, 2004.